Functional characterization of Cytoplasmic Polyadenylation Element Binding proteins in the developing and diseased brain

Dissertation

zur

Erlangung des Doktorgrades (Dr. rer. nat.)

der

Mathematisch-Naturwissenschaftlichen Fakultät

der

Rheinischen Friedrich-Wilhelms-Universität Bonn

vorgelegt von

Magdalena Skubal

aus

Tarnogrod, Polen

Bonn, 2016

Angefertigt mit Genehmigung der Mathematisch-Naturwissenschaftlichen Fakultät der Rheinischen Friedrich-Wilhelms-Universität Bonn

1. Gutachter:	**Prof. Dr. Christian Steinhäuser** Institut für Zelluläre Neurowissenschaften Universität Bonn
2. Gutachter:	**Prof. Dr. Walter Witke** Institut für Genetik Universität Bonn

Tag der Promotion: 29.11.2016

Erscheinungsjahr: 2016

“**One of the ultimate challenges for biology is to understand the brain's processing of unconscious and conscious perception, emotion, and empathy**“

Eric R. Kandel

ACKNOWLEDGEMENTS

First of all, I would like to sincerely thank my supervisor Prof. Dr. Christian Steinhäuser for the scientific guidance, support and many constructive discussions.

I am honestly grateful to PD Dr. Andreas Waha for co-supervising my project, giving valuable suggestions and encouraging me throughout my work.

My special thanks go to my former supervisor Prof. Dr. Martin Theis for giving me the opportunity to work on this interesting project.

I would like to thank Prof. Dr. Walter Witke, Prof. Dr. Volkmar Gieselmann and Prof. Dr. Dieter Meschede for accepting my request to be part of the examination committee and for their effort in reviewing this work.

I am especially grateful to PD Dr. Gerald Seifert, Dr. med. Gerrit Gielen, Dr. Lech Kaczmarczyk and Dr. Peter Bedner for their help in multiple analyses and writing CPEB manuscripts. I want to thank PD. Dr. Ronald Jabs for introduction to the confocal microscopy. In addition, I would like to thank Prof. Dr. Christian Henneberger and Dr. Anne Boehlen for fruitful discussions and constructive suggestions.

My special thanks go to the present and the former lab members: Aline, Björn, Camille, Daniel, Dimitri, Dilaware, Julia, Kirsten, Michel, Stefan, Steffi Anders, Steffi Griemsmann, and Tushar. Thank you for the great time together! I also would like to thank for administrative assistance to Dr. Silke Kunzel and Dr. Ines Heuer and for excellent technical support to Anja Matijevic, Thomas Erdmann, Dorota Denkhaus, Evelyn Dörfer, Verena Dreschmann, and Jennifer Hammes.

Last but not least, I would like to express my deepest gratitude towards my family, especially my parents and Nicolas for their constant encouragement and incredible support.

CONTENTS

ABBREVIATIONS

°C	degree Celsius
α-tubulin	alpha tubulin
β-ME	β-mercaptoethanol
µg	microgram
µl	microlitre
µM	micromolar
4EBP	eIF 4E-binding protein
AII	diffuse astrocytoma, WHO II
AAIII	anaplastic astrocytoma, WHO III
APS	ammonium persulfate
ATP	adenosine triphosphate
BCA	bicinchonic acid
Bcl-2	B-cell lymphoma 2
bp	base pair
BSA	bovine serum albumin
CaMKII	calcium-calmodulin dependent protein kinase II
cAMP	cyclic adenosine monophosphate
cDNA	complementary DNA
CNS	central nervous system
CPE	cytoplasmic polyadenylation element
CPEB	cytoplasmic polyadenylation element binding protein
CpG	cytosine-phosphate-guanine dinucleotide
CPSF	cleavage and polyadenylation specificity factor
CSC	cancer stem cell
CT	threshold cycle
DAB	3,3'-diaminobenzidine-tetrahydrochloride
dATP	deoxyadenosine triphosphate
dCTP	deoxycytidine triphosphate
ddH2O	double-distilled water
dGTP	deoxyguanosine triphosphate
dH2O	distilled water
DMEM	Dulbecco's modified eagle's medium
DMSO	dimethyl sulfoxide
DNMT	DNA methyltransferases
dNTP	deoxyribonucleotide phosphate
DPBS	Dulbecco's phosphate buffered saline
DTT	dithiothreitol
dTTP	deoxythymidine triphosphate
EDTA	ethylene diamine tetra acetic acid
EGFP	enhanced green fluorescent protein
eIF	eukaryotic translation initiation factors
eIF3	eukaryotic translation initiation factors 3
eIF4A	eukaryotic initiation factor 4A
eIF4E	eukaryotic initiation factor 4E
eIF4F	eukaryotic initiation factor 4F
eIF4G	eukaryotic initiation factor 4G
EMT	epithelial-to-mesenchymal transition
EphA4	ephrin receptor A4
ER	endoplasmic reticulum
EV	extracellular vesicle
FACS	fluorescence-activated cell sorting
FAM	fluorescein amidite
FCS	fetal calf serum
fw	forward primer
g	gram
GBM	glioblastoma multiforme, WHO IV
G-CIMP	glioma-CpG island methylator phenotype
GFAP	glial fibrillary acidic protein
GFP	green fluorescent protein
Gld2	germline development 2 poly(A) polymerase
GluN2A	NMDA receptor 2A
h	hour

HEK	human embryonic kidney cell
HEPES	4-(2-hydroxyethyl)-1-piperazineethanesulfonic acid
HIF-1α	hypoxia inducible factor-1α
HNF4	hepatocyte nuclear factor 4
HRP	horse radish peroxidase
ICC	immunocytochemistry
IDH	isocitrate dehydrogenase
IgG	immunoglobulin G
IHC	immunohistochemistry
kDa	kilo Dalton
KO	knockout
l	liter
LAR	luciferase assay reagent
LTP	long term potentiation
m7GpppG	7-methyl-guanosine
M	molar
mA	milliampere
MAP2	microtubule associated protein 2
MEF	mouse embryonic fibroblast
min	minute
miRNA	micro RNA
ml	milliliter
mM	millmolar
MMP7	matrix metallopeptidase 7
n	number
NDUFV2	ubiquinone oxidoreductase core subunit V2
Neo	neomycin
NEAA	non-essential amino acids
ng	nanogram
NGS	normal goat serum
nM	nanomolar
NMDA	N-methyl-D-aspartate
NP-40	nonidet P-40
NSC	neural stem cell
oct4	octamer-binding transcription factor 4
MEM	minimum essential media
OS	overall survival
p	probe
PABP	poly(A)-binding protein
PARN	poly(A) ribonuclease
PARP	phycoerythrin- cleaved poly (ADP-ribose) polymerase, Asp214
PARV	parvalbumin
PBGD	porphobilinogen deaminase
PBS	phosphate buffered saline
PCR	polymerase chain reaction
PDA	pancreatic ductal carcinomas
PFA	paraformaldehyde
pGBM	primary glioblastoma multiforme
pHH3	Alexa fluor 647-phospho(Ser10) histone H3
PI3K/Akt	phosphatidylinositol-4,5-bisphosphate 3-kinase/ protein kinase B
PKA	protein kinase A
PLB	passive lysis buffer
poly Q	polyglutamine
ps	pyrosequencing primer
PSD	postsynaptic density protein
PVDF	polyvinylidene fluoride
rev	reverse primer
RIPA	RNA immunoprecipitation assay
RNP	ribonucleoprotein complex
rpm	rotations per minute
RPS6K	ribosomal S6 kinase
RRM	RNA recognition motif
RT	room temperature
RT-PCR	reverse transcription polymerase chain reaction
sec	second
SEM	standard error of the mean
SDS	sodium dodecyl sulphate
sGBM	secondary glioblastoma multiforme

sqRT-PCR	semi quantitative real-time polymerase chain reaction	UTR	untranslated region
		v	transcript variant
TBS-T	tris buffered saline with tween 20	V	volt
TEMED	tetramethyl ethylene diamine	WB	Western blot
TGFβ	transforming growth factor β	WHO	World Health Organization
tPA	tissue plasminogen activator	Znf	zinc finger
Tris	tris (hydroxymethyl) aminomethane	ZO-1	zona occludens-1

1 INTRODUCTION

1.1 Gliomas

1.1.1 Cellular origin of gliomas

The cellular origin of gliomas is a matter of investigation. Evidence from glioma mouse models and human clinical data indicate that gliomas are developing from neural stem cells (NSCs), glial progenitor cells or differentiated progeny. The cell of origin has the potential to initiate oncogenic mutations that drive gliomagenesis (Modrek et al., 2014). There are two working hypothesis postulating that cellular heterogeneity and propagation of gliomas is regulated by clonal or cancer stem cell (CSC) model (Reya et al., 2001). The hypothesis of clonal growth of cancer postulates that single cancer cell has the ability to proliferate, self-renew and acquire genetic mutations, thus creating clonally derived subpopulations within the tumor (Schonberg et al., 2014). The CSC model assumes that a population of cells in the tumor possesses stem cell-like properties, such as the ability to self-renew, differentiate and proliferate. CSCs give rise to the cells that after reaching a fully differentiated stage reach limited tumorigenic potential (Schonberg et al., 2014). According to both models, the CSC and the clonal model, glioma cells acquire genetic mutations, accounting for the cellular and genetic heterogeneity (Modrek et al., 2014).

Cells having the ability to form gliomas are widely spread throughout the Central Nerves System (CNS), mostly developing within the cerebral hemispheres (Zong et al., 2012). Some of the glioblastomas occur in the subventricular zone adjacent to the lateral ventricles, while others arise in the subcortical white matter (Bohman et al., 2010; Lim et al., 2007). Region-specific features of the brain microenvironment and properties of the local progenitor population may affect the tumor phenotype (Gibson et al., 2010; Johnson et al., 2010). Distinct cells of origin may give rise to the same pathological manifestations, but it is also possible that different genetic mutations might transform the same cell into

different types of gliomas (Zong et al., 2012). Hence, defining the key driver mutations and cell types giving rise to gliomas is a prerequisite to understand the cancers biology, develop prevention strategies and effective treatments (Modrek et al., 2014; Zong et al., 2012).

1.1.2 **Histopathological and molecular classification of gliomas**

Gliomas are classified based on histopathological features, with reference to their association with specific glial lineages (Vigneswaran et al., 2015). The principles of histological analysis include findings of nuclear atypia, proliferative activity, microvascular proliferation, and necrosis (Louis, 2006). According to the grading of the World Health Organization (WHO) malignant gliomas are divided into astrocytic, oligoastrocytic, oligodendroglial, and ependymal tumors (Louis et al., 2007). Astrocytomas have morphological similarities with normal and reactive astrocytes, and express the astrocytic marker GFAP (Rousseau et al., 2006). Oligodendrogliomas are related to cells of the oligodendrocyte lineage, specifically oligodendrocyte progenitor cells, which express the markers including Olig2, NG2 and PDGFRα (Riemenschneider et al., 2004; Rousseau et al., 2006; Shoshan et al., 1999; Zong et al., 2012).

Malignant astrocytomas are further classified on the basis of tumor grade into less aggressive, diffuse astrocytomas, defined as WHO grade II (AII), aggressive, anaplastic astrocytomas, defined as WHO grade III (AAIII), and the most aggressive glioblastomas (GBMs) defined as WHO grade IV (Fig. 1.1.2-1) (Zong et al., 2012). Among astrocytomas, GBMs are the most frequent brain malignancies in adults (Louis et al., 2007). Based on clinical presentation GBMs are further classified as primary (pGBM) or secondary (sGBM) (Kim et al., 2013). Secondary GBMs are progressing from lower-grade precursor lesions, whereas primary GBMs develop *de novo* and usually at the time of diagnosis present advanced tumor features. Secondary GBMs are found in younger patients with median diagnosis age of ~45 years and occur less frequently than pGBM, i.e. in ~5% of GBM cases. The median age of diagnosis of pGBM patients is ~60 years (Olar and Aldape, 2012; Vigneswaran et al., 2015).

Due to histopathological similarity, GBMs require an identification of genetic alterations to describe their molecular subtypes (Ohgaki et al., 2004; Phillips et al., 2006; Verhaak et al., 2010). Phenotyping at a genome-wide level expanded the classification of gliomas by further dividing morphologically identical tumors into four subtypes, including classical, proneural, neural, and mesenchymal tumors (Verhaak et al., 2010; Vigneswaran et al., 2015; Zong et al., 2012). Secondary GBMs are usually classified as proneural, whereas primary GBMs may be of any of the subtypes (Cohen et al., 2013).

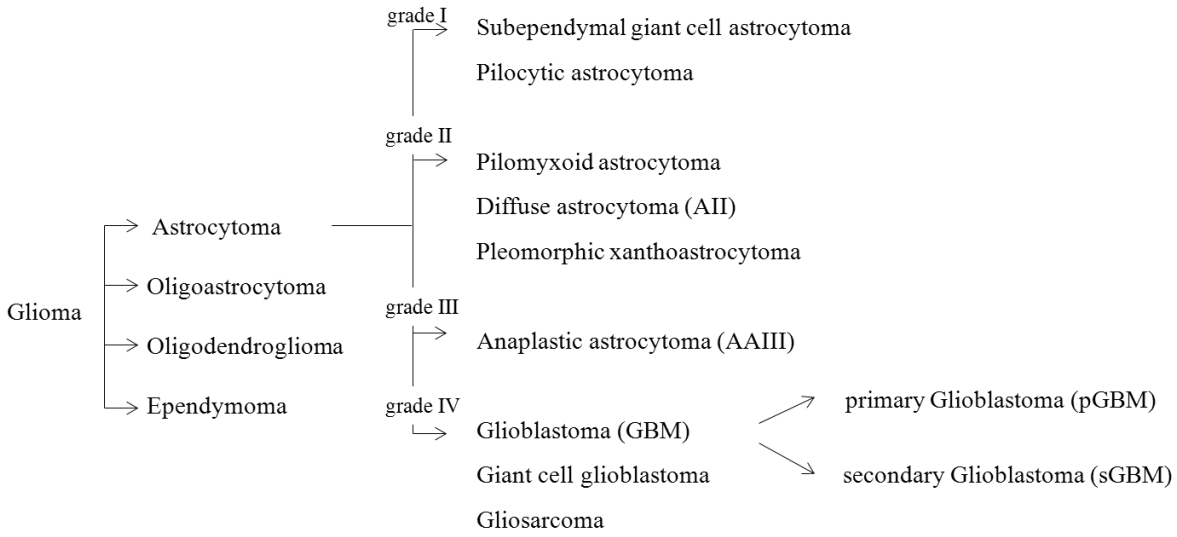

Figure 1.1.2-1. Simplified classification of gliomas based on WHO Classification of Tumors of The Central Nervous System (Louis et al., 2007). Classification is based on findings of histopathological features of cancer cells, including nuclear atypia, proliferative activity, microvascular proliferation, and necrosis. Figure adapted from the WHO Classification of Tumours of The Central Nervous System System (Louis et al., 2007).

The new WHO Classification of Tumors of The Central Nervous System (Louis et al., 2016) introduces molecular and cytogenetic information to assist glioma classification (Fig. 1.1.2-2). Detection of mutations in isocitrate dehydrogenase (IDH) (Bleeker et al., 2009; Parsons et al., 2008) is currently a prerequisite for tumors classification. The wild-type IDH1 catalyzes the oxidative decarboxylation of isocitrate to α-ketoglutarate. Whereas the mutant protein, with arginine 132 altered to histidine, converts α-ketoglutarate to R(-)-2-

hydroxyglutarate (Dang et al., 2010; Jin et al., 2011). Accumulation of 2-hydroxyglutarate, which acts as an oncometabolite, inactivates oxygenases (histone demethylases and TET 5'-methylcytosine hydroxylases) and leads to significant modifications in methylation profile, length of telomeres and gene expression (Cohen et al., 2013; Garber, 2010). Histologic assessment supported by genetic and epigenetic analysis in consequence produces more accurate and reproducible diagnostic criteria (Vigneswaran et al., 2015).

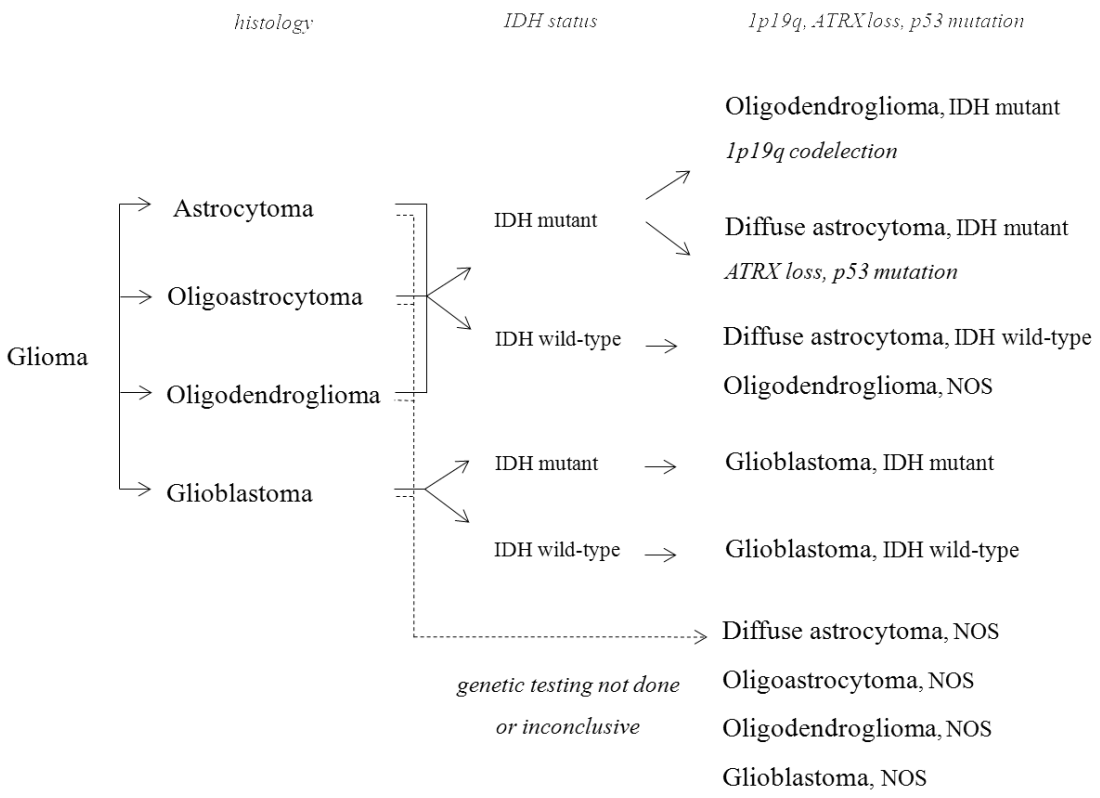

Figure 1.1.2-2. The new WHO Classification of Tumors of The Central Nervous System (2016). In contrast to the old grading, the new classification is based not only on histopathological features, but also includes IDH status and other genetic alternations. The IDH1 refers to isocitrate dehydrogenase 1, ATRX to alpha-thalassemia/mental retardation syndrome X-linked, and NOS to not otherwise specified. Figure adapted from the WHO Classification of Tumours of The Central Nervous System (Louis et al., 2016).

1.1.3 **Microenvironment of glioblastoma**

Solid tumors exist as tightly connected entities depending on their cellular environment. Individual cells may adapt to the local environment, but also change the surrounding to accommodate their own needs. For this reason, a complex communication involving interaction between tumor cells and non-malignant neighboring cells is required (Godlewski et al., 2015). GBMs are predominantly composed of cells resembling immature glia (Zong et al. 2013). The heterogeneous GBM tissue consists of tumor cells, surrounding blood vessels, immune cells, and extracellular matrix. Additionally, its structure includes stem cell-like cells and parenchymal cells. Tumor-associated non-neoplastic parenchymal cells include vascular cells, microglia, peripheral immune cells, normal astrocytes and neural precursor cells that play an essential role in cell-cell communication. The vasculature supports GBM cells with nutrients, oxygen and provides a specialized niche for stem-cell like cells. Microglia contribute to the tumor mass and support cell invasion. Normal astrocytes not only can be transformed into reactive cells under the pressure of the environment, but also can secrete a number of factors that alter tumor biology (Fig. 1.1.3-1). Altogether, cytokines, growth factors, and chemokines released in extracellular vesicles (EV) may support tumor initiation, angiogenesis, proliferation, and invasion (Pollard et al., 2004; D'Asti et al., 2016), thus providing an additional level of complexity and network communication (Godlewski et al., 2014).

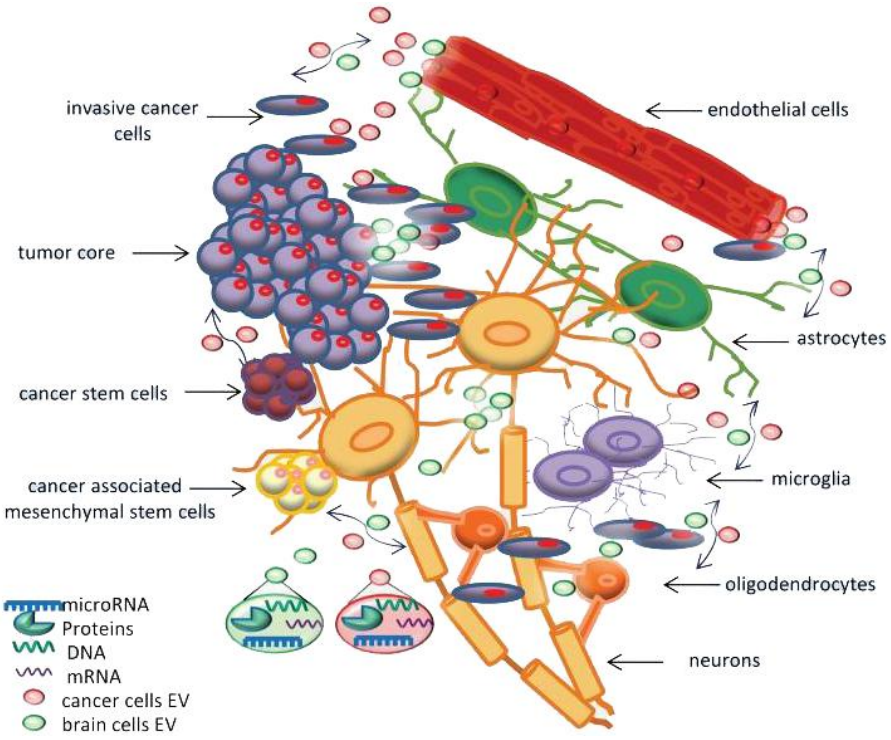

Figure 1.1.3-1. The microenvironment of glioblastoma. Tumor surrounding is composed of specialized cell types, which may support tumor growth or invasion. Different cell types from the tumor microenvironment communicate both locally and at distant ranges via the release and uptake of EVs. Such communication can contribute to tumor progression by transferring bioactive molecules. Figure from Godlewski et al., 2014.

1.1.4 **Implications for diagnosis and therapy**

Gliomas characterized by an astrocytic phenotype have a poorer prognosis than oligodendroglias of a corresponding grade (Ohgaki et al., 2004). Genetic alterations associated with good predictions, such as loss of heterozygosity of 1p19q (Barbashina et al., 2005), IDH1 mutation (Yan et al., 2009) and glioma-CpG island methylator phenotype (G-CIMP) (Noushmehr et al., 2010) are also more common in oligodendrogliomas and sGBMs (Zong et al., 2012). Among gliomas, the most common and lethal CNS tumors are GBMs. Despite surgical resection and aggressive treatment the prognosis for GBM patients is typically very poor. In the United States, the GBM incidence rate is 3.19/100000 people (Thakkar et al., 2014). The mean survival for GBM patient under currently available treatment is approximately 14.6 months from the time of diagnosis. The therapy commonly

includes surgical resection, radiotherapy and adjuvant temozolomide application (Stupp et al., 2005).

The failure of conventional approaches in curing GBM indicates the need for novel therapies, which target the cells of origin (Zong et al., 2012) or residual tumor cells (Wilson et al., 2014). Until now, molecule-targeted therapies, including inhibition of growth factor, and intracellular signaling pathways provided very limited or no therapeutic benefit. Similarly, immunotherapy or gene therapy, including cytotoxic gene therapies, or oncolytic viral vectors demonstrated minimal efficacy (Wilson et al., 2014). To understand the complex biology of GBMs, a variety of therapeutic approaches were undertaken but despite promising results in the preclinical phase, the therapies had limited or no effects in clinical trials (Wilson et al., 2014). Therefore, treatment of GBMs remains highly challenging.

1.2 Translational control by CPEBs

1.2.1 Principles of translation

Translation of mRNAs is tightly regulated in three major phases: initiation, elongation and termination (D'Ambrogio et al., 2013; Groppo and Richter, 2009). Regulation of translation efficiency is predominantly controlled at the initiation phase and involves eukaryotic translation initiation factors (eIFs) and other auxiliary proteins interacting with eIFs and with mRNAs. Initiation factors assemble on the 7-methyl-guanosine (m7GpppG) cap structure at the 5′end of RNAs (Sonenberg and Hinnebusch, 2009) and form the eIF4F complex. The complex is assembled with eIF4E, a cap binding factor, eIF4G, a scaffold protein interacting with eIF4E, eIF4A, an RNA helicase, and eIF3, a factor binding eIF4G. The integrated activity of eIFs recruits the 40S ribosomal subunit on the 5'end of the mRNA and allows formation of the pre-initiation complex (Dever, 2002).

Upon overexpression, one of the initiation factors, eIF4E elicits the preferential translation of mRNAs with long-structured 5'untranslated regions (UTRs) (D'Ambrogio et al., 2013) that usually encode growth factors and proto-oncogenes, like c-myc or cyclin D1 (Sonenberg, 1993). Knowing that eIF4E initiates the translation of proto-oncogenes

(Sonenberg, 1993), its excess is strongly correlated with cancer etiology (Lazaris-Karatzas et al., 1992; Ruggero et al., 2004). Proto-oncogenic activity of eIF4E is controlled by eIF4E-binding proteins (4EBPs). The 4EBPs impair association of the 40S subunit to the cap structure of mRNAs (Teleman et al., 2005) and counteract recruitment of eIF4G (Darnell and Richter, 2012). 4EBPs mimic eIF4G, bind the eIF4E, and as a result interrupt the eIF4E-eIF4G interaction, which downregulates the translation of many mRNAs (Richter and Sonenberg, 2005). Therefore, the key components of the translational machinery involved in the initiation step may either promote or suppress cancer formation. Translational control is additionally regulated by auxiliary mRNA-binding proteins. One of such group of factors is the family of CPEBs (D'Ambrogio et al., 2013).

1.2.2 **CPEBs**

Cytoplasmic polyadenylation element binding proteins (CPEBs) are translational factors that associate with consensus sequences present in 3'UTRs of mRNAs and regulate their translation (Darnell and Richter, 2012; Richter, 2007). The family of CPEBs in vertebrates comprises four genes. Each member of the family consists of an N-terminal regulatory domain and a C-terminal RNA binding domain (Fig. 1.2.2-1) (Kaczmarczyk et al., 2016; Theis et al., 2003). Although all CPEBs have two RNA recognition motifs (RRM), and two zinc fingers (ZnF), vertebrate CPEB 2–4 are more closely related to each other, forming a subfamily (Huang et al., 2006; Mendez and Richter, 2001), whilst CPEB1, the founding member of the family, is evolutionarily most distinct. CPEBs were first discovered in *Xenopus laevis* oocytes, where they control meiosis (Hake and Richter, 1994; Stebbins-Boaz et al., 1996). CPEB 2-4 display ~98% sequence similarity in RRMs and phosphorylation sites (Theis et al., 2003). In addition, these proteins possess common splicing patterns (Wang and Cooper, 2010), similar miRNA regulatory motifs (Morgan et al., 2010) and overlapping mRNA targets, between themselves and CPEB1 (Fernández-Miranda and Méndez, 2012; Igea and Méndez, 2010; Novoa et al., 2010; Theis et al., 2003; Turimella et al., 2015).

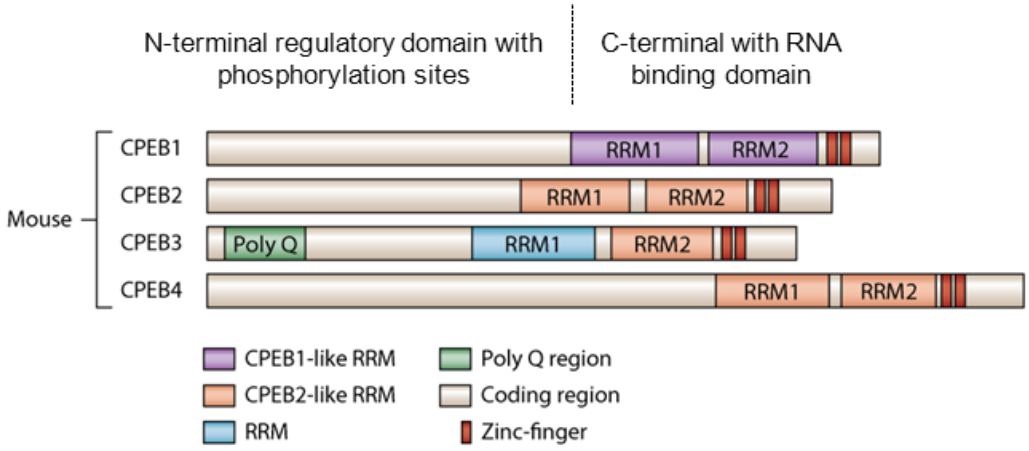

Figure 1.2.2-1. Structural relationships between CPEBs. CPEBs consist of an N-terminal regulatory domain and a C-terminal RNA binding domain containing two conserved RNA recognition motifs, two zinc-fingers, and poly Q regions corresponding to polyglutamine stretches. CPEBs with identically marked RRMs indicate strong similarity. Figure adapted from Ivshina et al., 2014.

1.2.3 Regulation of polyadenylation-induced translation

Cytoplasmic polyadenylation begins in the nucleus, where CPEB binds into uracil-rich (UUUUUAU, or similar) cytoplasmic polyadenylation elements (CPE) present in the 3'UTR of pre-mRNAs. Like most of the nuclear pre-mRNAs, the CPEB bound mRNAs have ~100 nucleotides long poly(A) tails (Lin et al., 2010). The cleavage and polyadenylation specificity factor (CPSF) associates with the AAUAAA sequence of mRNA and together with CPEB and Maskin shuttle to the cytoplasm (Lin et al., 2012). Following export, CPEBs recruit a number of molecules including symplekin, a scaffold protein, Gld2, a germline development 2 non-canonical poly(A) polymerase and PARN, a poly(A) ribonuclease to form the ribonucleoprotein (RNP) complex (Fig. 1.2.3-1) (Darnell and Richter, 2012; Kim and Richter, 2006).

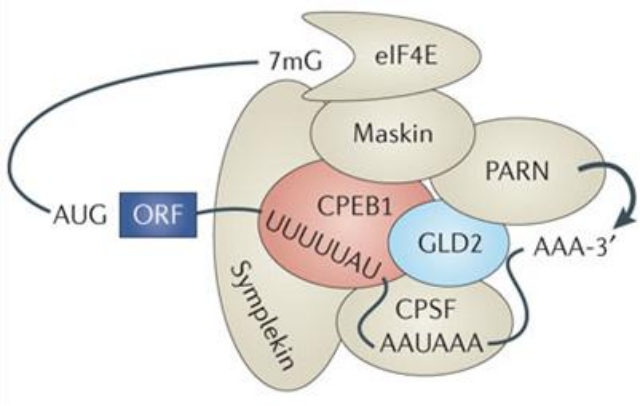

Figure 1.2.3-1. Polyadenylation-induced translation regulated by CPEB1. Cytoplasmic polyadenylation begins in the nucleus, where CPEB1 binds to the CPE elements present in 3'UTR of pre-mRNA. CPSF associates with the AAUAAA nuclear pre-mRNA cleavage and polyadenylation site. CPEB1 recruits RNP complex molecules, including symplekin, Gld2 polymerase, PARN ribonuclease and Maskin containing 4EBP activity. PARN activity shortens the long poly(A) tails added to the mRNA in the nucleus. Whereas Maskin binds eIF4E at the eIF4G binding site and thus inhibits translation initiation. Figure from D'Ambrogio et al., 2013.

Both of the RNP complex enzymes, PARN deadenylase and Gld2 polymerase are catalytically active. When the robust PARN activity exceed the activity of Gld2 polymerase, it shortens the poly(A) tails on CPE-containing RNAs to 20-40 nucleotides, thereby locks mRNAs in a dormant state (Kim and Richter, 2006). Hormonal stimulation leads to Aurora kinase A activation and phosphorylation of CPEB1 on serine 174 (Mendez et al., 2000a; Sarkissian et al., 2004). These modifications result in expulsion of PARN deadenylase from the RNP complex (Kim and Richter, 2006). As a consequence, Gld2 catalyzes polyadenylation and poly(A)-binding protein (PABP) associates with the newly elongated poly(A) tail (Barnard et al., 2004; Kim and Richter, 2006, 2007). The length of the poly(A) tail is correlated with the ribosome density and association of PABPs. Changes in the RNP complex potentiate the assembly of the initiation complex at the 5'end of the mRNA at the expense of the Maskin-eIF4E interaction (Fig. 1.2.3-2) (Cao and Richter, 2002; Kim and Richter, 2007). Phosphorylation of Maskin allows for its dissociation from eIF4E and beginning or resuming translation (Cao et al., 2006). Cytoplasmic polyadenylation takes place in sequential waves and is synchronized with the partial

destruction of CPEB, the number and location of CPEs within a 3'UTR, and the presence of other RNA binding proteins (Ivshina et al., 2014).

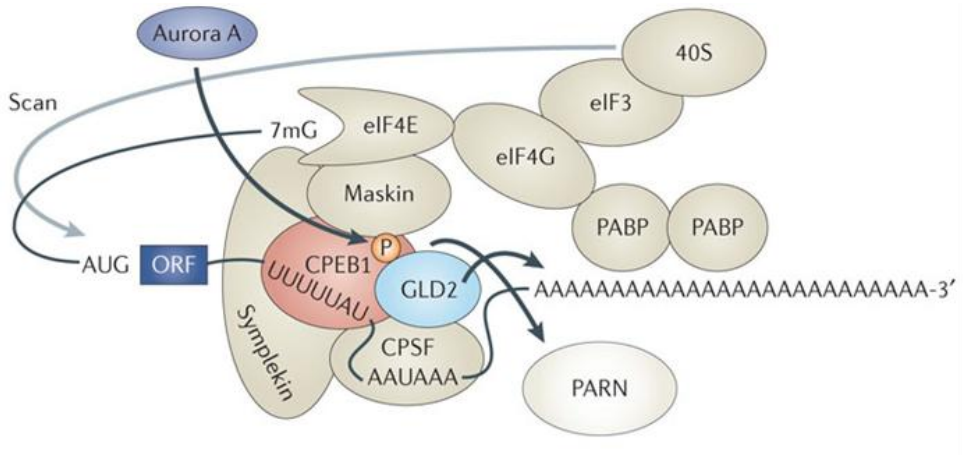

Figure 1.2.3-2. Polyadenylation-induced translation regulated by CPEB1. The RNP complex remains dormant until cell stimulation. Stimulation activates Aurora kinase A, which further phosphorylates CPEB1. PARN is removed from the complex and that allows Gld2-mediated polyadenylation. PABP and eIF4G attach to the newly elongated poly(A) tail. eIF4G replaces Maskin from eIF4E and, through the eIF3 complex, shifts the 40S ribosomal subunit to the 5' end of the mRNA. Figure from D'Ambrogio et al., 2013

1.3 Role of CPEBs in germline and somatic cells

1.3.1 CPEBs in cell cycle progression

In vertebrates, meiotic cell divisions occur in the absence of transcription, but depend on translational control of mRNAs. Many of these mRNAs may undergo regulation by CPEBs (Novoa et al., 2010). In *Xenopus* oocytes, CPEBs mediate both, meiotic progression and mitotic divisions. For instance, entry into the M phase is guided by CPEB1 phosphorylation by Aurora kinase A, while switch from M to S phase is regulated by CPEB1 dephosphorylation catalyzed by protein phosphatase 2A (Cao et al., 2006; Groisman et al., 2002). As oocyte maturation is similar to the somatic cell cycle (Liu and Maller, 2005; Peng and Maller, 2010) apart from meiosis, CPEBs were detected in mitosis of mammalian cells (Giangarrà et al., 2015; Groisman et al., 2002; Novoa et al., 2010). Based on this

finding, cytoplasmic regulation of the poly(A) tails length is not only needed to compensate for the lack of transcription in cell divisions but is a general mechanism of controlling cell cycle progression (Novoa et al., 2010). In addition to CPEB1, CPEB2 and CPEB4 were recently found to be necessary in the phase-specific polyadenylation and translational activation in the mitotic cell cycle. Accordingly, CPEB1 is essential for entrance into prophase, CPEB2 for metaphase and CPEB4 for cytokinesis (Giangarrà et al., 2015).

1.3.2 **CPEBs in metabolism and senescence**

In contrast to normal cells that generate energy required for cellular processes by mitochondrial oxidative phosphorylation, cancer cells rely on anaerobic glycolysis (Vander Heiden et al., 2009). Human primary fibroblasts with reduced CPEB1 expression demonstrated lower mitochondria number, which resulted in decreased respiration rates. Interestingly, ATP content remained unchanged. To maintain constant ATP level, cells increased glycolysis while reducing oxygen consumption. This process, known as the Warburg effect, is characteristic for transformed cancer cells (Burns and Richter, 2008). Metabolic balance between mitochondrial respiration and glycolysis is mediated by mRNAs containing CPEs, such as *p53* and *c-myc* (Burns and Richter, 2008; Groisman et al., 2006). Therefore, knockout of CPEB1 in mouse embryonic fibroblasts (MEF) results in reduced polyadenylation and translation of p53 mRNA that subsequently renders cells immortal and escaped senescence (Groisman et al., 2006; Ivshina et al., 2014).

During increased oxidative stress CPEB1 and CPEB2 bind to the hypoxia-inducible factor-1α (HIF-1α) mRNA and regulate its expression (Hägele et al., 2009). HIF-1α regulates homeostatic responses to oxidative stresses, by stimulating transcription of genes involved in angiogenesis, metabolism and cell survival. At normal oxygen concentration, HIF-1α is continuously synthesized at a reduced level and undergoes proteasome-mediated degradation. This type of protein synthesis confirms that HIF-1α mRNA remains ribosome-associated, thereby promoting quick responses to stress. Under hypoxia or increased oxidative stress, the level of HIF-1α is immediately increased (Chen and Huang, 2012;

Chen et al., 2015). Thus, by regulating HIF-1α (Chen et al., 2015) or p53 (Burns and Richter, 2008) CPEBs mediate important alterations in cellular metabolism.

1.3.3 **CPEBs in cancer**

CPEBs mediate control of cellular senescence, proliferation, and migration (Fernández-Miranda and Méndez, 2012; Jones et al., 2008), thus alterations in their expression are crucial for malignant transformation. Recently published meta-analysis shows the extensive correlation between the level of CPEB mRNA expression and human cancers (Fig. 1.3.3-1) (D'Ambrogio et al., 2013). CPEB expression is downregulated in many tumors, affecting the reproductive and digestive system, head and brain, including gliomas. Transcript expression level of CPEB1, CPEB2 and CPEB3 appears to be reduced in gliomas and only CPEB4 expression is upregulated in oligo-lineage tumors (D'Ambrogio et al., 2013).

Downregulation of CPEB1 was observed in several types of human tumors, including ovarian and gastric, as well as in breast-, myeloma- and colorectal cancer-derived cell lines (Caldeira et al., 2012; Hansen et al., 2009; Heller et al., 2008), where it was associated with the capacity of malignant cells to promote invasion and angiogenesis (Caldeira et al., 2012). Moreover, by mediating apical localization and translation of zona occludens-1 (ZO-1) mRNA, CPEB1 participates in maintaining the polarity of mammary epithelial cells. In the absence of CPEB1, a randomly distributed ZO-1 mRNA cause the loss of cell polarity (Nagaoka et al., 2012) that further leads to an epithelial-to-mesenchymal transition (EMT) (Nagaoka et al., 2016). This often results in cell dedifferentiation and metastasis (Tam and Weinberg, 2013). Therefore, deprivation of CPEB1 in mammary epithelial cells changes the gene expression profile and increases its metastatic potential (Nagaoka et al., 2016).

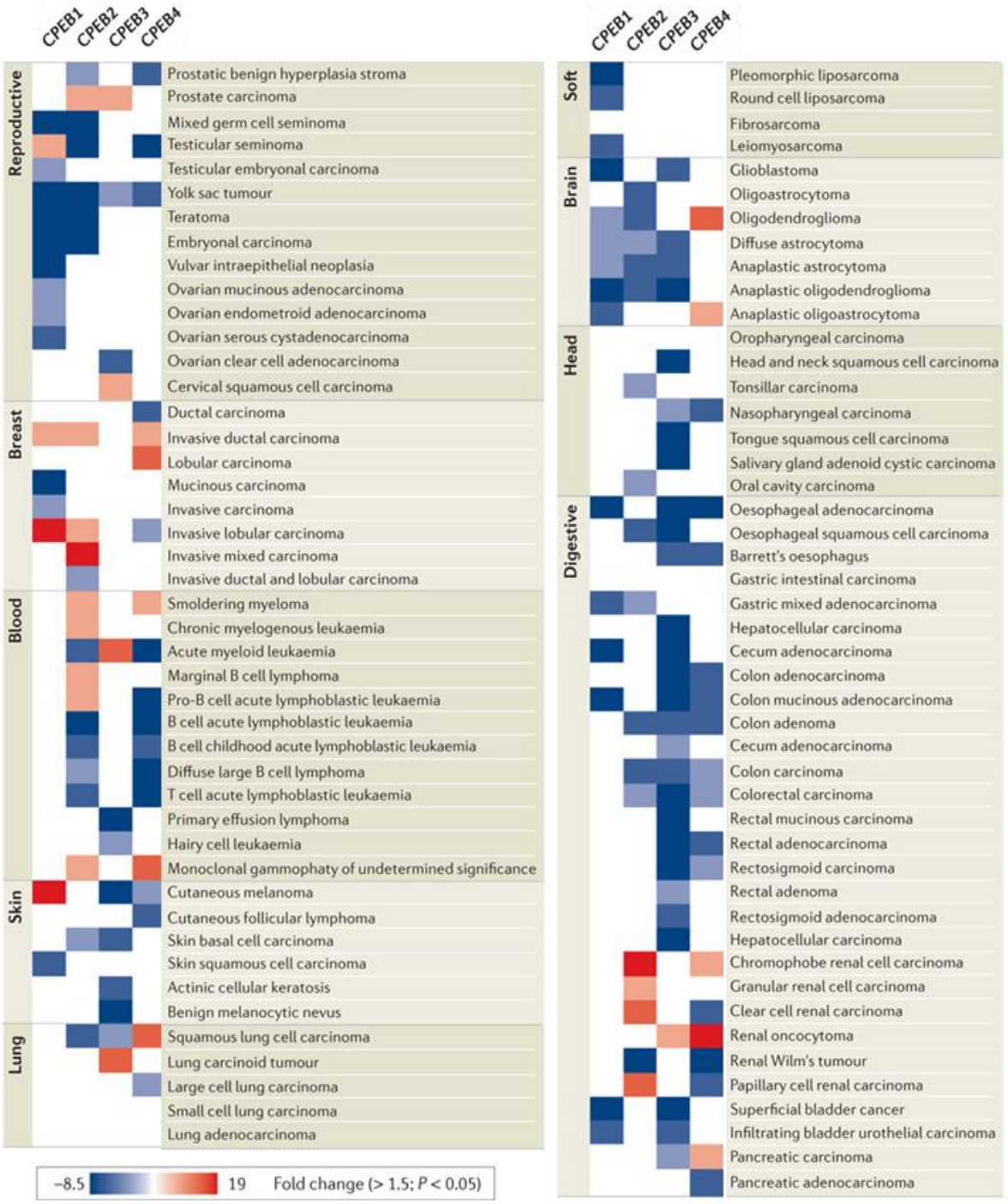

Figure 1.3.2-1. CPEB expression in cancers. Blue color indicates downregulation, while red color indicates upregulation of CPEB mRNA levels in cancer after comparison with reference samples. Figure adapted from the D'Ambrogio et al., 2013.

Thus far, CPEB2 was found to be involved in the progression of breast cancer. One study showed that CPEB2 downregulates *TWIST1*, a transcription factor that supports epithelial to mesenchymal transition, during oncogenesis but not in metastatic cells (Nairismägi et al., 2012). Moreover, CPEB2 regulates metastatic potential of human triple negative breast cancer (TNBC) cells (Johnson et al., 2015). The high metastatic potential of TNBC cells is especially correlated with increase in expression of CPEB2 isoform lacking the B-region. Downregulation of the CPEB2b induces cell death, whereas overexpression of the CPEB2b increases metastatic potential of TNBC cells (Johnson et al., 2015).

Cancer etiology is also mediated by CPEB4. Its expression is increased in GBMs and pancreatic ductal carcinomas (PDA). PDA tumors have particularly elevated translation of tissue plasminogen activator (tPA) mRNA that is regulated by CPEB4. tPA is absent in normal pancreas but overexpressed in most of PDA, where it supports tumor vascularization and cells proliferation, migration, and invasion. The expression of CPEB4 is absent in normal astrocytes, but abundant in high-grade gliomas. CPEB4 mediates tumor growth and vascularization in GBMs. Downregulation of CPEB4 levels results in reduction of tumor size, cellular proliferation and microvessel density (Ortiz-Zapater et al., 2011; Fernández-Mirandaa and Méndez, 2012). Other mRNAs linked to tumorigenesis regulated by CPEB4 include Smad3, B-cell lymphoma 2 (Bcl-2), and matrix metallopeptidase 7 (MMP7) (Ortiz-Zapater et al., 2011). Therefore CPEB4 seems to have a significant role in the development of tumors, and might be the element of a more general mechanism of carcinogenesis.

In summary, all CPEBs are involved in growth of cancer, but it is noteworthy that CPEB3 is not well investigated, yet. Furthermore, although CPEB isoform are structural very similar, they are functionally different (Ivshina et al., 2014).

1.3.4 **CPEBs in the nervous system**

Long-term memory formation takes place in the hippocampus and requires new protein synthesis to modulate synaptic plasticity (Kang and Schuman, 1996). Synaptic plasticity is the ability of synapses to undergo morphological and biochemical changes in response to stimulation (Kandel, 2001; Mayford et al., 2012; Richter and Klann, 2009; Sutton and Schuman, 2006). Then the newly synthesized proteins either constitute the synaptic tags or influence synaptic activity (Ivshina et al., 2014).

At the postsynaptic sites of hippocampal neurons reside mRNA molecules. Their translation might be initially repressed by CPEB binding, and activated in response to synaptic stimulation (Huang et al., 2002; Richter, 2001; Udagawa et al., 2012; Wu et al., 1998). CPEB1, Gld2, and Neuroguidin comprise a complex that regulates mRNA translation at synapses and, thereby, synaptic efficacy. Several important mRNAs undergo activity-dependent polyadenylation, including calcium-calmodulin protein kinase II (CaMKII), tissue plasminogen activator (tPA) or GluN2A (N-methyl-D-aspartate (NMDA) receptor subunit) that is crucial for synaptic plasticity (Du and Richter, 2005; Shin et al., 2005; Wu et al., 1998).

CPEB1 represses translation until glutamatergic activation initiates its phosphorylation by either Aurora kinase A (Huang et al., 2002; Mendez et al., 2000a) or CaMKII (Fig. 1.3.4-1) (Atkins et al., 2004, 2005). Upon stimulation, CPEB1 induces long-term potentiation, GluN2A mRNA translation (Udagawa et al., 2012) and the latter is inserted into the synaptic membrane as an NMDA receptor subunit (Swanger et al., 2013). The CPEB1 protein is responsible for dendritic transport of mRNAs. Therefore, CPEB1 associates with the motor proteins, kinesin and dynein and transport curtail mRNAs as CaMKII in into dendrites (Huang et al., 2003; Ivshina et al., 2014). The contribution of CPEB1 to local protein translation is confirmed by its localization in dendrites (Wu et al., 1998) and enrichment of phospho-CPEB1 in a fraction of postsynaptic density of neurons (Atkins et al., 2004, 2005; Darnell and Richter, 2012).

Knockout (KO) of CPEB1 activity in mouse models leads to defects in synaptic plasticity, learning, and memory (Alarcon et al., 2004; Berger-Sweeney et al., 2006; Darnell and

Richter, 2012). However, KO of another CPEB, CPEB3 results in enhancement of hippocampus-dependent learning. This process is possibly induced by expression of plasticity-regulating molecules, including PSD-95 and the NMDA receptor subunit GluA1, previously shown to be regulated by CPEB3 (Huang et al., 2006). KO of CPEB4 has no effect on hippocampal plasticity or on learning and memory (Ivshina et al., 2014; Tsai et al., 2013).

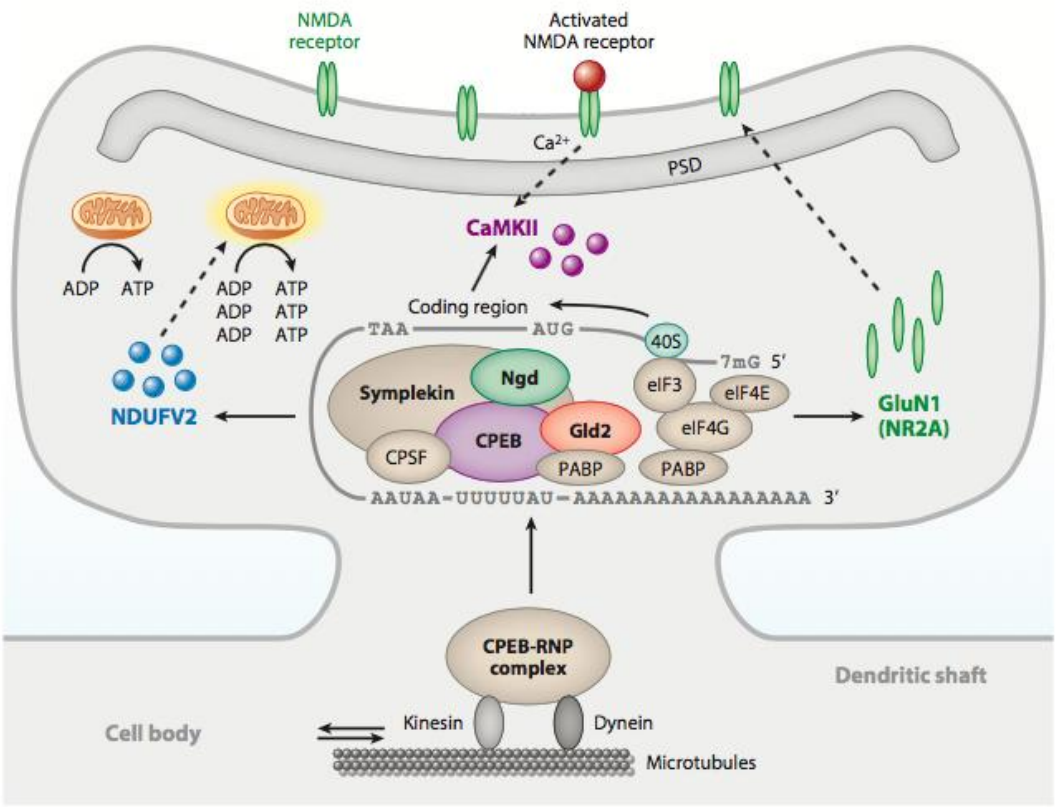

Figure 1.3.4-1. Impact of CPEB1 in neurons. The RNP complex containing CPEB1 is transported in dendrites along microtubules by the motor proteins - kinesin and dynein. Synapse stimulation and cytoplasmic polyadenylation initiate GluN2A, CaMKII and NDUFV2 activation. GluN2A encodes an NMDA receptor subunit, CaMKII, is associated with the postsynaptic density and has kinase activity while NDUFV2 is a part of mitochondrial electron transport chain that supplies ATP. Figure from Ivshina et al., 2014.

1.4 Alterations regulating expression and activity of CPEBs

1.4.1 DNA methylation

Heritable alterations in gene function that occur without modification in the DNA sequence are called epigenetic changes. To the major epigenetic mechanisms belong: DNA methylation, histone modifications, and RNA-mediated gene silencing (Sharma et al., 2010). Methylation is the most common covalent modification of DNA in eukaryotes that plays an important role in biological processes, including genomic imprinting (Wilkins, 2005), aging (Jung and Pfeifer, 2015) and cancerogenesis (Chen et al., 2014). DNA methylation occurs at cytosine residues, in the cytosine-phosphate-guanine (CpG) dinucleotides (Fig.1.4.1-1) (Weber et al., 2007). CpG dinucleotides are concentrated in the genome in the CpG-rich DNA fragments called CpG islands, which are clustered around gene regulatory regions (Weber et al., 2007; Yamada et al., 2004).

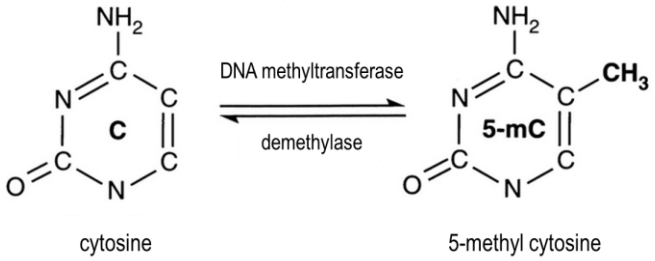

Figure 1.4.1-1. Cytosine methylation pathway. Methylation of DNA occurs at cytosine residues, in CpG dinucleotides. Upon a reaction catalyzed by the DNA methyltransferases, cytosine is converted to 5-methyl cytosine. As a result the methyl group donor, S-adenosylmethionine, is transformed into S-adenosylhomocytosine.

Methylation is catalyzed by DNA methyltransferases (DNMT), including DNMT1, DNMT3A and DNMT3B. DNMT1 is required to maintain the methylation status, while DNMT3A and DNMT3B are needed for *de novo* DNA methylation during the embryo formation process (Bernstein et al., 2007; Chen et al., 2014). Generally, methylation takes place during DNA replication. Following replication, DNMT1 (Goll and Bestor, 2005) complements the missing methylation on the newly synthesized strand. It allows

maintenance of DNA methylation patterns through many rounds of cell division (Zilberman and Henikoff, 2007). Methylation does not alter nucleotide sequences and does not affect the specificity of DNA base pairing (Chen et al., 2014).

In normal cells, regions of the gene promoter containing CpG islands are commonly not methylated, while coding regions are often methylated. This is to sustain the transcriptionally active euchromatin structure (Fig. 1.4.1-2). A reverse methylation pattern is observed in cancer. Cancerous cells undergo alterations in promoter methylation that result in abnormal gene expression and a malignant phenotype. Genomic hypomethylation of proto-oncogenes usually results in genome instability and their enhanced expression (Ehrlich, 2002). In contrast, local promoter hypermethylation results in functional silencing of tumor-associated genes. Enhanced methylation at the promoter region results in their inactivation by change in the open euchromatin conformation to a compact heterochromatin structure (Fig. 1.4.1-2) (Chen et al., 2014). Therefore, DNA hypermethylation suppresses the activity of genes transcription though blocking the binding of a transcription factor (Herman and Baylin, 2003; Watt and Molloy, 1988), or by recruiting methylation binding proteins that support inhibition of gene expression (Nan et al., 1998).

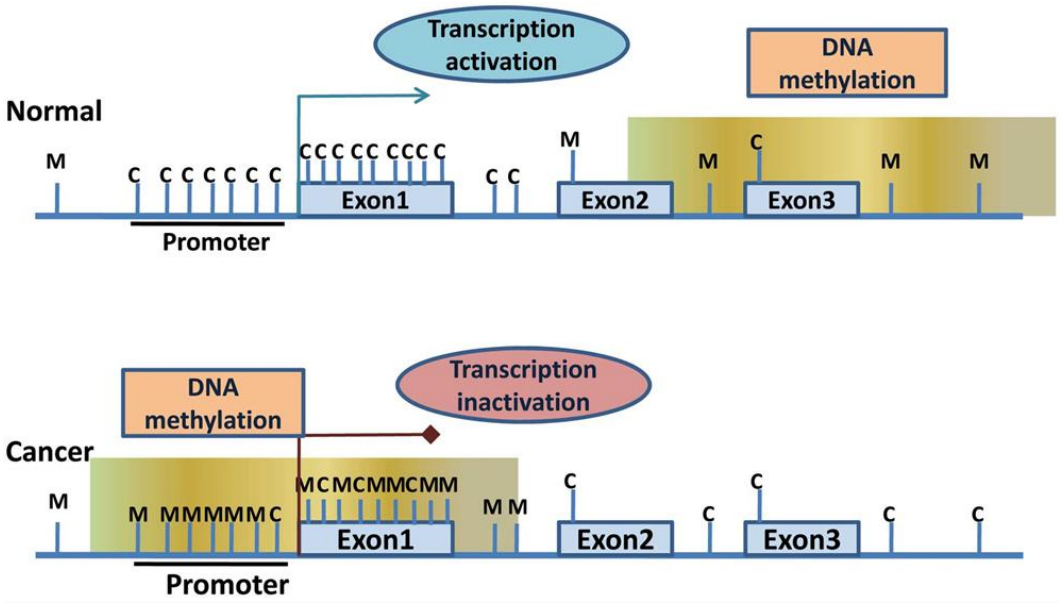

Figure 1.4.1-2. DNA methylation in normal and cancer cells. In normal cells, regions of the gene promoters containing CpG islands are commonly not methylated. This is to sustain the transcriptionally active euchromatin structure. Cancer development drives hypermethylation of many genes. Increased methylation at the promoters regions containing CpG islands results in their inactivation. Through changing of the open euchromatin conformation to a compact heterochromatin structure expression of these genes is silenced. On the illustration above, cytosine residues are marked with C, while 5-methyl cytosine residues are marked with M. Figure from Chen et al., 2014.

1.4.2 **Alternative splicing**

The process of removing introns and joining exons in pre-mRNA complexes is known as splicing. RNA splicing is controlled by splice sites, the specific sequences present at the intron-exon borders, and carried out by spliceosomes, the complexes that assemble around splice sites at introns and catalysis the splicing reaction (Wessagowit et al., 2005). Depending on the similarity to the canonical splicing consensus sequences, splice sites are considered to be strong or weak (Kornblihtt et al., 2013). The strong splice sites allow identification of consensus sequences that leads to the constitutive splicing, while the weak splice sites are suboptimal for consensus sequences and their use depends on the cellular context (Wessagowit et al., 2005). The proximity of competing weak and strong sites along the pre-mRNA allows the synthesis of numerous gene transcripts with different properties (Kornblihtt et al., 2013). Therefore, alternative splicing of pre-mRNA molecules forms an additional level of regulation that occurs between transcription and translation (Berget et al., 1977; Chow et al., 1977). This process tightly controls expression of multiple mRNA variants from a single gene and determines signal transduction and chromatin modification (Kornblihtt et al., 2013). However, in the cell itself this is not clearly separated because splicing and alternative splicing are combined with transcription, thus factors that regulate transcription also affect alternative splicing (Kornblihtt et al., 2013).

All four *CPEB* genes are subject to alternative splicing (Theis et al., 2003; Turimella et al., 2015; Wang and Cooper, 2009, 2010), however the biological importance of this phenomenon is not fully known. Alternative splicing leads to differences in the protein sequence, affecting further their function and altering where, and how CPEBs bind with their target mRNAs (Wang and Cooper, 2010). Alternative splicing of CPEBs is

particularly relevant in the context of cytoplasmic polyadenylation. This is because the alternatively spliced regions contain regulatory phosphorylation sites (Kaczmarczyk et al., 2016; Skubal et al., 2016; Theis et al., 2003; Turimella et al., 2015).

Regions of high similarity between CPEB 2-4 are found in the 8-aa B-region. Less similarity is observed in the 17-30-aa C-region. The hexamer and octamer sequences present in the RRMs, as well as the linkers between RRMs are similar, thus it is possible that CPEB 2-4 share the same regulatory mechanisms and target similar populations of RNAs (Fig. 1.4.2-1). Compared to CPEB 2-4, CPEB1 demonstrates significant differences within the described domains. This implies that CPEB1 may not only be involved in different mechanisms for RNA interaction, but also recognizes different targets (Wang and Cooper, 2010). CPEB1 harbors a site for alternative splicing in the RRM. For CPEB1, the full-length isoform (Gebauer and Richter, 1996) and the isoform with 5-aa deletion in RRM1 (Δ5) (Wilczynska et al., 2005) have been described. The N-terminal regulatory domain of CPEB 2-4 harbor regions of alternative splicing and give rise to multiple splice isoforms. Alternative splicing of CPEB 2-4 results in either inclusion or removal of the C- and B-region and gives rise to four splice variants including a (full length), b (lacking the B-region), c (lacking the C-region), and d (lacking both regions) (Theis et al., 2003; Wang and Cooper, 2010). Recent studies report that CPEB2 contains and additional 3-aa long region that undergoes alternative splicing, however its function is unknown (Turimella et al., 2015).

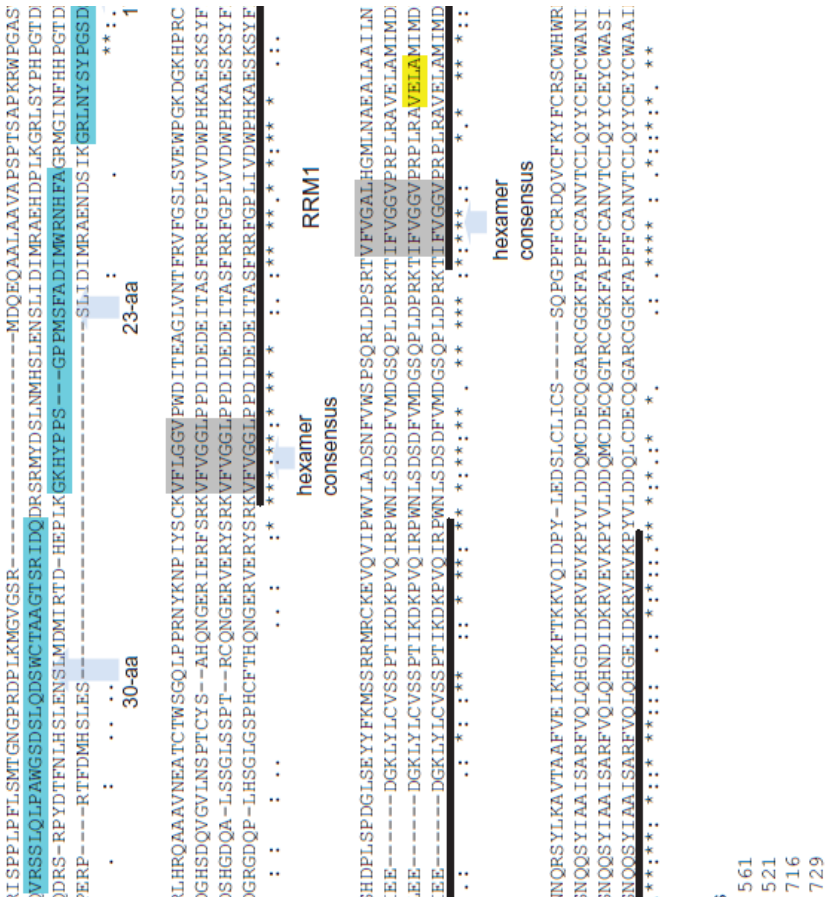

Figure 1.4.2-1. Comparison of mouse CPEB 1-4 containing regions undergoing alternative splicing. The alternatively spliced 17-30-aa long regions are marked in blue, 8-aa in red, 9-aa in orange. The underlined sequences refer to RRMs. The RRMs regions labeled in grey are consensus hexamer and octamer sequences. Asterisks mark perfect matches, colons indicate substitutions with similar amino acids, and gaps represent substitutions with distinct amino acids. Figure from Wang and Cooper, 2010.

1.4.3 **Phosphorylation**

Phosphorylation has been previously shown to regulate the activity of CPEBs (Theis et al., 2003). In *Xenopus* oocytes, CPEBs undergo phosphorylation by Aurora kinase A on serine 174, which subsequently triggers cytoplasmic polyadenylation and translation (Kim and Richter, 2006; Mendez et al., 2000b). In mouse brain, upon NMDA receptor activation, CPEB1 is phosphorylated and activated by Aurora A or CaMKII kinase (Tay and Richter, 2001; Tay et al., 2003; Hodgmanet al., 2001; Kaczmarczyk et al, 2016). The structural and functional differences that influence CPEB phosphorylation are generated during alternative splicing (Wang and Cooper, 2010). The splice variants of CPEB 2-4 differ

between each other by the presence or absence of B- and C-regions (Fig. 1.4.3-1). Especially important is the B-region located upstream of the two serine residues, that harbors the kinase recognition sites for cyclic AMP-dependent protein kinase A (PKA), protein kinase B (PI3K/Akt), ribosomal S6 kinase (RPS6K) and CaMKII (Kaczmarczyk et al., 2016; Theis et al., 2003; Wang and Cooper, 2010).

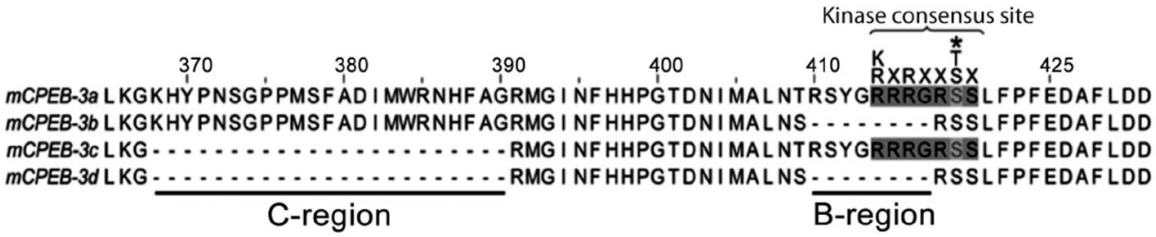

Figure 1.4.3-1. Comparison of CPEB3 isoforms in mouse brain. The CPEB3 isoform differs by the presence or absence of the alternatively spliced B- and C-regions. Splicing results in expression of four isoforms, including CPEB3a (containing both regions), CPEB3b (lacking the B-region), CPEB3c (lacking the C-region), and CPEB3d (lacking both regions). Phosphorylated residues S419 and S420 are marked by an asterisk, the consensus phosphorylation sites for PKA and CaMKII kinase are labeled above the alignment. Figure from Kaczmarczyk et al., 2016.

2 AIM OF THE STUDY

The present study aimed at elucidating principles of translational regulation by CPEBs and their function in the healthy brain and in tumor tissue. Three main aspects were investigated in detail.

Expression of CPEBs in the context of human glioma pathogenesis recently became an object of intensive investigation, and first reports already pre-described CPEB expression patterns (Galardi et al., 2016; Hu et al., 2015). However, the question how CPEB expression is regulated in gliomas remains largely unanswered. Therefore, the first part of the present work aimed at determining CPEB expression patterns in high- and low-grade human gliomas and assessing a potential contribution of CPEBs to the survival of glioma patients. Selected mechanisms involved in the regulation of CPEBs, such as methylation, alternative splicing and phosphorylation were subjected to further analysis. DNA methylation was considered due to its role in transcriptional silencing of tumor suppressor genes (Baylin, 2005), while analysis of phosphorylation and alternative splicing were relevant in the context of cytoplasmic polyadenylation (Kaczmarczyk et al., 2016).

Although altered expression of CPEBs in gliomas unequivocally indicates the importance of translational regulation in the brain tumors, the exact impact of CPEB dysregulation on GBM cells is unclear. Therefore the second part of the present study aimed at investigating the relationship between CPEB activity, growth properties and cancer-relevant parameters in a simplified cell culture model. The answer to the question whether overexpression of CPEB1 and CPEB2 in cultured GBM cells is associated with the change of cancer-related signaling pathways may help identifying new putative CPEB targets. Likewise, inquiring the effect of potential CPEB1 and CPEB2 overexpression on migration, apoptosis and proliferation may provide important information about the characteristics of altered CPEB expression in GMB cells.

All members of CPEB family are expressed in the mouse hippocampus, a region crucial for memory formation (Theis et al., 2003). In this context, CPEB1 was implicated in regulation of the local protein synthesis (Theis et al., 2003; Udagawa et al., 2012). However, beyond a general description, not much is known about the function of other family members. The main objective of the final part of the study was to determine the CPEB2 expression profile in mouse brain. Additionally, the study intended to validate whether CPEB2 subcellular localization resembles CPEB1 expression in primary hippocampal cultures and whether CPEB2 expression varies between different cellular populations, brain regions, and stages of development.

3 MATERIALS

3.1 Antibodies

Table 3.1-1. Primary antibodies

antigen	*host*	*type*	*concentration*	*application*	*company*	*catalogue no.*
CPEB1	Rb	P	1:100	ICC, IHC, WB	Eurogentec, Cologne	custom-made
CPEB2	Rb	P	1:250 (ICC), 1:50 (IHC, WB)	ICC, IHC, WB	Eurogentec, Cologne	custom-made
CPEB3	Rb	P	1:100	ICC, IHC, WB	Abcam, Cambridge	ab10833
CPEB4	Rb	P	1:250	ICC, IHC	Eurogentec, Cologne	custom-made
GFP	Ch	P	1:500	IHC	Abcam, Cambridge	ab13970
MAP2	Ms	M	1:100	IHC	Sigma, Saint Louis	M4403
PARP	Ms	M	1:5	FACS	BD Biosciences, San Jose	552933
PARV	Ms	M	1:250	IHC	Millipore, Temecula	MAB1572
PKA	Rb	P	1:500	IHC	Abcam, Cambridge	ab59218
pHH3	Rb	P	1:20	FACS	Cell Signaling, Danvers	9716
antigen	*host*	*type*	*concentration*	*application*	*company*	*catalogue no.*
phospho-	Rb	M	1:1000	IHC	Cell Signaling,	3361

CaMKII					Danvers	
phospho-CPEB3	Rb	P	1:50	ICC, IHC, WB	Eurogentec, Cologne	custom-made
TYH	Ms	M	1:500	IHC	Millipore, Temecula	MAB318

Ch: chicken; M: monoclonal antibody; Ms: mouse: P: polyclonal antibody; PARP: anti-cleaved poly(ADP-ribose) polymerase (Asp214); PARV: anti-parvalbumin; pHH3: phospho-histone H3 (Ser10); Rb: rabbit; TYH: anti-tyrosine hydroxylase

Table 3.1-2. Custom primary antibodies

antigen	*peptide sequence*
CPEB1	RGIHDQLPDFQDSEETVT
CPEB2	LQLPAWGSDSLQDSWC
CPEB4	KPPSPWSSYQSPSPTP
phospho-CPEB3	RRGRSSLFPFED

Table 3.1-3. Secondary antibodies

antigen	*host*	*concentration*	*application*	*company*	*catalogue no.*
Alexa 488	goat anti-mouse	1:500	ICC	Invitrogen, Rockford	A11006
Alexa 488	goat anti-rabbit	1:500	ICC	Invitrogen, Rockford	A11034

antigen	*host*	*concentration*	*application*	*company*	*catalogue no.*
Alexa 568	goat anti-mouse	1:500	ICC	Invitrogen, Rockford	A11031
Alexa 568	goat anti-rabbit	1:500	ICC	Invitrogen, Rockford	A11011

Alexa 594	goat anti-mouse	1:500	ICC	Invitrogen, Rockford	A11032
Alexa 594	goat anti-rabbit	1:500	ICC	Invitrogen, Rockford	A11037
IgG HRP	goat anti-mouse	1:10 000	WB	GE Healthcare, Amersham	31430
IgG HRP	goat anti-rabbit	1:10 000	WB	GE Healthcare, Amersham	31460

3.2 **Cell cultures**

3.2.1 **Reagents**

Dulbecco's Modified Eagle Medium with 25 mM glucose (DMEM)	Gibco, Darmstadt
Dulbecco's Phosphate Buffered Saline (DPBS)	Gibco, Darmstadt
Fetal Calf Serum heat-inactivated (FCS)	Gibco, Darmstadt
L-Glutamine	Gibco, Darmstadt
MEM Non-Essential Amino Acids (NEAA)	Gibco, Darmstadt
MEM Sodium Pyruvate	Gibco, Darmstadt
Opti-MEM (Reduced Serum Medium)	Gibco, Darmstadt
Penicillin/Streptomycin	Gibco, Darmstadt
Trypsin-EDTA 0,05%	Gibco, Darmstadt

3.2.2 **Media composition**

MEF cell culture medium:

DMEM with 25 mM glucose	500 ml
FCS (heat-inactivated)	10%
L-Glutamine	6 mM
MEM Non-Essential Amino Acids	0.1 mM

MEM Sodium Pyruvate	1 mM
Penicillin/Streptomycin	1%

Trans-MEF cell culture medium:

DMEM with 25 mM glucose	500 ml
FCS (heat-inactivated)	2%
L-Glutamine	6 mM
MEM Non-Essential Amino Acids	0.1 mM
MEM Sodium Pyruvate	1 mM
Penicillin/Streptomycin	1%

Serum-starved MEF cell culture medium:

DMEM with 25 mM glucose	500 ml
FCS (heat-inactivated)	1%
L-Glutamine	6 mM
MEM Non-Essential Amino Acids	0.1 mM
MEM Sodium Pyruvate	1 mM
Penicillin/Streptomycin	1%

Opti-MEM with 5% FBS:

Opti-MEM	500 ml
FCS (heat-inactivated)	5%

Opti-MEM with 10% FBS and 1%NEAA:

Opti-MEM	500 ml
FCS (heat-inactivated)	10%
MEM Non-Essential Amino Acids	0.1 mM

3.2.3 **Cell culture consumables**

6-well plate	Thermo Fisher Scientific, Roskilde
24-well plate	Thermo Fisher Scientific, Roskilde

96-well plate	Thermo Fisher Scientific, Roskilde
50 ml, 25 cm^3 flask	Greiner Bio-One, Frickenhausen
2 ml serological pipette	Greiner Bio-One, Frickenhausen
5 ml serological pipette	Costar Stripette, Corning
10 ml serological pipette	Greiner Bio-One, Frickenhausen
25 ml serological pipette	Costar Stripette, Corning
1 ml syringe	BD Plastipak, Madrid
25 ml tube	Greiner Bio-One, Frickenhausen
50 ml tube	Greiner Bio-One, Frickenhausen
cell scraper	Sarstedt, Newton
glass pipettes	Carl Roth, Karlsruhe
hypodermic needle, 27G	Braun, Melsungen
microscopic slides	Thermo Fisher Scientific
pipettes	BRAND, Wertheim
pipette tips	Greiner Bio-One, Frickenhausen

3.3 **Chemicals**

Chemicals were purchased from AppliChem (Darmstadt), Carl Roth (Karlsruhe) and Sigma-Aldrich (Saint Louis). Cell culture media, antibiotics and serum were purchased from Gibco (Darmstadt). Primers were purchased from Biolegio (Nijmegen) and Eurogentec (Cologne).

3.4 **Extraction of nucleic acids**

RNeasy Mini Kit	Qiagen, Hilden

content:

Buffer RLT

Buffer RW1

Buffer RPE

RNase-Free Water

3.5 **Fragment analysis**

3.5.1 **Reagents**

$_{dd}H_2O$	Fresenius Kabi, Bad Homburg
50 mM $MgCl_2$	Invitrogen, Carlsbad
10 mM dNTP	Invitrogen, Carlsbad
5x First-Strand Buffer	Invitrogen, Carlsbad
PlatinumTaq DNA Polymerase	Invitrogen, Carlsbad

3.5.2 **Primers**

Table 3.5.2-1. Primers for CPEB1-4 alternative isoforms identification

primer sequence	*binding position*	*predicted length*	*genebank association no.*	*detected length*	*isoform*
CPEB1					
fw 5’ GGATTGGTTAACACCTTCCGTGTTTTTGGC 3’					
	967 (v1)				
	751 (v2)				
rev 5’ AGGCCATCTGGGCTCAGCGGG 3’					

	1131 (v1)	176 bp (v1)	NM_030594	169 bp	Δ5
	921 (v2)	191 bp (v2)	NM_001079533	182 bp	full-length

CPEB2

fw 5’ AACTCCATCACTGACTCCAAAATCT 3’

1860

rev 5’ CAAGCCATCATCTATTGGAAAGAGGGAAGA 3’

	2206	375 bp (v4)	NM_001177382	375 bp	2a
	2182	352 bp (v2)	NM_182485	351 bp	2b
	2125	295 bp (v3)	NM_001177381	294 bp	2 c*
	2116	286 bp (v5)	NM_001177383	286 bp	2c
	2101	271 bp (v6)	NM_001177384	271 bp	2d*
	2092	262 bp (v1)	NM_182646	262 bp	2d

primer sequence	*binding position*	*predicted length*	*genebank association no.*	*detected length*	*isoform*

CPEB3

fw 5’ CAAAAAGCCCTTCTCCAGCAAC 3’

876

rev 5’ TTCAGCTTTGTGAGGCCAGTCTA 3’

	1478	604 bp (v1)	XM_006717715	600 bp	3a
	1433	580 bp (v3)	XM_011539514	576 bp	3b
	1388	535 bp	*	531 bp	3c
	1364	511 bp	*	507 bp	3d

CPEB4

fw 5’ CAGCTCTGCCTTTGCACCTAAAT 3’

1053

rev 5’ GGCCATCATCCAAGAATCCATC 3’

1309	278 bp (v1)	NM_30627	277bp	4a
1286	255 bp	*	254bp	4b
1258	227 bp (v2)	NM_001308189	226bp	4c
1234	203 bp (v3)	NM_001308191	203bp	4d

*"fw" and "rev" mark forward and reverse primers, * marks constructs based on a transcript variant alignment*

3.6 **Immunocytochemistry**

3.6.1 **Reagents**

DAPI	Sigma, Saint Louis
Hoechst	Life Technologies, Carlsbad
Mounting Medium, PermaFluor	Thermo Scientific, Fremont
Normal Goat Serum	Abcam, Cambridge
Triton X-100	Carl Roth, Karlsruhe

3.6.2 **Buffers and solutions**

10xPBS (pH 7.4):

NaCl	80 g
KCl	2 g
Na_2HPO_4	14.4 g
KH_2PO_4	2.4 g
$_dH_2O$	1l

0.01% NaN_3 in 1xPBS (pH 7.4):

NaN_3	0,1 g
1xPBS (pH 7.4)	1l

30% sucrose in 1xPBS (pH 7.4):

sucrose	30 g
1xPBS (pH 7.4)	1l

4% PFA:

PFA	4 g
$_dH_2O$	90 ml
NaOH	1M
10xPBS (pH 7.4)	10 ml

poly-L-lysine:

poly-L-lysine	500 µl of 2 mg/ml
$_dH_2O$	50 ml

3.7 **Immunohistochemistry**

3.7.1 **Reagents**

Cytoseal XYL medium	Thermo Scientific, Runcorn
Hematoxylin	Merck, Darmstadt
Permafluor	Thermo Scientific, Runcorn
PT Modul Buffer	Medac, Hamburg
Xylene	Merck, Darmstadt
100% ethanol	AppliChem, Darmstadt

90% ethanol	AppliChem, Darmstadt
70% ethanol	AppliChem, Darmstadt

3.7.2 **CSA II staining system for immunohistochemistry**

CSA II Biotin-free Tyramide Signal Amplification System — Dako, Carpinteria

content:

- TBS-T (Tris Buffered Saline- Tween)
- Peroxidase Block
- Protein Block
- Anti-Rabbit Immunoglobulins-HRP
- Amplification Reagent
- Anti-Fluorescein-HRP
- DAB Substrate Buffer
- Liquid DAB Chromogen

3.8 **Laboratory equipment**

3130 Genetic Analyzer	Applied Biosystems, Foster City
ABI 7900HT fast real time PCR system	Applied Biosystems, Darmstadt
Advanced Tissue Arrayer	Chemicon, Rolling Meadows
Axiophot	Carl Zeiss Microimaging GmbH, Göttingen
Axio Imager Z1 fluorescence microscope	Carl Zeiss Microimaging GmbH, Jena
BD FACS Canto II digital benchtop analyzer	BD Biosciences, Heidelberg
Centrifuge HERAEUS	Thermo Fisher Scientific, Schwerte
Centrifuges	Eppendorf GmbH, Wesseling
Fast Real-Time PCR System 7900HT	Applied Biosystems, Darmstadt
Gel electrophoresis chamber	Biorad, Munich
GeneGenome Syngene Bioimaging	Synaptics ltd. Cambridge
GeneTools System	Synaptics ltd. Cambridge
GloMax 96 Microplate Luminometer	Promega, Madison
Heat block	VWR International, Darmstadt

Lab Vision PT Modul	Thermo Scientific, Fremont
Leica TCS confocal	Leica Microsystems, Wetzlar
Mirax Slide Scanner	Carl Zeiss Microimaging GmbH, Jena
Nanophotometer Pearl	Implen GmbH, München
Novex Minicell WB module	Invitrogen, Darmstadt
Olympus BX53 research microscope	Olympus, Tokyo
PCR machines (MyCycler thermal cycler)	Biorad, München
pH meter	Mettler Toledo, Giessen
Pyromark Q24 instrument, Biotage	Qiagen, Hilden
Refrigerators (-80°C)	Thermo Fisher Scientific, Schwerte
Semi-automated IHC Stainer	Tecan, Crailsheim,
Shaker	Heidolph Rotomax120, Schwabach
Shaking incubator (GFL)	Progen Scientific, London
Shaking water bath	Memmert GmbH, Schwabach
Surgery equipment	Fine Science Tools (F.S.T), Heidelberg
VWR benchtop centrifuge	VWR International, Darmstadt
Thermoblock	Biometra, Goettingen
Vibratome, VT1000S	Leica, Nussloch
Vortexer	VWR International, Darmstadt
Mini-Protean 3 cell	Biorad, Munich
WB power supply	Biorad, Munich
Weigh balance	Sartorius group, Güottingen

3.9 **Methylation**

3.9.1 **Bisulfite conversion reagents**

EpiTect Fast DNA Bisulfite Kit	Qiagen, Hilden
content:	
Bisulfite Solution	
DNA Protect Buffer	
Buffer BL	
Buffer BW	

Buffer BD

Buffer EB

Carrier RNA

3.9.2 **Bisulfite-DNA amplification reagents**

$_{dd}H_2O$	Fresenius Kabi, Bad Homburg
PyroMark PCR Kit	Qiagen, Hilden

content:

Master Mix 2x

CoralLoad Concentrate 10x

3.9.3 **Pyrosequencing reagents**

Streptavidin-Sepharose High Performance Beads	GE-Healthcare, Solingen
PyroMark PCR Kit	Qiagen, Hilden

content:

PyroMark Annealing Buffer

PyroMark Binding Buffer, pH 7.6

PyroMark Denaturation Solution

PyroMark Enzyme Mixture

PyroMark Nucleotides (dATP, dCTP, dGTP, dTTP)

PyroMark Substrate Mixture

PyroMark Wash Buffer, pH 7.6

3.9.4 **Primers**

Table 3.9.4-1. Primers for amplification of bisulfite treated DNA

gene	*primer sequence*
CPEB1	fw 5’ GGGGGTTAGAGATTTAAGTTTGAG 3’
	rev 5’ ACTCCCATCCAAAAAAAACCAATAATATCT 3’
CPEB2	fw 5’ GGGGGTTATTAGTTTAAGTGAGAGTG 3’
	rev 5’ TCCCCTACCCAAATTCACT 3’
CPEB3	fw 5’ GGGGGTTATTAGTTTAAGTGAGAGTG 3’
	rev 5’ ACCACCAACCCATCATAAC 3’
CPEB4	fw 5’ GGGGAAAAGAGAGAGAAAGT 3’
	rev 5’ ACTTCCTCTCCCCCATAA 3’

"fw" and "rev" mark forward and reverse primers

Table 3.9.4-2. Primers for pyrosequencing

gene	*primer sequence*
CPEB1	ps 5’ AAGAGGGTAAGATTTATAAG 3’
CPEB2	ps 5’ TGGGGGAGTGGGAGA 3’
CPEB3	ps 5’ CCAACCCATCATAACC 3’
CPEB4	ps 5’ GGTTTTAGTATTTTTAG 3’

"ps" mark pyrosequencing primers

3.10 **Pathways activity assay**

Cignal 45-Pathway Reporter Array SABioscience, Frederick

Dual-Luciferase Reporter Assay	Promega, Madison
content:	
PLB	5x Passive Lysis Buffer (PLB) dissolved in 4 volumes of $_{d}H_2O$
LAR II	Luciferase Assay Substrate suspended in Luciferase Assay Buffer II
Stop & Glo Reagent	200 µl of 50x Stop& Glo Substrate dissolved in10 mL of Stop& Glo Buffer

3.11 **Semi-quantitative real time PCR**

3.11.1 **Reverse transcription reagents**

5x First-Strand Buffer	Invitrogen, Carlsbad
0.1 M DTT	Invitrogen, Carlsbad
50 mM $MgCl_2$	Invitrogen, Carlsbad
10 mM dNTP	Invitrogen, Carlsbad
250 ng Random Hexamer Primer	Invitrogen, Carlsbad
SuperScript III Reverse Transcriptase	Invitrogen, Carlsbad
$_{dd}H_2O$	Fresenius Kabi, Bad Homburg

3.11.2 **TaqMan semi-quantitative real time PCR reagents**

TaqMan Universal PCR Master Mix	Applied Biosystems, Warrington
900 nM forward primer	Eurogentec, Cologne
900 nM reverse primer	Eurogentec, Cologne
100 nM probe	Eurogentec, Cologne
$_{dd}H_2O$	Fresenius Kabi, Bad Homburg

3.11.3 **Primers and probes**

Table 3.11.3-1. Primers and probes for semi-quantitative real time PCR

primers and probes sequences	*binding position*	*length*

CPEB1; genebank association no: NM_030594		
fw 5’ GCACCCAGGACTCAGATTCC 3’	335 (v1), 110 (v2)	73 bp (v1),
rev 5’ CCCAGTGGGTTATGGAGCAT 3’	358 (v1), 134 (v2)	73 bp (v2)
p 5’ CCCAGAGCAGCACACACTCGGTACTG 3’	358 (v1), 134 (v2)	
CPEB2; genebank association no: NM_001177382		
fw 5’ TGCAGCAGAGGAACTCCTATAACC 3’	1631 (v1-v6)	81 bp (v1-v6)
rev 5’ CCCAGCCACTGCTCTGATG 3’	1693 (v1-v6)	
p 5’ CCAGCCTCTTCTGAAACAGTCTCCCTGG 3’	1659 (v1-v6)	
PBGD; genebank association no: NM_000190		
fw 5’ GCTATGAAGGATGGGCAACT 3’	808 (v1), 756 (v2), 688 (v3), 637 (v4)	149 bp (v1-v4)
rev 5’ GTGATGCCTACCAACTGTGG 3’	936 (v1), 886 (v2), 817 (v3), 766 (v4)	
p 5’ TGCCCAGCATGAAGATGGCC 3’	906 (v1), 855 (v2), 786 (v3), 735 (v4)	

"fw"and "rev" mark forward and reverse primers, "p" probe and "v" transcript variant

3.12 **Transfection**

3.12.1 **Reagents**

Forskolin	Cell Signaling, Danvers
Lipofectamine 3000 Transfection Kit	Invitrogen, Carlsbad
Staurosporine S4400	Sigma, Saint Louis

3.12.2 **Expression vectors**

Table 3.12.2-1. Expression vectors

host	*insert*	*vector*	*company*
human	CPEB1	pCMV6Neo	OriGene, Rockville
human	CPEB2	pCMV6Neo	OriGene, Rockville
human	-	pCMV6Neo	OriGene, Rockville
human	-	pmaxGFP	Lonza, Cologne
mouse	CPEB3a	pEGFP-N1	Clontech Laboratories, Heidelberg
mouse	CPEB3aKD	pEGFP-N1	Clontech Laboratories, Heidelberg
mouse	CPEB3b	pEGFP-N1	Clontech Laboratories, Heidelberg

CPEB3a-EGFP, CPEB3aKD-EGFP and CPEB3b-EGFP vectors were generated by Dr. Vamshidhar Vangoor (Institute of Cellular Neurosciences, University of Bonn), vector maps are provided in appendix I

3.13 **Western blotting**

3.13.1 **Protein lysis buffer**

Protein lysis buffer:

modified RIPA buffer

pH 7.5, stored at -20°C

Tris	6.05 g	50 mM
NaCl	8.76 g	150 mM
NP40	5 ml	0.5%
Sodium deoxycholate	5 g	0.5%
Triton X-100	10 ml	1%

Halt Protease Phosphatase Single Use Inhibitor Cocktail (Thermo Scientific, Rockford)

Contents (except NP40 and triton) were dissolved in 800 ml $_{dd}H_2O$; pH was adjusted to 7.5; NP40 and Triton X-100 were added; volume was adjusted to 1l; buffer was aliquoted 10 ml each and stored at -20^{o}C. Modified RIPA lysis buffer was supplemented with Inhibitor Cocktail directly before use.

3.13.2 **BCA Protein Assay**

BCA Protein Assay Kit — Thermo Scientific, Rockford

content:

Albumin Standard 2mg/mL

BCA Reagent A

BCA Reagent B

3.13.3 **SDS-PAGE and protein transfer**

Consumables:

Methanol	AppliChem, Darmstadt
PVDF membrane	GE Healthcare Life Sciences, Buckinghamshire
Roti Load 1 4x Sample buffer	Carl Roth GmbH, Karlsruhe
Whatman paper	Whatman International, Maidstone

Buffers and solutions:

Tris, 1.5 M, pH 8.8:

Tris	18.16 g/100 ml $_dH_2O$

Tris, 0.5 M, pH 6.8:

Tris	6.05 g/100 ml $_dH_2O$

10% APS:

APS	0.1 g/1 ml $_dH_2O$

10% SDS:

SDS	10 g/100 ml $_dH_2O$

Resolving gel (10%):

$_dH_2O$	7.94 ml
1.5 M Tris (pH 8.8)	5 ml
10% SDS	0.2 ml
Acrylamide	6.66 ml
10% APS	0.2 ml
TEMED	0.02 ml

Stacking gel (4%):

$_dH_2O$	2.81 ml
0.5 M Tris (pH6.8)	1.25 ml
10% SDS	0.05 ml
Acrylamide	0.83 ml
10% APS	0.05 ml
TEMED	0.005 ml

10x TBS-T, pH 7.4:

25 mM Tris	30.3 g
150 mM NaCl	87.7 g
0.05% Tween-20	10 g
$_dH_2O$	1l

Running buffer:

10x Tris-Glycine-SDS buffer, pH 8.3:

25 mM Tris	30.3 g
192 mM Glycine	144 g
0.1% SDS	10 g
$_{d}H_2O$	1l

Blotting buffer:

10x Tris-Glycine buffer, pH 8.3:

25 mM Tris	30.3 g
192 mM Glycine	144 g
$_{d}H_2O$	1l

3.13.4 **Blocking and antibody solutions**

General blocking solution:

5% milk powder	0.5 g
1x TBS-T (pH 7.4)	10 ml
0.05% Tween-20	0.5 ml

Blocking solution for phospho-specific antibody:

3% BSA	0.3 g
1x TBS-T (pH 7.4)	10 ml

Solution for incubation with primary and secondary antibody:

2,5% milk powder	0.25 g
1x TBS-T (pH 7.4)	10 ml

Solution for incubation with phospho-specific primary antibody:

2% BSA	0.2 g
1x TBS-T (pH 7.4)	10 ml

4 METHODS

4.1 Animals

Maintenance and handling of animals was according to the local government regulations. Animals were housed in a 12 h/12 h dark-light cycle, food and water ad libitum. C57Bl6J wild-type mice were purchased from Charler River Laboratories (Sulzfeld). Thy1-GFP mice were provided by Prof. Valentin Stein (Institute of Physiology, University of Bonn).

4.2 Cell cultures

4.2.1 Glioblastoma cell cultures

Human glioblastoma cell lines A172, A178, LN229, U373MG, U87MG and T98G were obtained from the Ludwig Institute for Cancer Research (San Diego). Individual cell lines identity was confirmed by STR DNA profiling of 15 loci and sex-determining marker amelogenin (Genetica DNA Laboratories, Cincinnati). Cells were grown in DMEM with 25 mM glucose (Gibco, Darmstadt) supplemented with 10% FCS (Gibco, Darmstadt), 1% penicillin/streptomycin (Gibco, Darmstadt), 200 mM L-glutamine (Gibco, Darmstadt) and 100 mM sodium pyruvate (Gibco, Darmstadt) at 37°C, 5% CO_2.

4.2.2 HEK-293FT cell cultures

Cultured HEK-293FT cells were grown in DMEM with 25 mM glucose supplemented with 10% FCS, 1% penicillin/streptomycin, 200 mM L-glutamine and 100 mM sodium pyruvate at 37°C, 5% CO_2.

4.2.3 **Primary hippocampal cultures**

Primary hippocampal cultures were provided by Prof. Susanne Schoch (Institute of Neuropathology, University of Bonn).

4.3 **Human specimens**

Human glioma specimens were received from 69 patients (26 females, 43 males) admitted to the University Hospital of Bonn (ethics volume no. FKZ. 01GS08187). Histological characterization performed by neuropathologists of the German Brain Tumor Reference Center in Bonn confirmed that each specimen used further for extraction of nucleic acids and immunohistochemical staining consisted of at least 80% tumor cells. To avoid a possible tumor infiltration, human normal cerebellar tissues were used as a control. Tumors were graded according to the World Health Organization (WHO) classification of tumors of the central nervous system (Louis et al., 2007) into the following groups: diffuse astrocytoma (AII), anaplastic astrocytoma (AAIII), primary glioblastoma multiforme (pGBM), and secondary glioblastoma multiforme (sGBM) (Fig. 1.1.2-1). All patients agreed to preform molecular analysis on their samples. Specimens were treated in an anonymous manner approved by the ethics committee at the University of Bonn.

Table 4.3-1. Investigated human tissues

diagnosis	*WHO grade*	*no. of patients*
diffuse astrocytoma	II	11
anaplastic astrocytoma	III	22
primary glioblastoma multiforme	IV	28
secondary glioblastoma multiforme	IV	8

4.4 Extraction of nucleic acids for methylation and fragment analysis studies

Extraction of DNA and RNA for methylation and fragment analysis was carried out using ultracentrifugation of homogenized tumor tissue through a CsCl gradient. Extraction was performed by Johannes Freihoff (Institute of Neuropathology, University of Bonn) according to instructions described before by Ichimura et al. (1996).

4.5 Methylation of CPEB1-4 genes

4.5.1 Bisulfite conversion

DNA methylation occurs on cytosine residues in regions with a high content of CpG dinucleotides known as CpG islands. The methylation status of CpG islands of CPEB1-4 genes was determined by bisulfite conversion according to instructions provided in the EpiTect Fast DNA Bisulfite Conversion Kit (Qiagen, Hilden). The bisulfite reaction consists of steps necessary for DNA denaturation, subsequent sulfonation and cytosine deamination. Isolated DNA samples were incubated with high bisulfite salt concentrations at high temperature and low pH to convert unmethylated cytosine residues into uracyl. Methylated cytosines remained unchanged. Afterwards converted single-stranded DNA was purified on MinElute DNA columns. Membrane-bound DNA was washed with 500 µl of washing buffer and desulfonated by incubation for 15 min with 500 µl of desulfonation buffer. Next, DNA was washed again with 500 µl of washing buffer to remove the desulfonation agent and eluted with 15 µl of elution buffer. Finally, bisulfite converted DNA was amplified in PCR reaction and sequenced.

Table 4.5.1-1. Analyzed samples

no. of glioblastoma cell lines:	5
no. of reference tissues:	3-6
no. of glioma specimens:	63
AAIII	12
SGBM	10
pGBM	41

Table 4.5.1-2. Bisulfite conversion reaction and program

reagent	*amount*
DNA template	5 µl
$_{dd}H_2O$	15 µl
bisulfate solution	85 µl
DNA protection solution	35 µl
total volume:	140 µl

denaturation	95°C	5 min
incubation	60°C	10 min
denaturation	95°C	5 min
incubation	60°C	10 min
hold	20°C	∞

Table 4.5.1-3. Bisulfite-DNA amplification PCR reaction and program

reagent	*amount*
bisulfite - DNA	3 µl
master mix	12.5 µl
coral load	2.5 µl
forward primer	1.5 µl
reverse primer	1.5 µl
$_{dd}H_2O$	4 µl
total volume:	25 µl

initial denaturation	95°C	15 min	
denaturation	94°C	30 sec	45x
annealing	56°C	30 sec	
extension	72°C	30 sec	
final extension	72°C	10 min	

4.5.2 **Pyrosequencing**

Pyrosequencing of the PCR products containing methylation sites was performed using pyrosequencing primers and the PyroMarkGold Reagents (Qiagen, Hilden). 20 µl of each bisulfite converted PCR product was pipetted into fresh 96-well reaction plates, complemented by 20 µl mastermix and placed on a shaker to maintain dispersion of beads. The mastermix composed of 1.5 µl streptavidin-sepharose beads and 18.5 µl binding buffer. Afterwards, 1 µl of pyrosequencing primers mixed with 24 µl of annealing buffer was pipetted into the fresh pyrosequencing annealing plate. With the use of a vacuum prep tool all DNA-beads samples were uniformly sucked from the plate. Attached samples were transferred into the 70% ethanol, denaturation solution, washing buffer and beads were released into the already prepared annealing plate. The pyrosequencing plate was incubated at 80°C for 2 min, cooled down and placed in the sequencing Pyromark Q24 instrument (Qiagen, Hilden). Additional cartridge containing PyroMark enzyme, substrate and nucleotides were attached to the sequencing instrument. Bisulfite conversion and pyrosequencing were performed by Jennifer Hammes (Institute of Neuropathology, University of Bonn).

4.5.3 **Data analysis**

Pyrogram outputs were analyzed using the PyroMark Q24 software (Qiagen, Hilden). Values obtained by CpG-islands pyrosequencing of individual tumor and normal brain sample were averaged and compared between each other. Normal brain tissues of age-matched patients were considered as controls. As a cut-off level for methylation the three fold the standard deviation of mean methylation of normal brain samples was chosen. Ultimately, values obtained by pyrosequencing were imported into MultiExperiment Viewer and visualized as a heat map.

4.6 **Fragment analysis of CPEB1-4 alternative splice isoforms**

4.6.1 **Fragment analysis**

Identification of CPEB1-4 alternative splice variants was performed using RT-PCR products with primers spanning previously defined splice variants. CPEB1-4 cDNA was amplified by Platinum Taq DNA Polymerase and CPEB primers. One of each primer pairs was labeled with a specific fluorescent dye allowing sensitive detection and sizing of the PCR products. CPEB splice forms were estimated by electrophoretic separation of fluorescently labeled PCR products. Fragment sequencing was performed on thin capillaries allowing for distinction of 1bp differences.

Table 4.6.1-1. Analyzed samples

no. of glioblastoma cell lines:	5
no. of reference tissues:	4
no. of glioma specimens:	58
AII	1
AAIII	12
SGBM	8
pGBM	37

Table 4.6.1-2. PlatinumTaq reaction and PCR program

reagent	*amount*
$_{dd}H_2O$	13.7 µl
MgCl2	0.8 µl
dNTP	0.4 µl
5x First-Strand Buffer	2 µl
forward primer	1 µl
reverse primer	1 µl
PlatinumTaq DNA polymerase	0.1 µl
cDNA template in $_{dd}$H2O	1 µl
total volume:	20 µl

initial denaturation	95°C	15 min	
denaturation	95°C	45 sec	40x
annealing	54°C	45 sec	
extension	72°C	45 sec	
final extension	72°C	10 min	

4.6.2 **Data analysis**

RT-PCR products were generated in separate PCR reactions optimized for the individual CPEB and diluted to adjust optimal signal strength. Next, fluorescently labeled PCR products were pooled and loaded for each individual tumor specimen or cell line. Detection and separation of PCR products was performed on an automated DNA sequencing machine 3130 (Applied Biosystems, Foster City). Electropherogarams of the individual samples were analyzed using GeneMapper v3.7 software by reading out the length of the RT-PCR product given in base pairs and the signal intensity expressed in relative fluorescent unit, which was proportional to the amount of generated PCR product. The fragment analysis was performed by Jennifer Hammes (Institute of Neuropathology, University of Bonn).

4.7 **Generation of custom-made antibodies**

Custom-made rabbit polyclonal antibodies were raised against CPEB1, CPEB2, CPEB4 and the phosphorylated form of CPEB3a/c (phospho-CPEB3). Peptide antigens (Kaczmarczyk et al., 2016; Turimella et al., 2015) were based on antigenic index (Jameson and Wolf, 1988), hydrophobicity (Kyte and Doolittle, 1982) and surface probability (Emini et al., 1985) and generated by Eurogentec GmbH (Cologne, Germany). As a carrier protein the keyhole limpet hemocyanin was used. For every CPEB two specific pathogen-free (SPF) rabbits were injected 4 times with 200 µg of each peptide, in 2-week intervals. Three months after the first immunization animals were sacrificed, bled and antibodies were purified by affinity purification. The phospho-CPEB3 antibody was directed against a region surrounding the S419 and S420 serine residues. The RRGRSSLFPFEDC peptide was chosen for immunization and cross-affinity purification of antibody. Purified antibodies were directed to mouse as well as human CPEBs. Their specificity was tested by peptide competition assay and immunoblot analysis (Kaczmarczyk et al., 2016; Turimella et al., 2015). Antibodies bound specifically and did not cross-react with other CPEBs.

4.8 Immunohistochemistry

4.8.1 Staining of paraformaldehyde fixed tissues

4.8.1.1 Tissue preparation

Juvenile (p12) or adult (p90) C57Bl6J mice and juvenile (p12) Thy1-GFP mice (Feng et al., 2000) were perfused via the vascular system using 4% paraformaldehyde (PFA). Next, isolated brains were fixed for 24 h in 4% PFA at 4°C and transferred to phosphate buffered saline (PBS). Coronal sections of 40 µm thicknesses were prepared on a VT1000S vibratome (Leica, Nussloch) and stored in 0.01% NaN_3 in PBS at 4°C.

4.8.1.2 Immunohistochemical staining

Brain sections were washed three times for 10 min with PBS and blocked for 2 h in 10% of normal goat serum (NGS), 0.4% Triton X-100 in PBS. Following blocking, sections were incubated with the custom-made CPEB2 antibody– (1:50) and GFP– (1:500), MAP2– (1:100), PARV– (1:250) or TYH– (1:500) antibodies in 5% of NGS, 0.1% Triton X-100 in PBS for 48 h at 4°C. Afterwards, sections were washed with PBS and incubated for 90 min with secondary Alexa Fluor antibody– (1:500). Cell nuclei were stained with Hoechst for 10 min. Then sections were washed with PBS and mounted in Permafluor (Thermo Scientific, Runcorn).

4.8.1.3 Microscopy and data analysis

Images were taken with an Axio Imager Z1 fluorescence microscope (Carl Zeiss GmbH, Jena). For quantitative assessment of CPEB2 expression in excitatory, inhibitory, and dopaminergic neurons, GFP-parvalbumin-tyrosine hydroxylase-positive cells colocalizing with CPEB2 were counted (7-5 slices from three animals per type of neurons).

4.8.2 **Staining of formalin fixed paraffin-embedded tissues**

4.8.2.1 **Generation of tissue microarrays**

The tissue microarray technique allows for simultaneous analysis of multiple histological specimens assembled on one glass slide. Here, dissected glioma tissues were fixed with 4% PFA for 24–48 h at 4°C and embedded in a paraffin block. Microarrays were prepared by taking core needle biopsies from separate paraffin tissue blocks and re-embedding these tissues in an arrayed master block on Advanced Tissue Arrayer (Chemicon, Rolling Meadows). Afterwards, 4 µm thick tissue sections were prepared in the Lab Vision PT Modul (Thermo Scientific, Fremont) followed by pretreatment for 20 min at 99°C in PT Modul Buffer (Medac, Hamburg) and a 20 min cool-down phase at room temperature. Tissue microarrays were prepared by Brigitte Söndgen (Institute of Neuropathology, University of Bonn).

Table 4.8.2.1-1. Analyzed glioma samples

no. of specimens:		69
	AII	11
	AAIII	22
	SGBM	8
	pGBM	28

4.8.2.2 **Immunohistochemical staining**

Immunohistochemical staining was performed with a CSA II Biotin-free Tyramide Signal Amplification System (Dako, Carpinteria). Endogenous peroxidase activity forming high non-specific background staining was eliminated by pretreatment of tissue with hydrogen peroxide. Five min peroxidase blocking was followed by 60 min protein block prior to incubation of primary antibody. Next, specimens were incubated overnight at 4°C with the following antibodies: GFAP– (1:1000), CPEB1– (1:100), CPEB2– (1:250), CPEB3–

(1:100), phospho-CPEB3– (1:50), CPEB4– (1:250), phospho- CaMKII– (1:1000) and PKA– (1:500). Afterwards sections were treated for 1h with poly-HRP-goat anti-mouse or anti-rabbit secondary antibody. Generated signal was enhanced with amplification reagent, anti-fluorescein-HRP and 3,3'-diaminobenzidine (DAB), 15 min each. Cell nuclei were stained with hematoxylin.

4.8.2.3 **Microscopy and data analysis**

Histological evaluation was performed by microscopic observation and digital scan of stained specimens. Stainings were observed with an Olympus BX53 research microscope (Olympus, Tokyo) and scanned by a Mirax Slide Scanner (Carl Zeiss GmbH, Jena). Tissues were categorized as positive or negative for the individual antibody by Dr. Gerritt Gielen (Institute of Neuropathology, University of Bonn). Specimens classified as a positive were further divided into three intensity groups: weak, intermediate and strong.

4.9 **Transfection and stimulation of cultured cells**

4.9.1 **Transfection of cultured cells**

Cells were seeded in 6-well plates, grown in complete mouse embryonic fibroblast (MEF) culture medium and transfected when ~75% confluency was obtained. One hour prior to transfection MEF medium was replaced by trans-MEF cell culture medium with reduced serum (2%). The transfection reaction was prepared in 250 µl of opti-MEM with 2 µg of expression plasmid and 3 µl of lipofectamine reagent. Transfected cells were incubated for 5h at 37°C, 5% CO_2 and trans-MEF medium was replaced by fresh MEF medium. Afterwards cells were incubated for another 48 h and collected for RNA and protein analysis.

4.9.2 **HEK-293FT cells stimulation with forskolin**

In order to test phosphorylation of CPEB3 protein, HEK-293FT cells were transiently transfected with CPEB3a-EGFP, CPEB3KD-EGFP and CPEB3b-EGFP constructs. 24 h post transfection cells were stimulated for 1 h with 200 μM forskolin, which increases the intracellular cAMP concentration and activates cAMP-dependent protein kinase (PKA). Control cells were treated with the same amount of dimethyl sulfoxide (DMSO). Following forskolin treatment cells were washed with ice-cold PBS and collected for protein analysis.

4.10 **Immunocytochemistry**

4.10.1 **Coating slides with poly-L-lysine**

Glass coverslips were coated with poly-L-lysine to enhance cell attachment. An aliquot of 500 μl poly-L-lysine (2 mg/ml) was diluted in 50 ml $_{dd}H_2O$ and incubated with coverslips for 2h at 37° C. Afterwards coverslips were washed with $_{dd}H_2O$ and dried.

4.10.2 **Immunocytochemical staining**

Glioblastoma A172 cells were seeded and grown on glass coverslips until obtaining approximately 80% of confluency. Next, cells were washed with PBS and fixed for 20 min with 4% sucrose in 4% PFA. Cell membranes were permeabilized with 0.5% Triton X-100 and blocked for 60 min with 10% NGS and 0.5% Triton X-100 at room temperature. Following blocking of unspecific binding, cells were stained overnight at 4°C with polyclonal antibodies directed to CPEB1-4. Primary antibodies were diluted in PBS supplemented with 5% NGS and 0.1% Triton X-100 at the following dilutions: CPEB1– (1:100), CPEB2– (1:250), CPEB3– (1:100), phospho-CPEB3– (1:50), CPEB4– (1:250). Afterwards, cells were washed with PBS and incubated for 60 min with Alexa secondary antibodies (Invitrogen, Rockford). Counterstaining was performed with DAPI dye (Sigma,

Saint Louis). Coverslips were mounted using the PermaFluor mounting medium (Thermo Scientific, Fremont).

4.10.3 **Microscopy and data analysis**

Images were taken with the Zeiss Axio Imager Z1 fluorescence microscope. For qualitative estimation of endogenous CPEB1-4 and phospho-CPEB3 expression, human glioblastoma A172 cells stained with individual CPEBs were compared to their expression pattern in human glioma tissues.

4.11 **Extraction of RNA for semi-quantitative real time PCR**

Isolation of RNA from glioblastoma cultured cells was carried out using the RNeasy Mini Kit (Qiagen, Hilden). Cells transfected with the CPEB1- pCMV6Neo, CPEB2- pCMV6Neo or pCMV6Neo vector were washed with ice-cold PBS and directly lysed with 350 µl of RLT buffer (Qiagen, Hilden) supplemented with 1% β-mercaptoethanol (β-ME). Samples were frozen in -20°C or the isolation procedure was immediately continued following the manufacturer's protocol.

4.12 **Semi-quantitative real time PCR**

4.12.1 **Reverse transcription**

1 µg of template RNA was reversely transcribed with SuperScript III reverse transcriptase. Isolated RNAs were mixed with 10 mM dNTPs, 50 mM $MgCl_2$, 0.1M DTT and 250 ng of random hexamers in a total of 20 µl reaction volume and transcribed to cDNA by reverse transcription PCR.

Table 4.12.1-1. Reverse transcription reaction and PCR program

reagent	amount
dNTP	1 µl
Random Hexamer Primer	1 µl
5x First-Strand Buffer	2 µl
$MgCl_2$	2 µl
DTT	2 µl
SuperScript III reverse transcriptase	0.25 µl
$_{dd}H_2O$	1.75 µl
1 µg/µL RNA template in $_{dd}H_2O$	10 µl
total volume:	20 µl

annealing	25 ° C	10 min
extension	42 ° C	50 min
reverse transcriptase inactivation	70 ° C	15 min
hold	4 ° C	∞

4.12.2 **Semi-quantitative real time PCR**

Semi-quantitative assessment was achieved by amplification of 1 µl cDNA with 900 nM of CPEB and PBGD primers, 100 nM of fluorogenic Taqman probes and TaqMan Universal PCR Master Mix (Applied Biosystems, Warrington). Probes consisted of a 6-FAM fluorophore attached to the 5'-end of oligonucleotide and 3'-end attached the TAMRA quencher. The final TaqMan reaction volume was 12.5 µl.

Table 4.12.2-1. TaqMan sqRT-PCR reaction and PCR program

reagent	amount
TaqMan Universal PCR Master Mix	6.25 µl
TaqMan Assay forward primer	1.125 µl
TaqMan Assay reverse primers	1.125 µl
TaqMan Assay probe	0.25 µl
$_{dd}H_2O$	2.75 µl
template cDNA	1 µl
total volume:	12.5 µl

UNG activation	50°C	2 min	
initial denaturation	95°C	10 min	
denaturation	95°C	15 sec	40x
annealing and extension	60°C	60 sec	

UNG (Uracil-N glycosylase)

4.12.3 **Data analysis**

The critical threshold cycle (CT) value for each reaction was determined using SDS 5.0 Software (Applied Biosystems, Warrington). Normalization was performed using the housekeeping porphobilinogen deaminase (PBGD) gene as a reference against the expression of *CPEB* genes transcripts. The transcript level of CPEB1 and PBGD genes was calculated using the following equation: $X_{CPEB}/X_{PBGD} = 2^{CT\ PBGD\ -\ CT\ CPEB}$, where X is the respective input copy numbers and CT is the threshold cycle numbers for CPEB1 and PBGD (Seifert and Steinhäuser, 2007).

4.13 **Western blotting**

4.13.1 **Tissue and cell culture lysates**

Tissue and culture cells were lysate with modified RIPA buffer supplemented with a phosphatase and protease inhibitor cocktail. Tissue was homogenized in a 1.5 ml tube with a pestle, whereas cells were scraped in cold lysis buffer. Samples were disrupted with a 27G needle, then sonicated for 10 min and incubated for 30 min on ice. Afterwards cells were centrifuged for 15 min at 4°C, 14.000 g and their supernatants were collected for the further analysis. Total protein content was estimated by a BCA protein assay. For this purpose 25 µl of protein standard (20-2000 µg/ml range; Thermo Scientific, Rockford) and 5 µl of lysate mixed with 20 µl $_{dd}H_2O$ was pipetted into a 96-well plate. The plate was gently shaken for 25 min at 37°C. Colorimetric detection and quantitation of total protein concentration was performed with an OptiMax Tunable Microplate Reader (Molecular Devices, Sunnyvale).

4.13.2 **SDS-PAGE and Western blotting**

30 µg of protein samples were mixed with denaturing sample buffer and heated for 5 min at 95°C. Next proteins were separated according to their molecular weight by SDS-PAGE (30

min at 80 V, 0.04 mA followed by 1.5h at 220 V, 0.06 mA) and blotted (2h at 100 V) on a PVDF membrane (GE Healthcare Life Sciences, Buckinghamshire). Afterwards, membranes with transferred non-phosphorylated proteins were blocked for 1h in 5% milk powder in T-BST and membranes with transferred phosphorylated proteins in 3% BSA in T-BST. Then membranes were incubated overnight with primary antibodies suspended in 2.5% milk powder (non-phosphorylated antibodies) or 2% BSA (phosphorylated antibodies) in T-BST. The next day membranes were washed with TBS-T buffer, incubated for 1h with horseradish peroxidase (HRP) secondary antibody in 2.5% milk powder in T-BST and visualized.

4.13.3 **Data analysis**

HRP activity was detected with Supersignal West Dura Substrate (Thermo Scientific, Rockford). Generated chemiluminescence was measured with the Gene Genome digital documentation system (Synoptics, Cambridge). Densitometry was performed with GeneTools System (Synoptics, Cambridge) and tested for significant differences.

4.14 **Measurement of cellular proliferation and viability**

4.14.1 **FACS samples preparation**

The dis-regulation of CPEB expression observed in glioma was the reason to study their influence on growth properties and apoptotic activity in *in vitro* conditions. Glioblastoma cells were transiently transfected with CPEB1-pCMV6Neo, CPEB2-pCMV6Neo or control pCMV6/Neo vector and subsequently their expression was monitored by sqRT-PCR and Western blot. Here, cells were additionally co-transfected with pmaxGFP to allow detection of CPEB-GFP positive cells by fluorescence-activated cell sorting (FACS). 24 h post transfection MEF medium was replaced with serum-starved MEF medium to induce apoptosis. The next day attached and detached cells of the flask were collected, washed with ice-cold PBS and transferred to the FACS tubes (polystyrene, non-pyrogenic). Cells

were fixed for 10 min in 4% PFA, permeabilized for 5 min in 0.5% Triton X-100 and stained. Proliferating cells were labeled with an Alexa Fluor 647-labeled antibody against phospho-(ser10)-histone H3 (pHH3; 1:20), whereas apoptotic cells were stained with a phycoerythrin-labeled antibody recognizing cleaved poly(ADP-ribose) polymerase (PARP; 1:5). Incubation with antibody for 30 min at room temperature was followed by 30 min DAPI staining (10 µg/ml) at 37°C.

4.14.2 **Proliferation and viability analysis**

Samples were analyzed with the use of BD FACS Canto II digital benchtop analyzer (BD Biosciences, Heidelberg). In each experiment at least 100000 GFP- CPEB1-pCMV6/Neo, GFP- CPEB2-pCMV6/Neo, GFP- pCMV6/Neo or pmaxGFP positive single cells were analyzed. Cells transfected with GFP- pCMV6/Neo or pmaxGFP vector were considered as reference samples. Non-transfected cells labeled only with pHH3 antibody or stimulated for 24 h with 1 µM staurosporine and stained with PARP antibody were used as a control to monitor proliferation and apoptosis, respectively.

4.15 **Measurement of cellular migration**

4.15.1 ***In vitro*** **scratch assay**

Migration of cultured glioblastoma cells transiently overexpressing CPEB1 and CPEB2 proteins was tested by an *in vitro* wound healing assay. A reproducible size scratch was created by the tip of a glass pipet on a confluent cell monolayer in the center of culture dish. Cell motility was monitored for 24 h.

4.15.2 **Cell migration analysis**

The motility of CEPB overexpressing cells was measured by the area covered by cells over time. 24 h after the scratch cells migrated into the center of the wound, which was imaged and quantified.

4.16 **Cancer associated pathway activity assay**

4.16.1 **Reverse transfection**

A pathway reporter array allowed for simultaneous analysis of 45 cancer-associated signaling pathways by screening their activities. Quantitative assessment was possible upon overexpression of CPEB1-pCMV6/Neo, CPEB2-pCMV6/Neo and control pCMV6/Neo plasmids in cultured cells and its reverse transfection with reporter constructs from array plates. Every construct was assembled of a constitutively expressed *Renilla* reporter and an inducible transcription factor responsive firefly luciferase reporter. Positive control was composed of a mixture of a constitutively expressed firefly luciferase and *Renilla* luciferase GFP constructs. Negative control was composed of non-inducible firefly luciferase reporter and constitutively expressed *Renilla* reporter. Reverse transfection was initiated by activation of reporter constructs from array plates by adding 50 µl of Opti-MEM. For each transfection reaction 0.3 µl lipofectamine in 50 µl of Opti-MEM was used. The mixture was added onto the plate, gently mixed and incubated for 20 min. A172 cells transiently expressing CPEB1-pCMV6/Neo, CPEB2-pCMV6/Neo and control pCMV6/Neo plasmids were washed with PBS without Ca^{2+} and Mg^{2+}, trypsinized, suspended in Opti-MEM with 5% FBS and counted. 15.000 cells per well in 50 µl of Opti-MEM with 10% FBS and 1% NEAA was added into each well and incubated for 24 h at 37°C. Afterwards the medium was replaced with MEF growth medium, incubated for another 24 h at 37°C and signals were detected by a dual-luciferase assay.

4.16.2 **Dual-luciferase reporter assay**

A dual luciferase assay was performed 48 h after reverse transfection. Grown medium was removed from cultures cells, cells were rinsed with PBS and 10 µl of PLB was added into each well of Cignal 45-Pathway Reporter Array plates. After 15 min of gentle shaking at room temperature firefly (*Photinus pyralis*) and *Renilla* (*Renilla reniformis*) luciferases activities were measured sequentially from each well. First the firefly luciferase reporter was measured by adding 50 µl of Luciferase Assay Reagent II to generate a stabilized luminescent signal. After quantification the firefly luminescence, reaction was quenched, and the *Renilla* luciferase reaction was initiated by 50 µl of Stop & Glo Reagent added to the same well. *Renilla* luciferase signal decayed slowly over the course of the measurement.

4.16.3 **Cancer associated pathways activity analysis**

Firefly and *Renilla* luciferase activities were analyzed using GloMax 96 Microplate Luminometer. Results were calculated by dividing the normalized luciferase activity of each pathway reporter reverse transfected into A172 cells overexpressing CPEB1-pCMV6/Neo or CPEB2-pCMV6/Neo plasmid by the normalized activity of pathway reporter transfected with the control pCMV6/Neo vector. Reporters showing minimum two-fold change of relative luciferase units were considered as up- or downregulated. Experiments repeated three times in duplicates were further tested for statistical significance using OrigeneLab Corporation software (Northampton, MA, USA).

4.17 **Statistics**

In chapters 5.1.1, 5.1.4 and 5.2.2, the subsequent statistical analysis was conducted. Each data set was tested for Gaussian distribution by the Shapiro-Wilk-test. Next, for the comparison of two independent variables the normally distributed data was further examined with the F-test for equivalence of variances. Accordingly, Student's t-Test

without or with Welsh correction was performed. For comparison of more than two independent variables one-way ANOVA with post-hoc Tukey-test was applied. Therefore, the data were tested for equal variances by the Levene-test and based on the result Welsh-correction was performed. Non-normal distributed data were analyzed with non-parametric tests. Therefore, data sets with two independent variables were tested with Mann-Whitney U test and sets with three or more independent variables with the Kruskal-Wallis-ANOVA and post-hoc Bonferoni-corrected Mann-Whitney U test. Data are represented as mean ± SEM. In chapter 5.1.2, *IDH1* mutation was correlated with CPEB1 and CPEB3 methylation by Fisher's two-sided exact test. While, in chapter 5.1.3.2, clinical course of glioma patients was correlated with CPEB expression data by Kaplan-Meier survival analysis.

5 RESULTS

5.1 Functional analysis of CPEB 1-4 in the pathogenesis of gliomas

5.1.1 Methylation of CPEB 1-4 genes in the 5'-CpG islands in gliomas

Methylation of DNA belongs to the heritable alternations in gene function, occurring without a change in the DNA sequence. Such epigenetic reaction may have inhibitory effects on gene expression. It neither alters nucleotide sequences nor affects the specificity of DNA base pairing. Differential methylation hybridization is a commonly used technique to identify changes in methylation patterns observed in cancers. Here, the methylation status of *CPEB1-4* genes was determined by bisulfide treatment and pyrosequencing of glioma (n=63), normal brain (n=3-6) and cultured glioblastoma samples (n=5) (Fig. 5.1.1-1). *De novo* hypermethylation in the investigated CpG-islands was detected in *CPEB1* (Fig. 5.1.1-1) and the gene was identified as a target for epigenetic inactivation in gliomas. In normal brain specimens of age-matched patients only trace methylation of up to 16% was observed (Fig. 5.1.1-2). The methylation cut-off was set to three-fold the standard deviation of the mean of normal brain samples (n=6; threshold methylation of 13.12%). *CPEB1* methylation was detected in most of the AAIII (9/11; mean methylation of 62.31 ± 2.93%), and sGBM specimens (10/10; mean methylation of 55.40 ± 8.79%) that developed following malignant progression of lower-grade precursor lesions (Fig. 5.1.1-1). Furthermore, all examined glioblastoma cell lines showed hypermethylation of *CPEB1* (mean methylation of 72.7 ± 4.89%, data not shown). In contrast to *CPEB1*, methylation of *CPEB3* was less abundant (mean methylation of 10.19 ± 0.43%). In the cohort of investigated samples only a few pGBM cases showed an increased methylation up to 19.09% (Fig. 5.1.1-1). *CPEB2* and *CPEB4* did not demonstrate methylation of CpG-islands in any of the investigated tumors. This is indicated by a blue color on the heat map, which corresponds to the lack of methylation (Fig. 5.1.1-1).

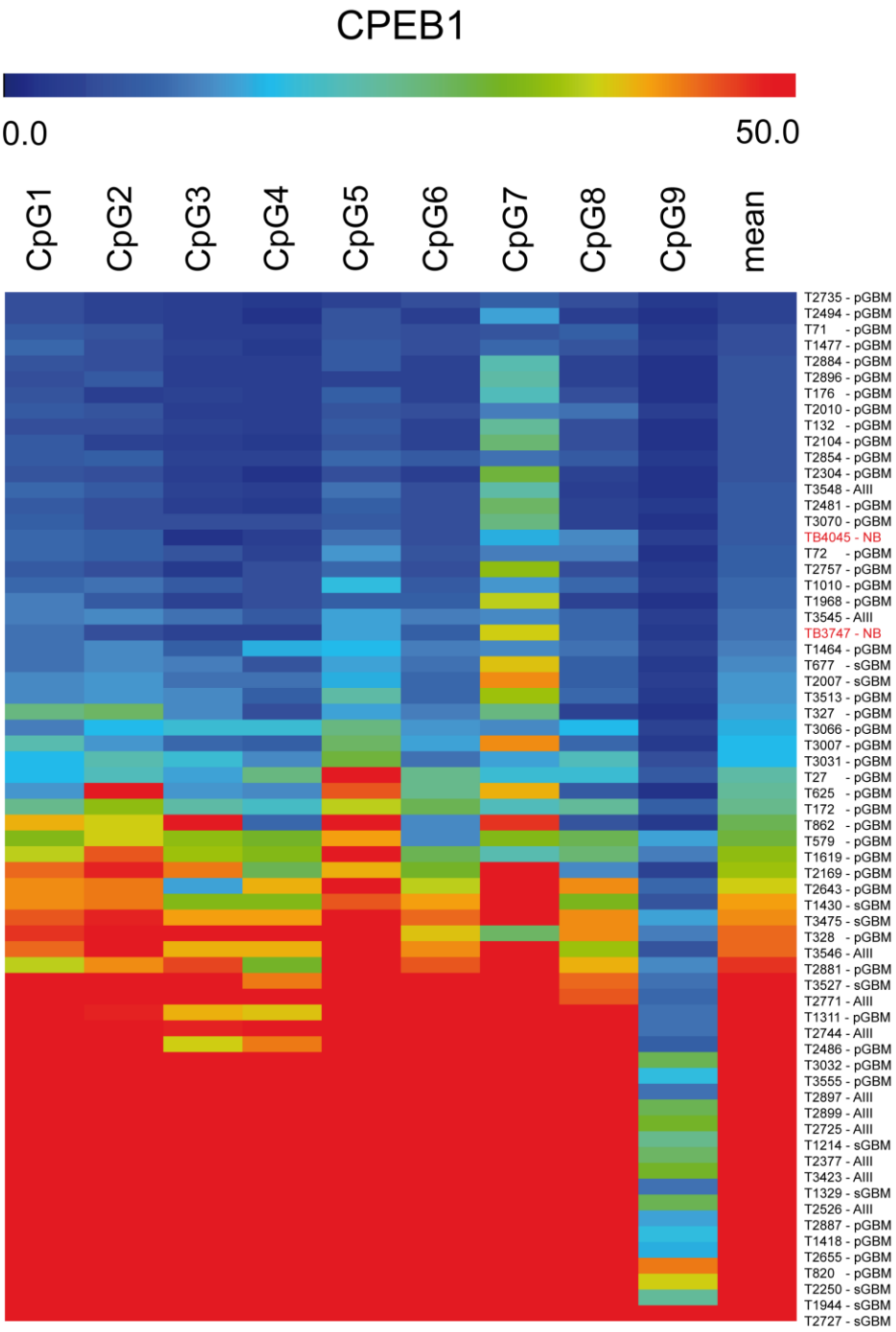
CPEB1
0.0
50.0
CpG1
CpG2
CpG3
CpG4
CpG5
CpG6
CpG7
CpG8
CpG9
mean
T2735 - pGBM
T2494 - pGBM
T71 - pGBM
T1477 - pGBM
T2884 - pGBM
T2896 - pGBM
T176 - pGBM
T2010 - pGBM
T132 - pGBM
T2104 - pGBM
T2854 - pGBM
T2304 - pGBM
T3548 - AIII
T2481 - pGBM
T3070 - pGBM
TB4045 - NB
T72 - pGBM
T2757 - pGBM
T1010 - pGBM
T1968 - pGBM
T3545 - AIII
TB3747 - NB
T1464 - pGBM
T677 - sGBM
T2007 - sGBM
T3513 - pGBM
T327 - pGBM
T3066 - pGBM
T3007 - pGBM
T3031 - pGBM
T27 - pGBM
T625 - pGBM
T172 - pGBM
T862 - pGBM
T579 - pGBM
T1619 - pGBM
T2169 - pGBM
T2643 - pGBM
T1430 - sGBM
T3475 - sGBM
T328 - pGBM
T3546 - AIII
T2881 - pGBM
T3527 - sGBM
T2771 - AIII
T1311 - pGBM
T2744 - AIII
T2486 - pGBM
T3032 - pGBM
T3555 - pGBM
T2897 - AIII
T2899 - AIII
T2725 - AIII
T1214 - sGBM
T2377 - AIII
T3423 - AIII
T1329 - sGBM
T2526 - AIII
T2887 - pGBM
T1418 - pGBM
T2655 - pGBM
T820 - pGBM
T2250 - sGBM
T1944 - sGBM
T2727 - sGBM

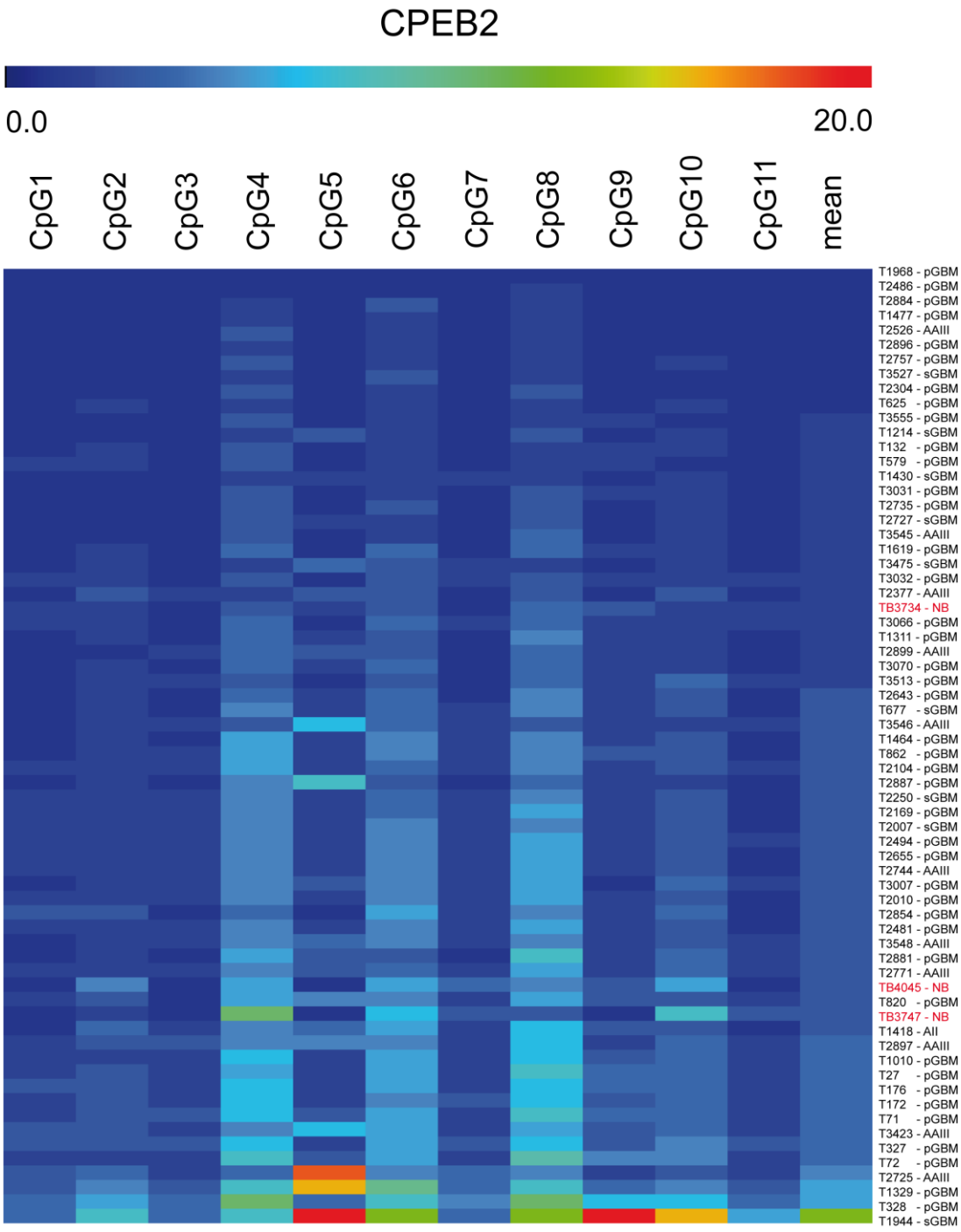
CPEB2
0.0
20.0
CpG1
CpG2
CpG3
CpG4
CpG5
CpG6
CpG7
CpG8
CpG9
CpG10
CpG11
mean
T1968 - pGBM
T2486 - pGBM
T2884 - pGBM
T1477 - pGBM
T2526 - AAIII
T2896 - pGBM
T2757 - pGBM
T3527 - sGBM
T2304 - pGBM
T625 - pGBM
T3555 - pGBM
T1214 - sGBM
T132 - pGBM
T579 - pGBM
T1430 - sGBM
T3031 - pGBM
T2735 - pGBM
T2727 - sGBM
T3545 - AAIII
T1619 - pGBM
T3475 - sGBM
T3032 - pGBM
T2377 - AAIII
TB3734 - NB
T3066 - pGBM
T1311 - pGBM
T2899 - AAIII
T3070 - pGBM
T3513 - pGBM
T2643 - pGBM
T677 - sGBM
T3546 - AAIII
T1464 - pGBM
T862 - pGBM
T2104 - pGBM
T2887 - pGBM
T2250 - sGBM
T2169 - pGBM
T2007 - sGBM
T2494 - pGBM
T2655 - pGBM
T2744 - AAIII
T3007 - pGBM
T2010 - pGBM
T2854 - pGBM
T2481 - pGBM
T3548 - AAIII
T2881 - pGBM
T2771 - AAIII
TB4045 - NB
T820 - pGBM
TB3747 - NB
T1418 - AII
T2897 - AAIII
T1010 - pGBM
T27 - pGBM
T176 - pGBM
T172 - pGBM
T71 - pGBM
T3423 - AAIII
T327 - pGBM
T72 - pGBM
T2725 - AAIII
T1329 - pGBM
T328 - pGBM
T1944 - sGBM

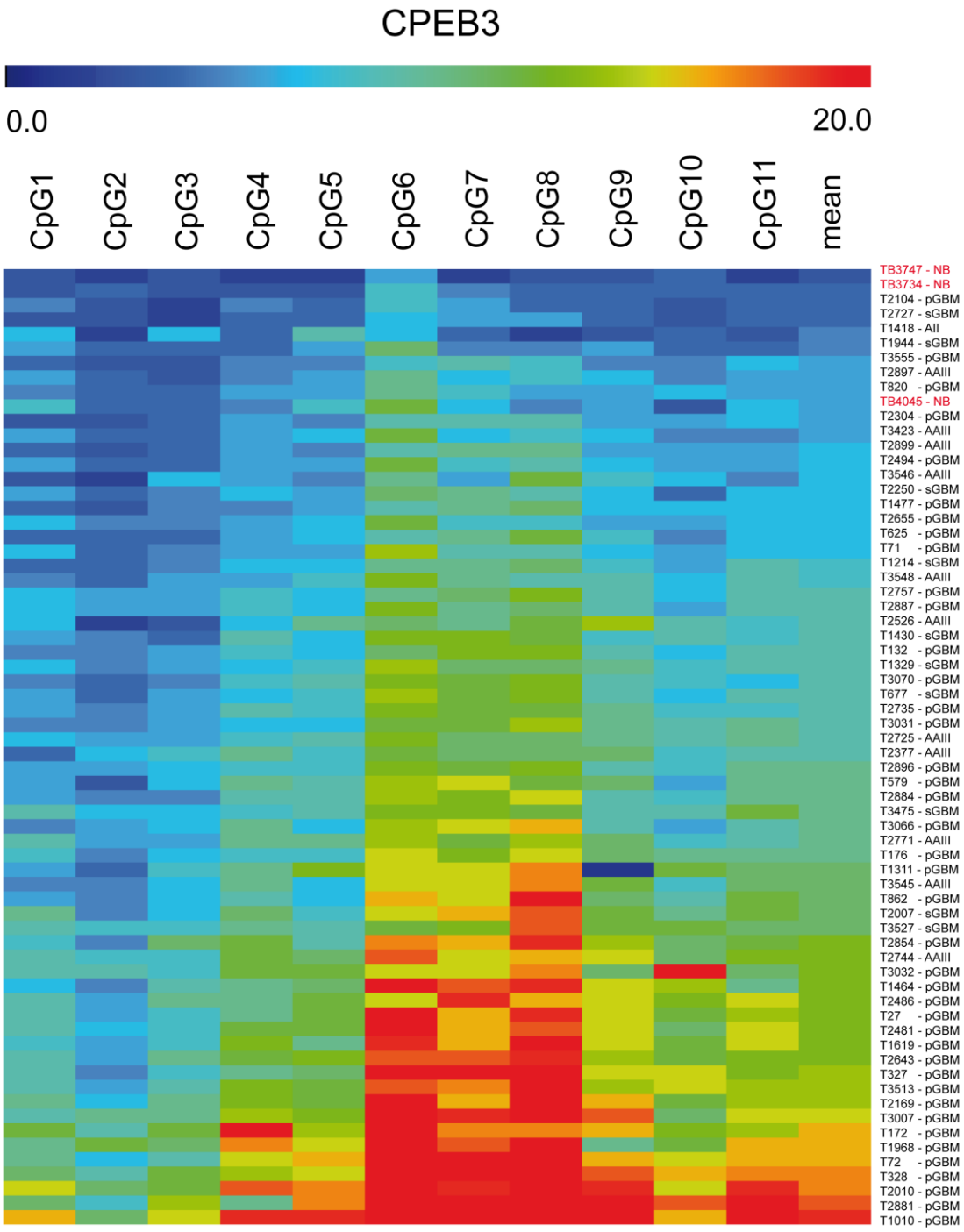
CPEB3
0.0
20.0
CpG1
CpG2
CpG3
CpG4
CpG5
CpG6
CpG7
CpG8
CpG9
CpG10
CpG11
mean
TB3747 - NB
TB3734 - NB
T2104 - pGBM
T2727 - sGBM
T1418 - AII
T1944 - sGBM
T3555 - pGBM
T2897 - AAIII
T820 - pGBM
TB4045 - NB
T2304 - pGBM
T3423 - AAIII
T2899 - AAIII
T2494 - pGBM
T3546 - AAIII
T2250 - sGBM
T1477 - pGBM
T2655 - pGBM
T625 - pGBM
T71 - pGBM
T1214 - sGBM
T3548 - AAIII
T2757 - pGBM
T2887 - pGBM
T2526 - AAIII
T1430 - sGBM
T132 - pGBM
T1329 - sGBM
T3070 - pGBM
T677 - sGBM
T2735 - pGBM
T3031 - pGBM
T2725 - AAIII
T2377 - AAIII
T2896 - pGBM
T579 - pGBM
T2884 - pGBM
T3475 - sGBM
T3066 - pGBM
T2771 - AAIII
T176 - pGBM
T1311 - pGBM
T3545 - AAIII
T862 - pGBM
T2007 - sGBM
T3527 - sGBM
T2854 - pGBM
T2744 - AAIII
T3032 - pGBM
T1464 - pGBM
T2486 - pGBM
T27 - pGBM
T2481 - pGBM
T1619 - pGBM
T2643 - pGBM
T327 - pGBM
T3513 - pGBM
T2169 - pGBM
T3007 - pGBM
T172 - pGBM
T1968 - pGBM
T72 - pGBM
T328 - pGBM
T2010 - pGBM
T2881 - pGBM
T1010 - pGBM

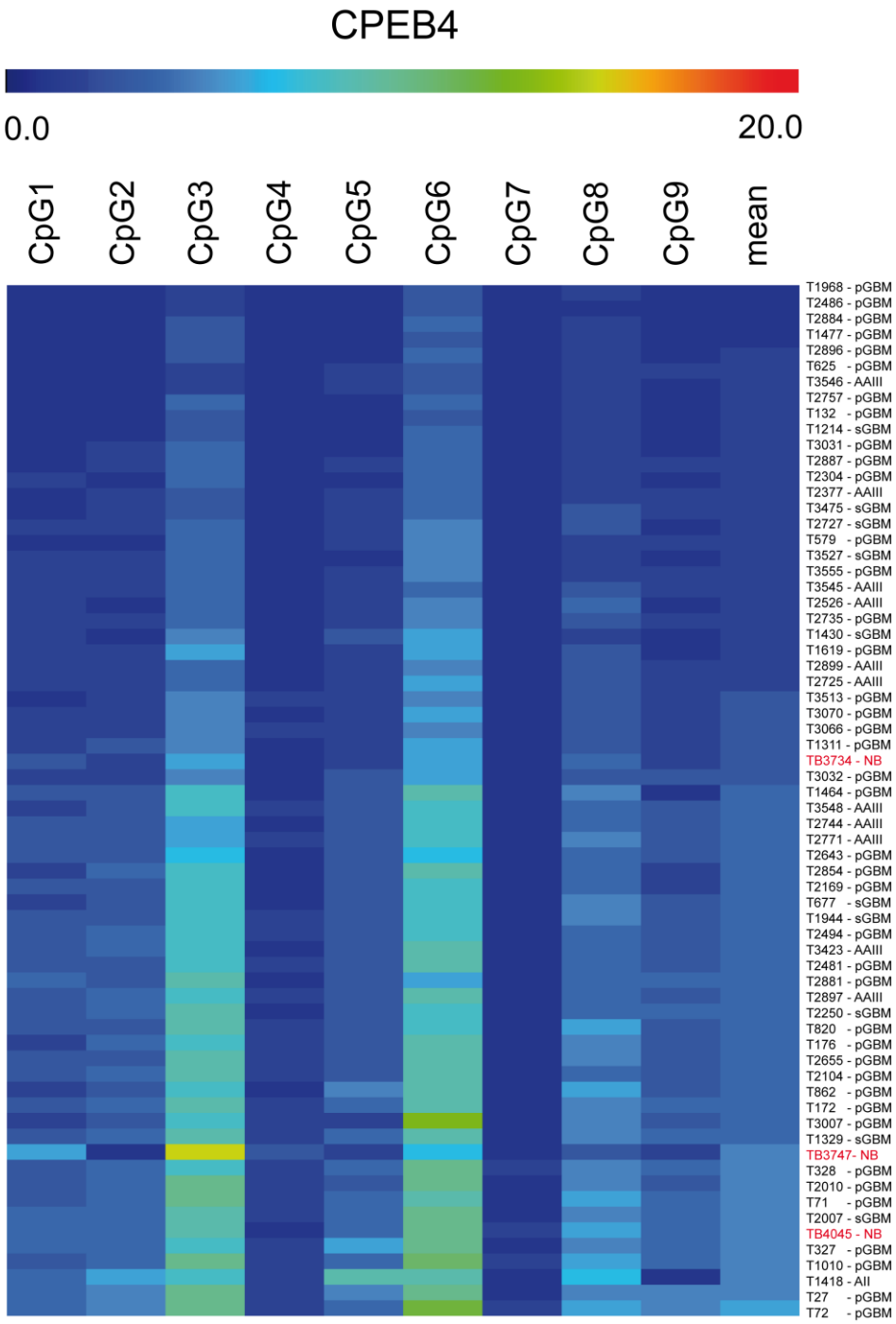
CPEB4
0.0
20.0
CpG1
CpG2
CpG3
CpG4
CpG5
CpG6
CpG7
CpG8
CpG9
mean
T1968 - pGBM
T2486 - pGBM
T2884 - pGBM
T1477 - pGBM
T2896 - pGBM
T625 - pGBM
T3546 - AAIII
T2757 - pGBM
T132 - pGBM
T1214 - sGBM
T3031 - pGBM
T2887 - pGBM
T2304 - pGBM
T2377 - AAIII
T3475 - sGBM
T2727 - sGBM
T579 - pGBM
T3527 - sGBM
T3555 - pGBM
T3545 - AAIII
T2526 - AAIII
T2735 - pGBM
T1430 - sGBM
T1619 - pGBM
T2899 - AAIII
T2725 - AAIII
T3513 - pGBM
T3070 - pGBM
T3066 - pGBM
T1311 - pGBM
TB3734 - NB
T3032 - pGBM
T1464 - pGBM
T3548 - AAIII
T2744 - AAIII
T2771 - AAIII
T2643 - pGBM
T2854 - pGBM
T2169 - pGBM
T677 - sGBM
T1944 - sGBM
T2494 - pGBM
T3423 - AAIII
T2481 - pGBM
T2881 - pGBM
T2897 - AAIII
T2250 - sGBM
T820 - pGBM
T176 - pGBM
T2655 - pGBM
T2104 - pGBM
T862 - pGBM
T172 - pGBM
T3007 - pGBM
T1329 - sGBM
TB3747- NB
T328 - pGBM
T2010 - pGBM
T71 - pGBM
T2007 - sGBM
TB4045 - NB
T327 - pGBM
T1010 - pGBM
T1418 - AII
T27 - pGBM
T72 - pGBM

Figure 5.1.1-1.

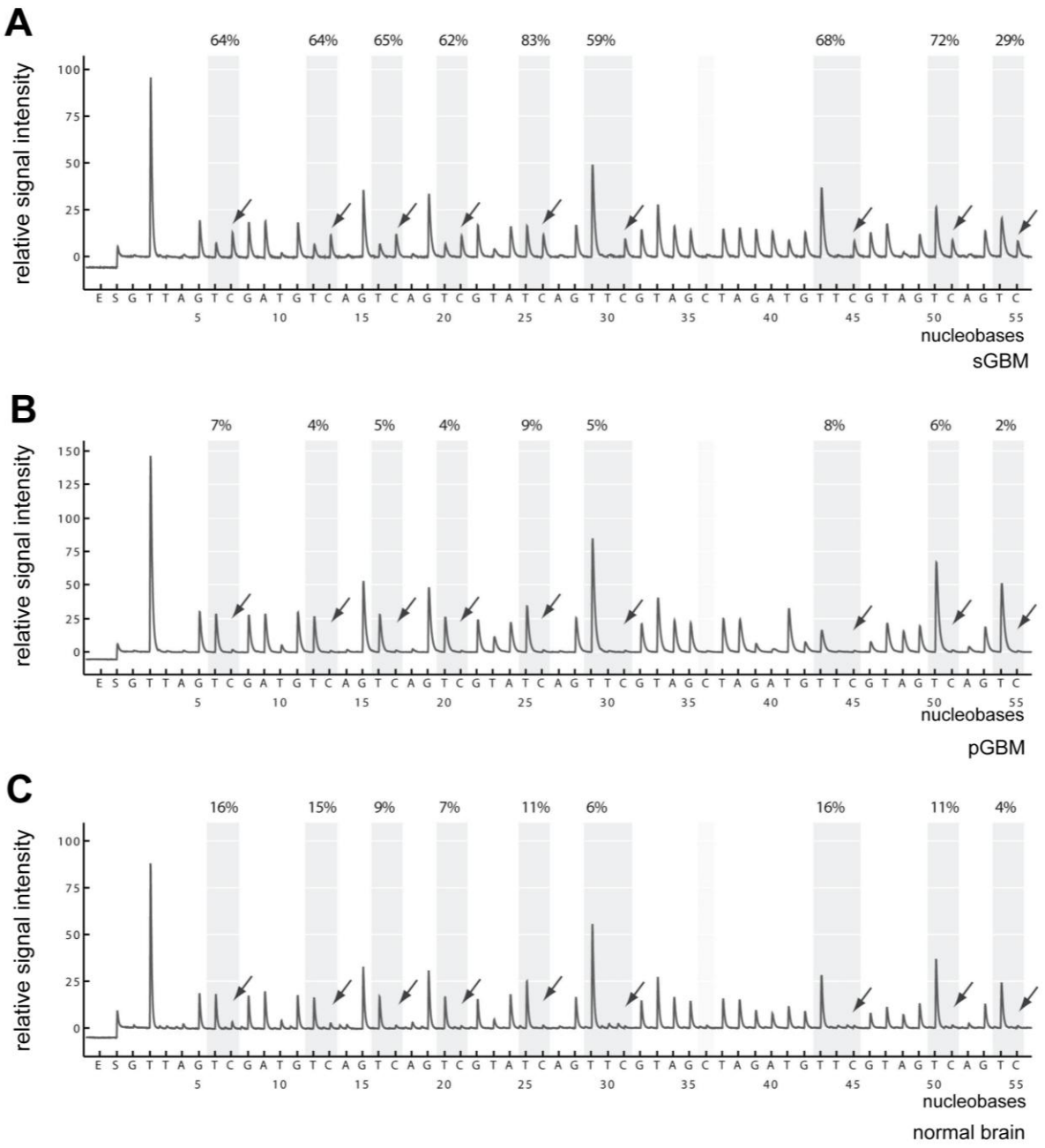

Figure 5.1.1-2.

Figure 5.1.1-1. Methylation profile of *CPEB1-4* genes in glioma and normal brain tissues. Bars above the heat maps indicate the methylation in % (range 0-50 for CPEB1; range 0-20 for CPEB2-4). Columns show investigated CpG dinucleotides, while rows present the individual glioma and control tissue samples. Blue

color corresponds to the lack of methylation, while red indicates increase in methylation of investigated tumors.

Figure 5.1.1-2. Pyrosequencing analysis of the CpG island in the 5'-region of *CPEB1* gene in sGBM, pGBM and normal brain tissue. The pyrogram of a sGBM (A) shows a strong methylation of up to 83% of the CpG positions. The pyrograms of a pGBM (B) and the normal brain tissue (C) show methylation of the investigated region up to 16%.

5.1.2 **IDH1 mutation in gliomas**

Mutation of *IDH1* gene occurs frequently in low-grade and secondary high-grade gliomas. *IDH* mutations drive increased methylation of DNA and are associated with improved prognosis for patients (Cohen et al., 2013). In the investigated cohort of gliomas, 1/1 AII, 9/11 AAIII, 7/10 sGBM and 4/41 pGBM revealed mutation in the *IDH1* gene. Secondary GBM tumors with mutated *IDH1* (n=7) demonstrated an average methylation of 69.37 ± 6.78%. Surprisingly, few pGBM samples with mutated *IDH1* (n=4) also disclosed a significant increase of *CPEB1* methylation (mean 73.53 ± 4.26%). Secondary GBMs without *IDH1* mutation (n=3) and pGBMs with wild type *IDH1* (n=37) showed an average methylation of 21.81 ± 8.93% and 19.84 ± 2.74% in the investigated region of *CPEB1* (Tab. 5.2.2-1). The described pattern indicates that *IDH1* mutation, are tightly linked to the *CPEB1* methylation status. *CPEB1* belongs to the methylation targets affected by the glioma associated CpG island methylator phenotype (G-CIMP) in *IDH1* mutant gliomas. In contrast to *CPEB1*, no correlation was observed between *CPEB3* methylation and *IDH1* mutation.

Table 5.1.2-1. Mutation of *IDH1* and methylation of *CPEB1* in human glioma specimens.

	mean± SEM	*mean*± SEM

IDH1 mutation	*no. of investigated samples*	*no. of samples with IDH1 mutation*	*CPEB1 methylation [%]*	*no. of samples without IDH1 mutation*	*CPEB1 methylation [%]*
AII	1	1	73.11	0	-
AAII	11	9	62.31±2.93	2	9.50
sGBM	10	7	69.37 ± 6.78	3	21.81 ± 8.93
pGBM	41	4	73.53 ± 4.26	37	19.84 ± 2.74%

5.1.3 **Expression profile of CPEB 1-4 in gliomas**

5.1.3.1 **Expression of CPEB 1-4 in human glioma specimens**

Histological characterization of CPEBs was the next step to understand their role in human brain cancer. Glioma specimens assembled on tissue microarrays were stained with custom CPEB antibodies and evaluated by microscopic observation and neuropathologic assessment (Fig. 5.1.3.1-1; Fig. 5.1.3.1-2; Tab. 5.1.3.1-1). All of the investigated specimens were stained with GFAP antibody to confirm their affiliation to the group of astrocytomas. CPEB1 was detected in the infiltration areas of tumor cells in normal brain tissue. However, the majority of cells in the tumor center, in the areas of angiogenesis and necrosis showed no CPEB1 expression (Fig. 5.1.3.1-1). Strong immunoreactivity against CPEB1 was present only in few (2/61) glioma tissues (Tab. 5.1.3.1-1). Downregulation of CPEB1 protein was observed with a rising grade of glioma malignancy (Fig. 5.1.3.1-2). The vast majority of astrocytoma specimens revealed a positive staining for CPEB1 (26/29: 8/8 AAII and 18/21 AAIII). 23/32 glioblastoma (6/7 sGBM and 17/25 pGBM) samples contained CPEB1 positive cells (Tab. 5.1.3.1-1). CPEB2 was present in reactive astrocytes of normal brain tissue and in endothelial cells of vessels residing within the tumor tissue (Fig. 5.1.3.1-1). Positive staining was revealed in most of the studied glioma specimens (8/9 AAII; 18/20 AAIII; 7/8 sGBM; 18/25 pGBM) (Tab. 5.1.3.1-1). Among CPEBs in gliomas, CPEB3 occurred to be the most abundant and widespread in the cytoplasm and processes of astrocytic tumor cells (Fig. 5.1.3.1-1). Strong immunoreactivity against CPEB3 was detected in 8/10 AAII, 19/20 AAIII, 7/7 sGBM and 23/24 pGBM (Tab.

5.1.3.1-1). Enhanced CPEB3 signal was associated with an increased grade of malignancy. The opposite trend was observed with a phosphospecific CPEB3 antibody. Here, phosphorylation of CPEB3 protein was observed mainly in low-grade gliomas (7/8 AAII; 17/20 AAIII) and distinctly reduced in glioblastomas (10/26 pGBM) (Tab. 5.1.3.1-1). Analogous to CPEB1, strong expression of CPEB4 was found in only few tumors (10/62) (Tab. 5.1.3.1-1). Proteins were distributed in tumor cell bodies and processes (Fig. 5.1.3.1-1). In conclusion, above experiments revealed a distinctive and differential expression pattern of individual CPEBs that could be correlated with the glioma malignancy grade.

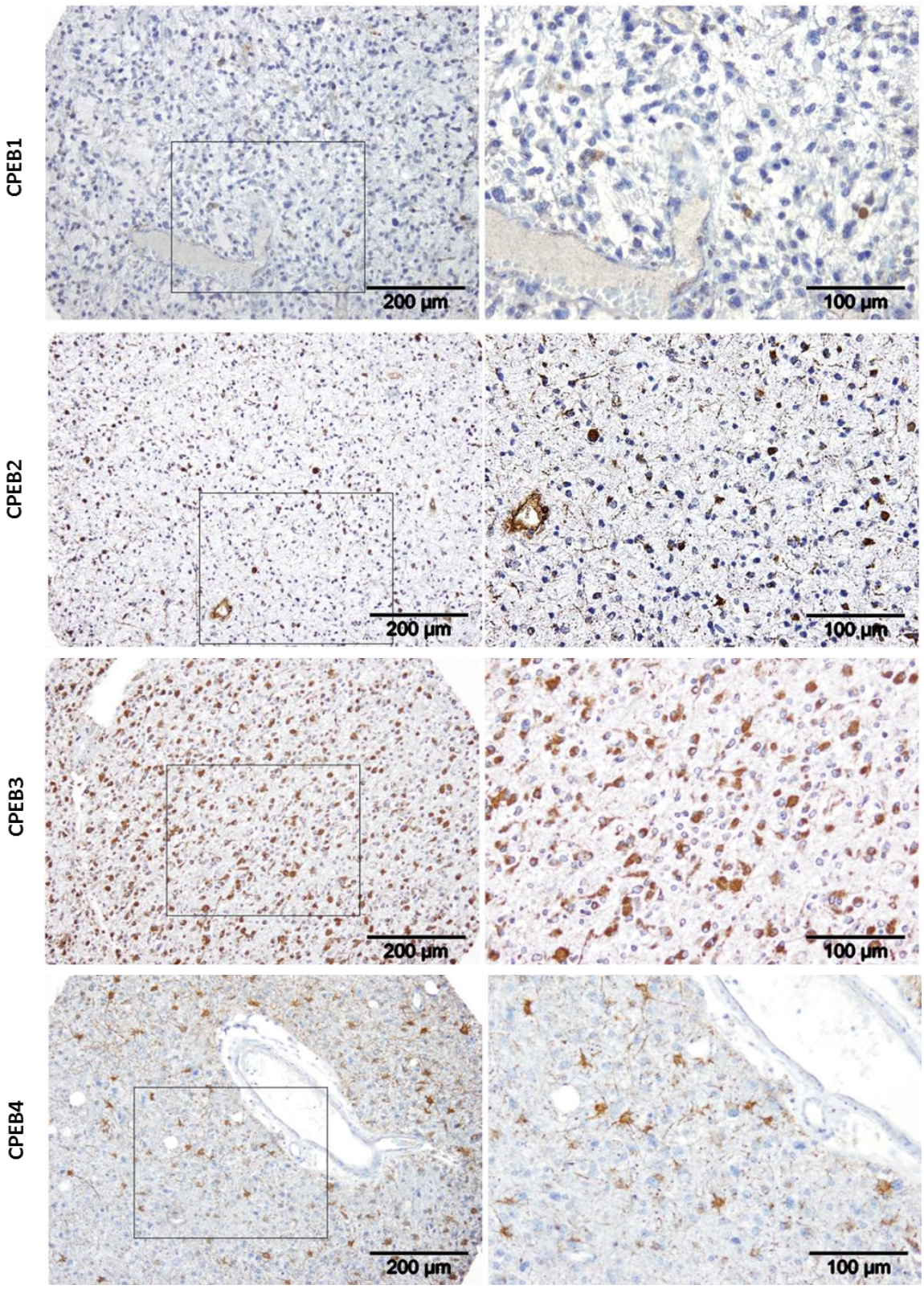

Figure 5.1.3.1-1.

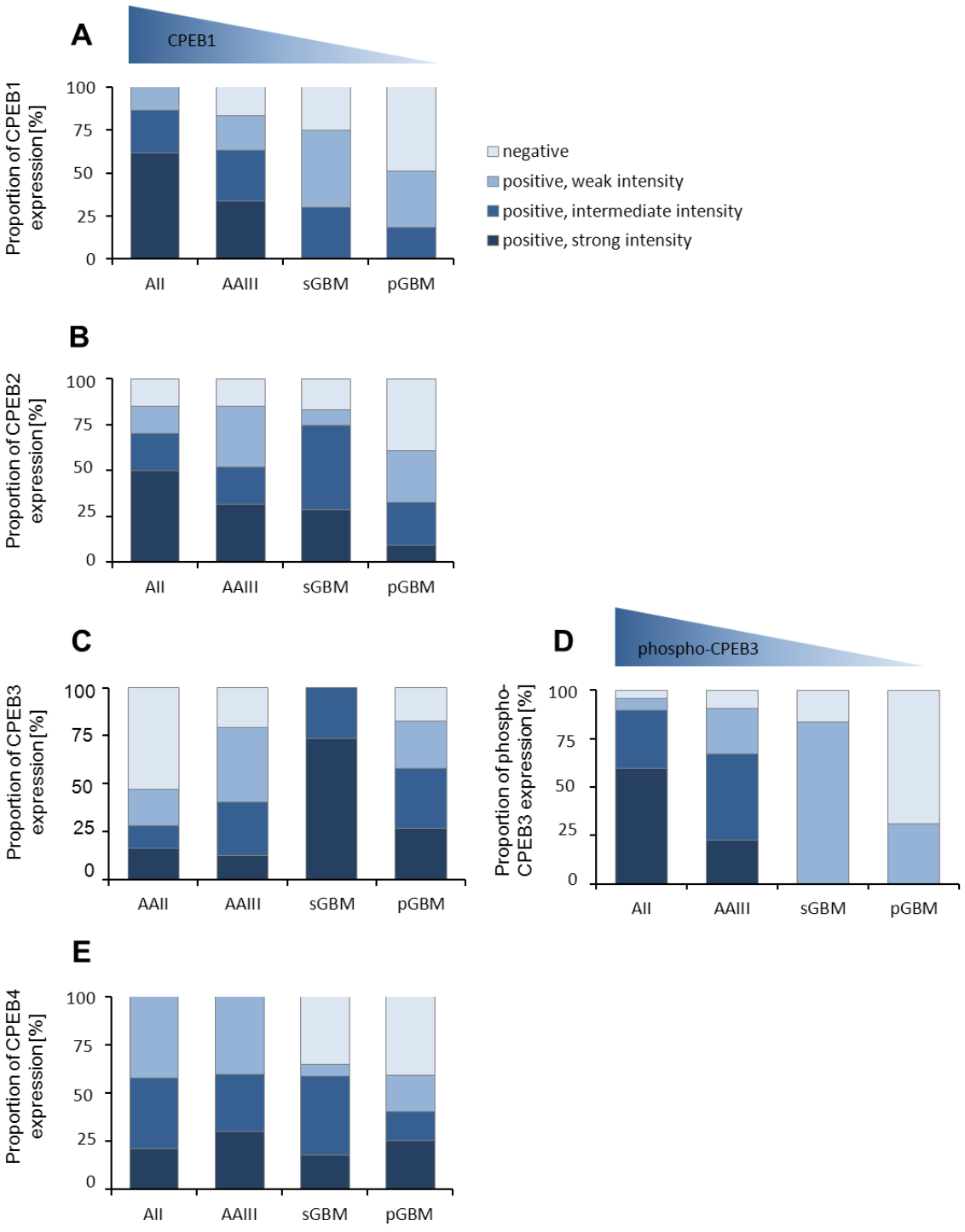

Figure 5.1.3.1-2.

Figure 5.1.3.1-1. Immunohistochemical analysis of CPEB1-4 protein expression in gliomas. Staining of AII (CPEB3) and AA III (CPEB1, CPEB2, and CPEB4) tissues with CPEB1, CPEB2, CPEB3 and CPEB4 antibodies. The brown areas represent CPEB protein deposits while the blue regions correspond to the cell nuclei.

Figure 5.1.3.1-2. Evaluation of CPEB1-4 and phospho-CPEB3 protein expression in glioma tissues. A: CPEB1, B: CPEB2, C: CPEB3, D: phospho-CPEB3, E: CPEB4: Light blue graph sections represent the lack of CPEB expression, while blue and dark blue sections correspond to the positive CPEB staining divided subsequently to intensity groups: weak, intermediate, and strong.

Table 5.1.3.1-1. Quantification of CPEB1-4 and phospho-CPEB3 expression in human glioma specimens. Table contains number of not accessible and investigated specimens assembled on tissue microarrays.

CPEB1 *expression*	*no. of not accessible samples*	*no. of investigated samples*	*no. of negative samples*	*no. of positive samples-weak intensity*	*no. of positive samples-intermediate intensity*	*no. of positive samples-strong intensity*
AII	3	8	0	3	4	1
AAII	1	21	3	8	9	1
sGBM	1	7	1	4	2	0
pGBM	3	25	8	12	5	0
sum:	8	**61**	**12**	**27**	**20**	**2**
percentage:		**100%**	**19.67%**	**44.26%**	**32.79%**	**3.28%**
CPEB2 *expression*						
AII	2	9	1	2	2	4
AAII	2	20	2	9	4	5
sGBM	0	8	1	1	4	2
pGBM	3	25	7	10	6	2
sum:	7	**62**	**11**	**22**	**16**	**13**
percentage:		**100%**	**17.74%**	**35.48%**	**25.81%**	**20.97%**
CPEB3 *expression*						
AII	1	10	2	3	3	2
AAII	2	20	1	8	9	2
sGBM	1	7	0	0	3	4
pGBM	4	24	1	6	12	5
sum:	8	**61**	**4**	**17**	**27**	**13**
percentage:		**100%**	**6.56%**	**27.87%**	**44.26%**	**21.31%**

phospho-CPEB3 *expression*	*no. of not accessible samples*	*no. of investigated samples*	*no. of negative samples*	*no. of positive samples- weak intensity*	*no. of positive samples- intermediate intensity*	*no. of positive samples- strong intensity*
AII	3	8	1	2	3	2
AAII	2	20	3	10	6	1
sGBM	0	8	1	7	0	0
pGBM	2	26	16	10	0	0
sum:	7	**62**	**21**	**29**	**9**	**3**
percentage:		**100%**	**33.87%**	**46.77%**	**14.52%**	**4.84%**
CPEB4 *expression*						
AII	1	10	0	6	3	1
AAII	2	20	0	12	5	3
sGBM	1	7	1	1	4	1
pGBM	3	25	4	11	5	5
sum:	7	**62**	**5**	**30**	**17**	**10**
percentage:		**100%**	**8.06%**	**48.39%**	**27.42%**	**16.13%**

5.1.3.2 **Correlation of CPEB 1-4 expression with clinical prognosis of glioma patients**

Clinical course of glioma patients was correlated with CPEB expression data by Kaplan-Meier survival analysis. Overall survival was determined as a time between surgery of primary tumor and death of the patient. When the expression of CPEB1 protein in all investigated samples (n=61) was compared with patients survival no correlation was detected (Fig. 5.1.3.2-1A). Nevertheless, if the studied group was narrowed to only low-grade astrocytoma samples (n=29), the Kaplan-Meier curve suggested a positive correlation between CPEB1 expression and longer patient survival (Fig. 5.1.3.2-1B). The remaining pGBM (17/25) and sGBM (6/7) specimens expressing CPEB1 protein did not reveal any significant relation with the life expectancy of patients. Despite a robust expression, neither CPEB2-3 nor CPEB4 showed correlation with survival of glioma patients (Fig. 5.1.3.2-1C, D, G). CPEB3 activation, as determined by phosphorylation was significantly correlated with longer patient survival in all investigated tumor samples (n=62) (Fig. 5.1.3.2-1E). Interestingly, in the analysis focused on low-grade astrocytomas (n=28), which are considered precursor lesions for sGBM and show a molecular pathology distinct from pGBM, a significant correlation between CPEB3 activity and prolonged patient survival

was observed (Fig. 5.1.3.2-1F). It indicates that phospho-CPEB3 protein might be a novel biological marker for a better prognosis of low-grade glioma patients. However, it may be also considered as a marker of glioma patients independently of histological entity or grading.

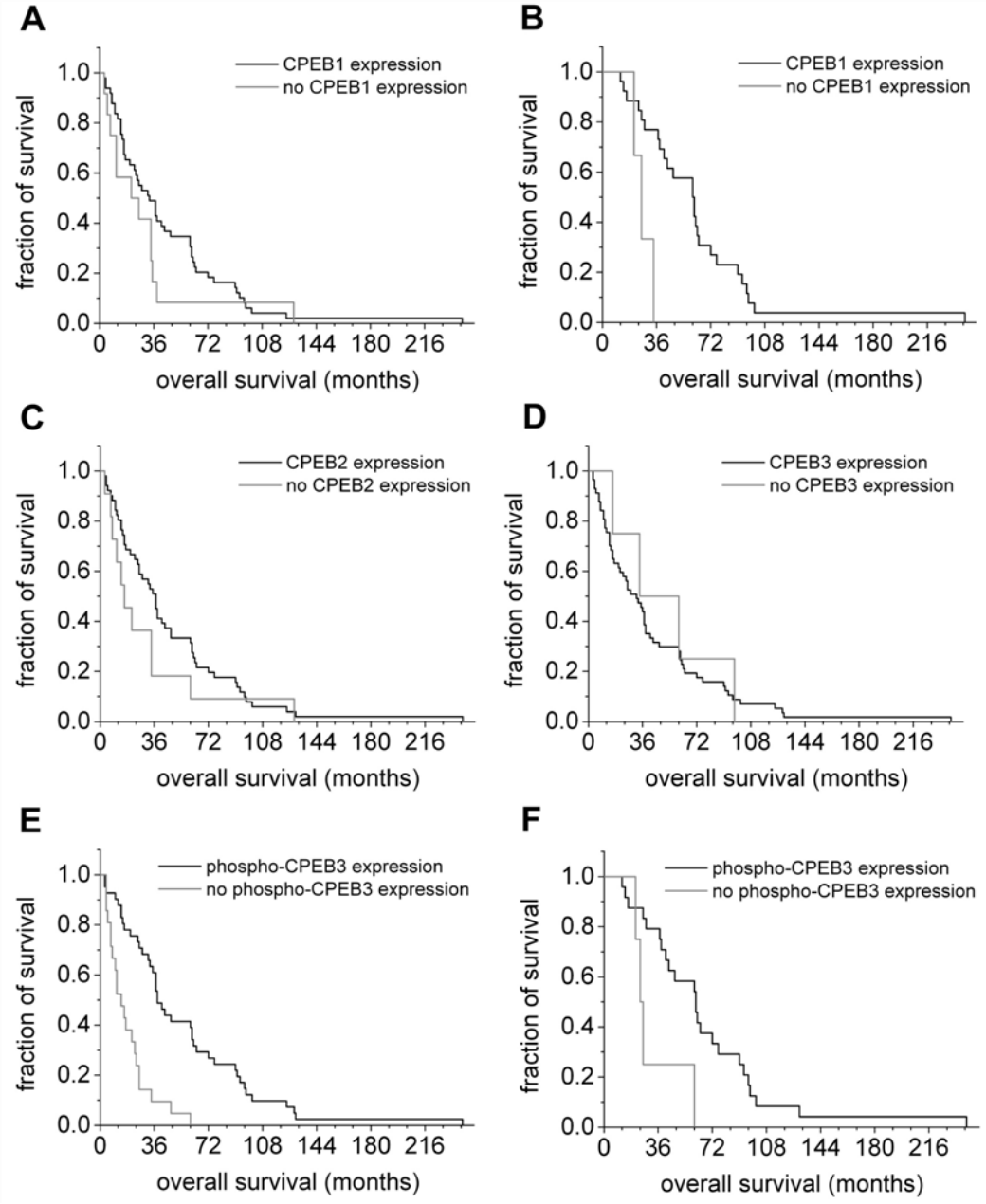

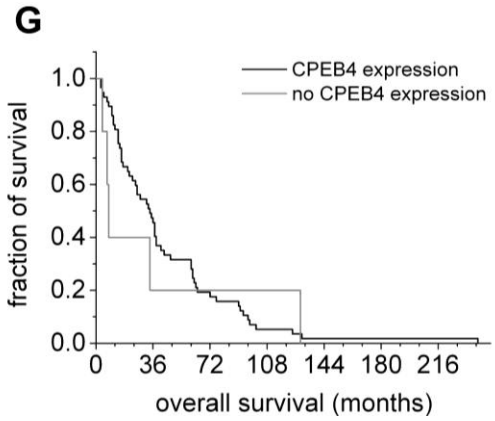

Figure 5.1.3.2-1. Correlations between expression of CPEB 1-4 and survival of glioma patients. A: Kaplan- Meier survival analysis showed no correlation between CPEB1 expression and longer survival in all investigated glioma patients B: Positive correlation between CPEB1 expression and patient survival was observed in a subpopulation of AAII and AAIII. C, D, G: No correlation was observed between CPEB2, CPEB3 and CPEB4 expression and patient survival. E: Significant correlation between phospho-CPEB3 expression and survival data was observed in all investigated glioma samples. F: Detail studies on AAII and AAIII (n=28) as well as primary (n=26) and secondary (n=8) GBM samples indicated that phospho-CPEB3 expression when compared to survival reach statistical significance only in the group of AAII and AAIII.

5.1.4 *CPEB1* gene methylation and its influence on expression profile.

The current study on expression of CPEBs in gliomas revealed an interesting dependency between tumor malignancy grade and the change in their expression level. In parallel to the increasing grade of glioma, expression of CPEB1 protein decreased (Fig. 5.1.3.1-2; Tab. 5.1.3.1-1). The observed effect was verified by sqRT-PCR transcript analysis in glioma (n=25) and reference normal brain (n=6) samples. Investigated specimens contained significantly reduced transcript level, as compared to the control tissue. In particular, CPEB1 expression was decreased by 37% in AAIII (n=6), 6 % and 9 % in sGBM (n=3) and pGBM (n=16) (Fig. 5.1.4-1A), respectively. Afterwards, the same set of specimens was analyzed for *CPEB1* gene methylation. A significant increase in methylation was detected in AAIII and sGBM, but not in pGBM, when compared to the control brain samples (Fig. 5.1.4-1B). As hypermethylation of DNA is considered to have an inhibitory effect on gene expression, the correlation between methylation and expression profile of CPEB1 was examined performing Pearson's correlation analysis (data not shown). However, despite the

strong trend indicating such dependence, *CPEB1* methylation and expression were not correlated.

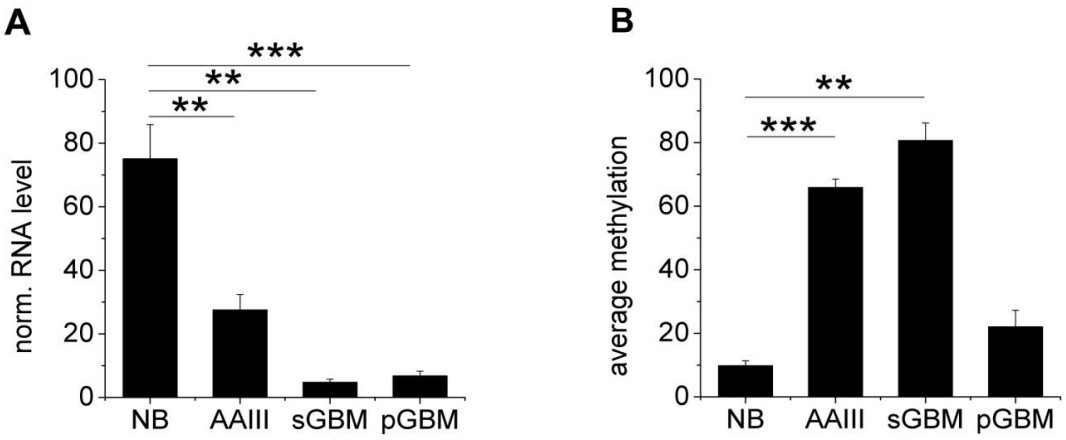

Figure 5.1.4-1. Comparison of *CPEB1* methylation and expression in glioma and reference samples. A: Significant decrease of CPEB1 transcript was observed with rising grade of tumor malignancy in AAIII, sGBM and pGBM samples. B: Significant increase in *CPEB1* methylation was observed in AAIII and sGBM, but not in pGBM samples.

5.1.5 **Activity dependent expression of CPEB3 protein in gliomas**

Evaluation of CPEB3 and the phospho-CPEB3 protein uncovered their differential expression patterns in human glioma specimens. In parallel to the rising grade of glioma malignancy, expression of CPEB3 increased, while expression of phospho-CPEB3 was reduced (Fig. 5.1.3.1-2C, D). To confirm the specificity of phospho-CPEB3 antibody, the splice variants of CPEB3a, CPEB3aKD (CPEB3a kinase dead) or CPEB3b were cloned into the pEGFP-N1 expression vector and overexpressed in HEK-293FT cells (Fig. 5.1.5-1). Transfection of CPEB3 plasmids was followed by cell stimulation with 200 μM forskolin, which increases the intracellular cAMP concentration and activates PKA. Afterwards, expression of CPEB3 variants was quantified by Western blot analysis. The full-length CPEB3a isoform was detected by both, CPEB3 and phospho-CPEB3 antibody. The effect of forskolin stimulation was observed as an increased intensity bands detected

by phosphospecific CPEB3 antibody in CPEB3a overexpressing cells. The CPEB3aKD variant contained two serines (S419; S420) in the phosphorylation site, which were mutated to alanine. Therefore, despite forskolin treatment, no phosphorylation was observed. Similarly, CPEB3b isoform lacking the B-region localized next to putative phosphorylation sites for PKA, CaMKII and RPS6K did not reveal any phosphorylation (Fig. 5.1.5-1). This finding confirmed that only the CPEB3 isoform comprising both, phosphorylation sites and the B-region, could be effectively activated by phosphorylation.

Next, in order to understand activity dependent CPEB3 expression, CPEB3, phospho-CPEB3 and kinases indicated before as putative CPEB3 activators, CaMKII and PKA, were further examined by immunostaining (Kaczmarczyk et al., 2016; Theis et al., 2003). Two groups of tumor samples were investigated. The first group of low-grade astrocytomas (n=6; AII and AAIII) was characterized by strong CPEB3 and phospho-CPEB3 expression. The second group contained primary GBMs samples (n=7) positive for CPEB3, but negative for phospho-CPEB3 antibody (Fig 5.1.5-2). Robust expression of PKA and phospho-CaMKII was detected in low-grade astrocytomas, which also contained active CPEB3 protein (Fig 5.1.6-1). However, despite the kinases activity in high-grade gliomas, the expression of phosphorylated CPEB3 protein was reduced (Fig 5.1.5-2). Therefore, lack of active kinases cannot explain the loss of CPEB3 phosphorylation in high-grade gliomas.

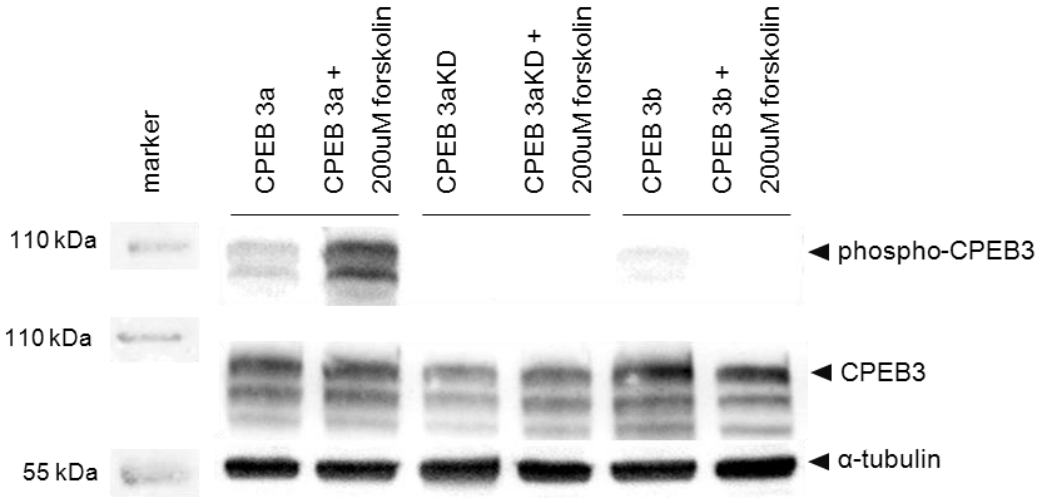

Figure 5.1.5-1.

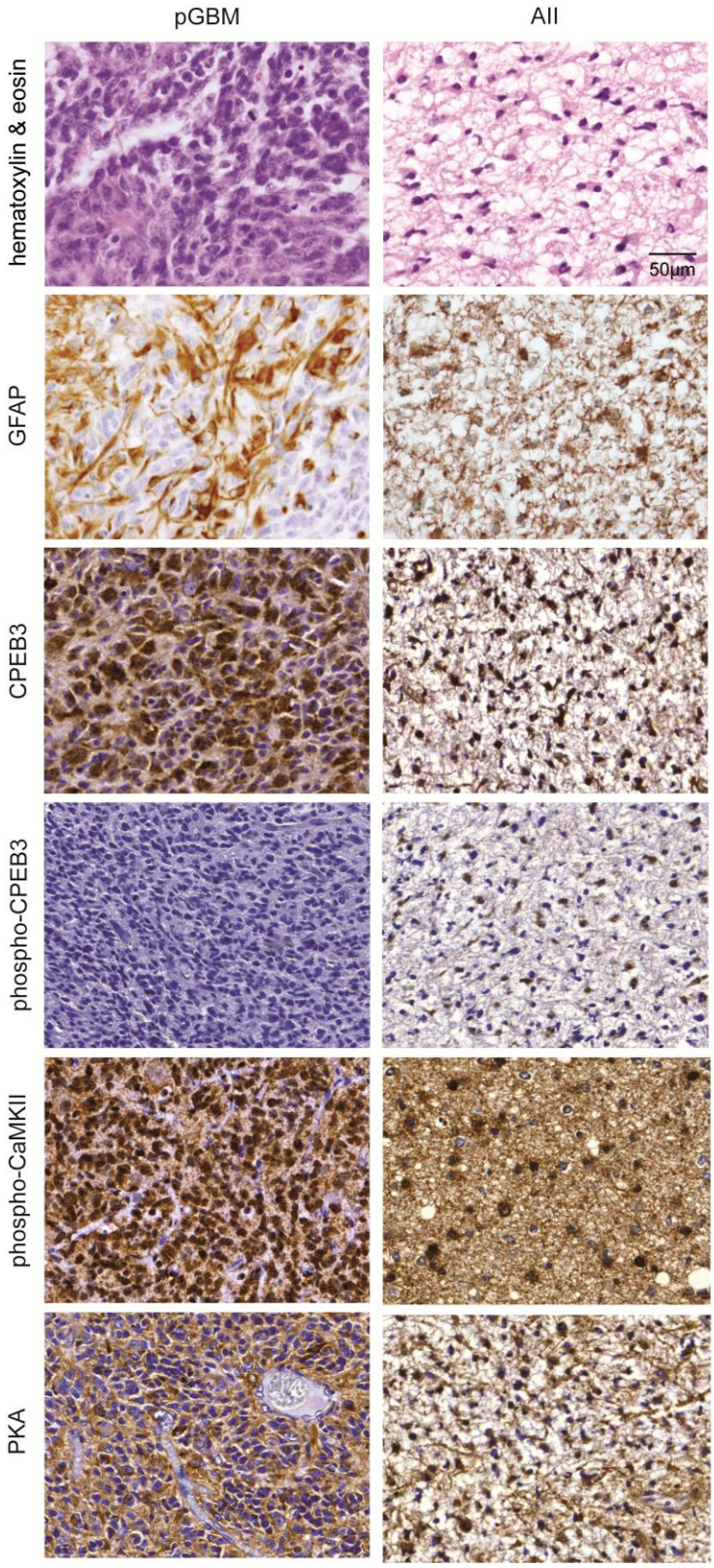
pGBM
AII
hematoxylin & eosin
50µm
GFAP
CPEB3
phospho-CPEB3
phospho-CaMKII
PKA

Figure 5.1.5-2.

Figure 5.1.5-1. Immunoblot presenting phosphorylation of CPEB3a-EGFP, CPEB3aKD-EGFP and CPEB3b-EGFP isoforms in HEK-293FT cells. Overexpressed CPEB3-EGFP protein was stimulated with forskolin to activate PKA. Immunoreactivity against CPEB3 antigene was detected in all investigated splice isoforms, while immunoreactivity against phospho-CPEB3 antigene was observed only in the CPEB3a variant.

Figure 5.1.5-2. Immunohistochemical analysis of altered CPEB3 activity in low-grade astrocytoma and primary GBM specimens. In the upper row of the figure cell nuclei (violet) and cytoplasm (pink) were stained by hematoxylin and eosin, respectively. The following lower rows represent brown areas of respective: GFAP; CPEB3; phospho-CPEB3; phospho- CaMKII; PKA antibody staining and dark blue areas corresponding to cell nuclei stained by hematoxylin.

5.1.6 **Alternative splice isoforms of CPEB1-4 in human gliomas**

The presence of multiple alternative splice isoforms of CPEB paralogs uncovered the complexity of their regulatory functions. Here, alteration in the abundance of CPEB1-4 splice variants was studied in primary glioma tissues (n=58), glioblastoma cell lines (n=5), and normal brain tissues (n=4) (Tab. 5.1.6-1). The optimized RT-PCR approach allowed for the quantitative assessment of CPEB variants by electrophoretic separation of fluorescently labeled PCR products. Differences between CPEB splice variants depend on presence or absence of respective B- and C-regions. Of particular importance is the B-region adjacent to the two serine residues (S419; S420), because it is responsible for phosphorylation and further activation of CPEBs (Fig. 5.1.6-1).

In the present study, a significant change in expression of alternative transcripts was observed between tumor and reference brain tissues. Most of the investigated AAIII specimens contained the same alternative transcripts, while GBMs lost several of the CPEB2-4 splice variants as compared to normal brain samples (Fig. 5.1.6-2). In the reference tissue the following alternative variants of CPEBs were the most abundant: CPEB1Δ5 (169bp); CPEB2a (375bp; full-length isoform), CPEB2c (286bp; lack of C- and E-region); CPEB3a (600bp; full-length isoform), CPEB3b (576b; lack of B-region), CPEB3c (531bp; lack of C-region), CPEB3d (507bp; lack of B- and C-region); CPEB4a (277bp; full-length isoform of CPEB4), CPEB4b (254bp; lack of B-region), CPEB4c

(226bp; lack of C-region), CPEB4d (203bp; lack of B- and C-region) (Fig. 5.1.6-2). Interestingly, the abundance of CPEB1 seemed not to be altered in gliomas. In all except two pGBM samples, which revealed the 182bp CPEB1 splice variant, corresponding to the full-length isoform, the only found CPEB1 transcript was 169bp CPEB1Δ5 (Fig. 5.1.6-2; Tab. 5.1.6-1). The abundance of the full-length isoforms of CPEB2-4 appeared to be reduced and instead the b/d variants, lacking the B-region were expressed. Consequently 20/37 pGBM and 5/8 sGBM samples were deprived of CPEB2a, 36/37 pGBM and 8/8 sGBM samples were deprived of CPEB3a and 30/37 pGBM and 6/8 sGBM were deprived of CPEB4a as compared to AAIII and reference tissues (Tab. 5.1.6-1). Furthermore, 11/37pGBM and 3/8 sGBM samples were devoid of the CPEB2c*, while 35/37 pGBM and 6/8 sGBM samples were devoid of the CPEB4c variant also containing the B-region (Tab. 5.1.6-1). Additionally, some of the detected CPEB2 isoforms contained the E-region (Tab. 5.1.6-1; Fig. 5.1.6-1), which was previously described in mouse CPEB2 (Turimella et al., 2015).

Differences between splice isoforms were further reflected by properties of the expressed proteins, because only CPEB a/c variants containing the B-region were subject to phosphorylation. As most of the splice variants missing the B-region were expressed in high-grade gliomas, alternative splicing seemed to play an important role in tumor progression.

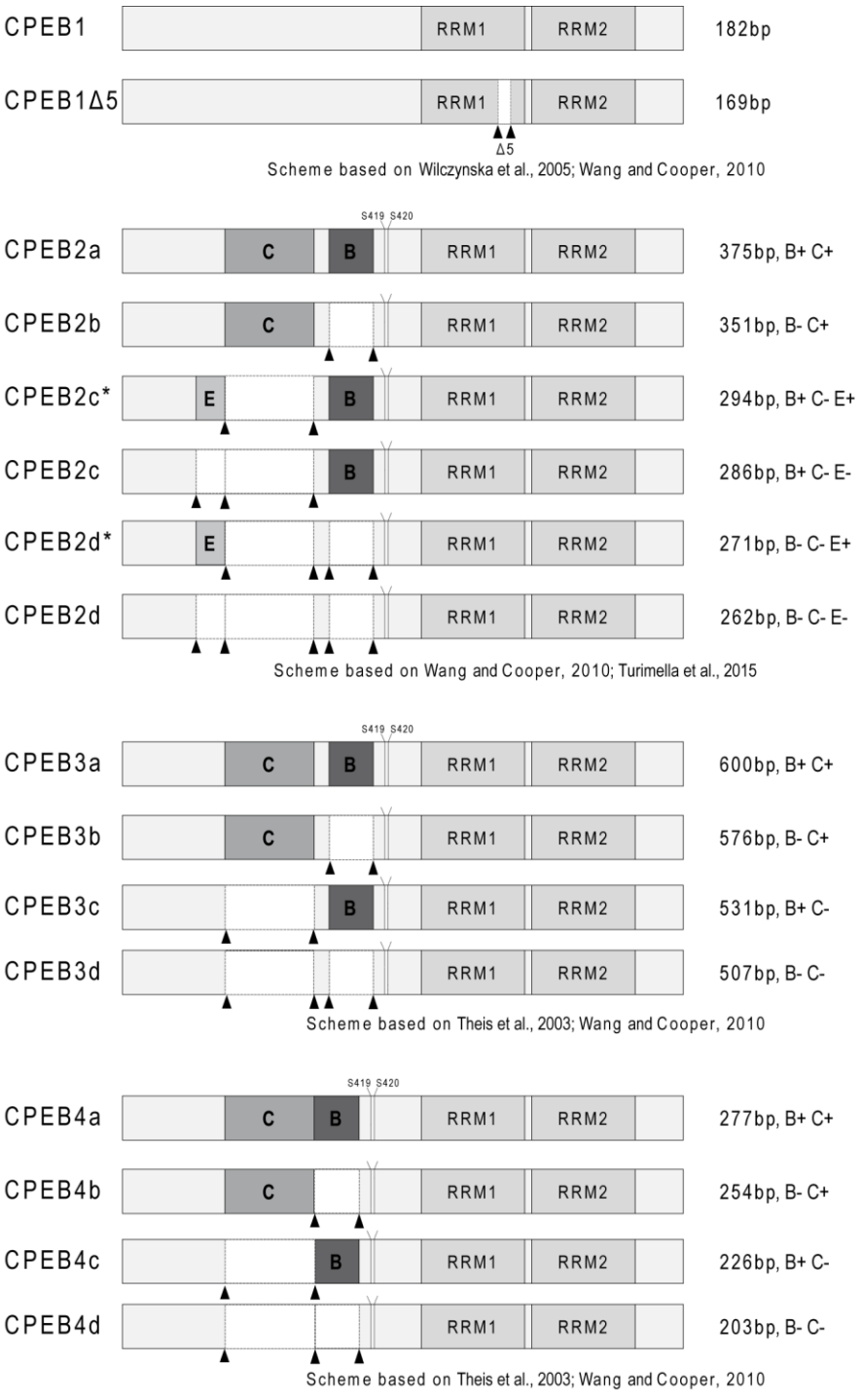
CPEB1
RRM1
RRM2
182bp
CPEB1Δ5
RRM1
RRM2
169bp
Δ5
Scheme based on Wilczynska et al., 2005; Wang and Cooper, 2010
S419 S420
CPEB2a
C
B
RRM1
RRM2
375bp, B+ C+
CPEB2b
C
RRM1
RRM2
351bp, B- C+
CPEB2c*
E
B
RRM1
RRM2
294bp, B+ C- E+
CPEB2c
B
RRM1
RRM2
286bp, B+ C- E-
CPEB2d*
E
RRM1
RRM2
271bp, B- C- E+
CPEB2d
RRM1
RRM2
262bp, B- C- E-
Scheme based on Wang and Cooper, 2010; Turimella et al., 2015
S419 S420
CPEB3a
C
B
RRM1
RRM2
600bp, B+ C+
CPEB3b
C
RRM1
RRM2
576bp, B- C+
CPEB3c
B
RRM1
RRM2
531bp, B+ C-
CPEB3d
RRM1
RRM2
507bp, B- C-
Scheme based on Theis et al., 2003; Wang and Cooper, 2010
S419 S420
CPEB4a
C
B
RRM1
RRM2
277bp, B+ C+
CPEB4b
C
RRM1
RRM2
254bp, B- C+
CPEB4c
B
RRM1
RRM2
226bp, B+ C-
CPEB4d
RRM1
RRM2
203bp, B- C-
Scheme based on Theis et al., 2003; Wang and Cooper, 2010

Figure 5.1.6-1.

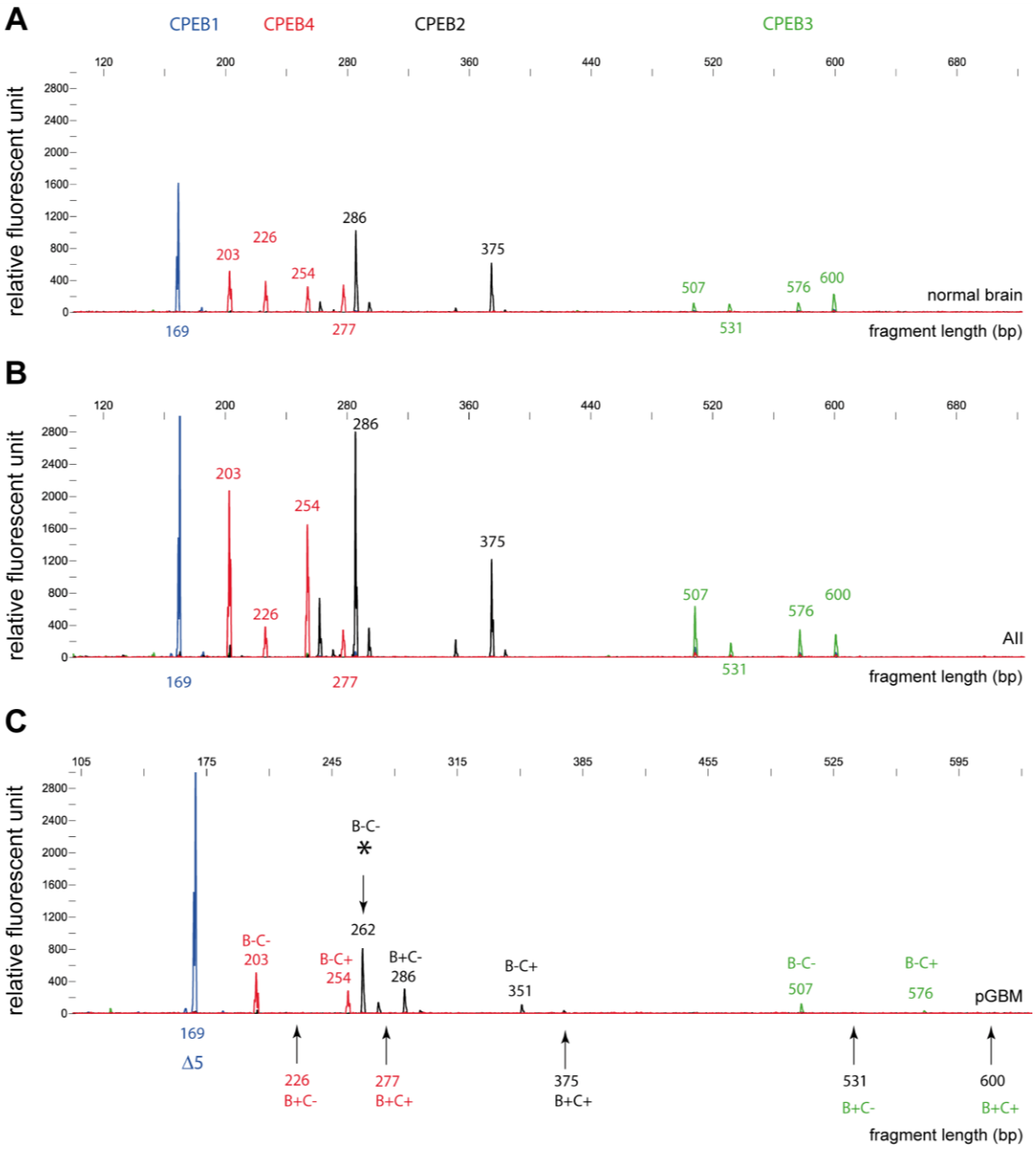
A
CPEB1
CPEB4
CPEB2
CPEB3
relative fluorescent unit
fragment length (bp)
normal brain
169
203
226
254
277
286
375
507
531
576
600
B
All
C
pGBM
B-C-
B-C+
B+C-
B+C+
262
351
Δ5
226 B+C-
277 B+C+
375 B+C+
531 B+C-
600 B+C+

Figure 5.1.6-2.

Figure 5.1.5-1. Scheme of CPEB1-4 splice variants detected by fragment analysis in normal brain and glioma samples. Individual panels contain labeled B, C or E-regions and phosphorylation sites of respective CPEB variants.

Figure 5.1.6-2. Relative abundance of respective splice variants of the four CPEB genes revealed by the RT-PCR fragment analysis. Values of the x-axis correspond to the fragment length of the RT-PCR product given in base pairs. The y-axis defines signal intensity (relative fluorescent units) which is proportional to the amount of generated PCR product. The size of the RT-PCR product generated by fragment analysis does not describe the actual length of the respective splice product, but length of fragments detected with primers spanning previously defined splice variants.

Table 5.1.6-1. The RT-PCR products of specific splice variants of the CPEB1-4 genes detected in AII; AAIII, pGBM, sGBM, normal brain tissues and GBM cultured cells. The upper values above the table correspond to the RT-PCR product (size in base pairs) generated by fragment analysis. The following alternative variants of CPEBs were detected: CPEB1Δ5 (169bp), CPEB1 (182bp); CPEB2d (262bp; lack of B, C, E-region) CPEB2d* (271bp; lack of B, C-region), CPEB2c (286bp; lack of C, E-region), CPEB2c* (294bp; lack of C-region), CPEB2b (351bp; lack of B-region), CPEB2a (375bp; full-length isoform); CPEB3d (507bp; lack of B, C-region), CPEB3c (531bp; lack of C-region), CPEB3b (576b; lack of B-region), CPEB3a (600bp; full-length isoform); CPEB4d (203bp; lack of B, C-region), CPEB4c (226bp; lack of C-region), CPEB4b (254bp; lack of B-region), CPEB4a (277bp; full-length isoform of CPEB4).

A

Detected splice isoforms:			CPEB1 Δ5	CPEB1		
Diagnose	ID-T-Nummer	CPEB1	169 bp	182 bp	508 bp	599 bp
AAIII	2377		26683			
AAIII	2526		30894			
AAIII	2725		21376			
AAIII	2744		23806			
AAIII	2771		31813			
AAIII	2897		37449			
AAIII	2899		24278			
AAIII	3423		54168			
AAIII	3545		28195			
AAIII	3546		45194			
AAIII	3548		34216			
AAIII	4045		32681			
pGBM	71		38072			
pGBM	72		32832			
pGBM	132		27337			
pGBM	172		21483			
pGBM	327		7186			
pGBM	328		25658			
pGBM	625		27745			
pGBM	862		19256			
pGBM	1010		25856			
pGBM	1311		30762			
pGBM	1619		20905			
pGBM	1968		26145			
pGBM	2010		34031			
pGBM	2104		23173			
pGBM	2169		18711			
pGBM	2304		25799			
pGBM	2481		27551			
pGBM	2486		26420			
pGBM	2494		30091			
pGBM	2735		43101			
pGBM	2757		20864			
pGBM	2854		30034			
pGBM	2884		21244			
pGBM	2896		19339			
pGBM	3007		52052			
pGBM	3031		37154			
pGBM	3032		26770			
pGBM	3066		7859			
pGBM	3070		16581	1909		
pGBM	3513		30871			
pGBM	3747		36070			
GBM oligo	2655		20061			
GBM RZ	3527		21366			
GBM sark	2643		17833			
GBM sark	3555		18439	2160		
Normal Brain	NBfrontal		17581			
Normal Brain	NBoccipital		14549			
Normal Brain	NBparietal					1864
Normal Brain	NBtemporal		24982			
All	1418		26306			
pGBM LÜ	820		38785			
pGBMsark	176		24154			
sGBM	677		18769		3412	
sGBM	1214		24461			
sGBM	1329		39085			
sGBM	1430		24163			
sGBM	1944		16999			
sGBM	2007		43109			
sGBM	2727		20646			
sGBM	3475		17974			
GBM cells	A172		38776			
GBM cells	LN229		20089			
GBM cells	LN428		27441			
GBM cells	T98G		23426			
GBM cells	U178		48217			

more abundant in normal brain tissue and reduced or lacking in tumors

more abundant in glioma tissue and reduced or lacking in normal brain tissues

B

Detected splice isoforms:					CPEB2d	CPEB2d*	CPEB2c	CPEB2c*	CPEB2b	CPEB2a
Diagnose	ID-T-Nummer	CPEB2	170 bp	203 bp	262 bp	271 bp	286 bp	294 bp	351 bp	375 bp
AAIII	2377				19243	3816	21200		7022	8456
AAIII	2526				15307		28051	4055		4453
AAIII	2725				13604	2454	17950	2852	3193	4612
AAIII	2744				7681		12972			4560
AAIII	2771				8959	1071	13648	1525	1776	2961
AAIII	2897				9514		34779	4853	2798	16075
AAIII	2899				5384		24686	4201		8263
AAIII	3423				9284		23739	2808		6835
AAIII	3545				19103		31827	3676	4930	10797
AAIII	3546				9080		34540	6921		7906
AAIII	3548				12417		23140	2490	3353	7882
AAIII	4045				3934		57221	4731		9744
pGBM	71				15391	2816	5999		1907	
pGBM	72				23004	3795	11148		5366	
pGBM	132				8845		9613		1354	
pGBM	172				16565		15177			5853
pGBM	327				19305		5559		2000	
pGBM	328				27750		20949			6870
pGBM	625				28744	3612	10825		7319	3753
pGBM	862				17776	2447	6002		1722	
pGBM	1010				15453	2242	9012	1193	3549	2778
pGBM	1311				39092	4376	12895		5148	
pGBM	1619				20667		14643			
pGBM	1968				22959		18904		6162	
pGBM	2010				21862	2844	16371	2312	7560	7230
pGBM	2104				20673	2917	32529	4586		4254
pGBM	2169				33190	4799	10029		4174	
pGBM	2304				20938	3913	8495		2218	
pGBM	2481				21328		23116			6976
pGBM	2486				23707		19784	3520		
pGBM	2494				10869		12771		2577	3845
pGBM	2735				30423	5149	16458		11587	8431
pGBM	2757				20331	3224	11469		5863	3850
pGBM	2854				16473	3507	31545	6160		4135
pGBM	2884				22520	3867	11169		3910	2412
pGBM	2896				18772	3692	21197			5594
pGBM	3007				35081	6034	25479	4176	7502	7393
pGBM	3031		422	567						
pGBM	3032				23106	4075	21910	3737	5109	5755
pGBM	3066				7374		4665		966	
pGBM	3070				11779		9861			
pGBM	3513				15812	2648	13211	1889	3364	3997
pGBM	3747				3935		35837	4589		9197
GBM oligo	2655				5707		16105	3979		
GBM RZ	3527				19454	3971	16649	3240	2610	2390
GBM sark	2643				15336		9016			
GBM sark	3555				15783	1412	8804		4047	2729
Normal Brain	NBfrontal						19221	2402		9947
Normal Brain	NBoccipital						17043	2654		8193
Normal Brain	NBparietal						27201	3259		15137
Normal Brain	NBtemporal						9943			5267
All	1418				10382		27422	3413		9416
pGBM LÜ	820				18678		17925			
pGBMsark	176				13646		6486			
sGBM	677				22717	4536	16365		6843	5106
sGBM	1214				14151		22018			
sGBM	1329				25454	4341	13992	2448	3946	3066
sGBM	1430				8732		13920			2573
sGBM	1944				2784		1408			
sGBM	2007				25122		13291		5809	4136
sGBM	2727				13130		13388	2144		
sGBM	3475				9065		25518	4897		6035
GBM cells	A172				31735	3767	4119		3787	
GBM cells	LN229				22869	5466	1544		2998	
GBM cells	LN428				32980	3384	8621			
GBM cells	T98G				43905				3575	
GBM cells	U178				48671					

more abundant in normal brain tissue and reduced or lacking in tumors

more abundant in glioma tissue and reduced or lacking in normal brain tissues

C

Detected splice isoforms:												CPEB3d	CPEB3c		CPEB3b	CPEB3a
Diagnose	ID-T-Nummer	CPEB3	100 bp	104 bp	122 bp	135 bp	143 bp	182 bp	203 bp	254 bp	452 bp	507 bp	531 bp	547 bp	576 bp	600 bp
AAIII	2377											14978			7471	
AAIII	2526											16481			5174	
AAIII	2725											8565			5827	
AAIII	2744									1336		8779			3911	
AAIII	2771											11567				
AAIII	2897											10303	3297		7329	6800
AAIII	2899											9728			5401	1662
AAIII	3423											8332			7130	3319
AAIII	3545											10263	1937		6631	5312
AAIII	3546											10090			7658	
AAIII	3548				2244		950					14927			5418	1641
AAIII	4045						2809		967	1267		6986				
pGBM	71				975							2644				
pGBM	72					890						12224			3767	
pGBM	132											2960				
pGBM	172														5473	
pGBM	327										4332					
pGBM	328											11773			3715	
pGBM	625				3411				1331			9924			4181	
pGBM	862				2902							4307				
pGBM	1010		2482									3189			3926	
pGBM	1311				1697							5664			4930	
pGBM	1619											8481			2164	
pGBM	1968								1309			12571			3929	
pGBM	2010				1832							11890		4069	5785	
pGBM	2104				1684							9475			5370	
pGBM	2169		2010		2775				2038	1369		7456				
pGBM	2304				3064							6016			5035	
pGBM	2481											4655			1948	
pGBM	2486											13216			5885	
pGBM	2494											7194			4258	
pGBM	2735				3702							19438			6404	
pGBM	2757											7269			3233	
pGBM	2854				2848							11950			4230	
pGBM	2884				906						2270	3166				
pGBM	2896											8291			3573	
pGBM	3007				3215				1769			12083	2690		8418	4942
pGBM	3031								1302		1394	13680	2416		5531	
pGBM	3032					1488			1435			11285			5442	
pGBM	3066				937							5000				
pGBM	3070				2843							2916				
pGBM	3513					1274			958			7020			5493	
pGBM	3747									1060		13025			5380	
GBM oligo	2655											6427			5669	
GBM RZ	3527											14338			8036	
GBM sark	2643					1052						2988				
GBM sark	3555							1790				7409			4267	
Normal Brain	NBfrontal											2786			3347	6109
Normal Brain	NBoccipital											2747	1313		3014	4169
Normal Brain	NBparietal											2224			4410	8886
Normal Brain	NBtemporal											2423				4662
All	1418											10694			3442	
pGBM LÜ	820					781						14046			9726	
pGBMsark	176											1821			994	
sGBM	677				1794							16129			5345	
sGBM	1214											10861			4527	
sGBM	1329											5077			3081	
sGBM	1430											2564			1991	
sGBM	1944															
sGBM	2007				1156							12615			5049	
sGBM	2727											3751			2626	
sGBM	3475											12062			4703	
GBM cells	A172		4055		4301							8985			4284	
GBM cells	LN229											2498			2219	
GBM cells	LN428											8673			5298	
GBM cells	T98G		1685		1524											
GBM cells	U178		9331	1442	10162				1469			9216			3498	

more abundant in normal brain tissue and reduced or lacking in tumors

more abundant in glioma tissue and reduced or lacking in normal brain tissues

D

Detected splice isoforms:							CPEB4d	CPEB4c	CPEB4b	CPEB4a			
Diagnose	ID-T-Nummer	CPEB4	115 bp	142 bp	182 bp		203 bp	226 bp	254 bp	277 bp	306 bp	507 bp	547 bp
AAIII	2377						21149		21655				
AAIII	2526						19619		19174			1675	
AAIII	2725						26046		20165				
AAIII	2744						21718		25345				
AAIII	2771						16637		12207		7133		
AAIII	2897						26150	5221	22566	4984			
AAIII	2899						19046	1503	15869	1628			
AAIII	3423						9538		8597	1103			
AAIII	3545						19463		25298				
AAIII	3546						22665		20903				
AAIII	3548						21383		22958	2407		2125	
AAIII	4045						26882		32885	2864			
pGBM	71						7320		4185				
pGBM	72						15172		15587				
pGBM	132						6518		5536				
pGBM	172						17460	4028	9620	6182			
pGBM	327						12086		8460				
pGBM	328						25485		21644				
pGBM	625					2634	30452		11702				
pGBM	862			3500			15071		5445				
pGBM	1010						22305		14188				
pGBM	1311						22087		17696				
pGBM	1619						14804		15511				
pGBM	1968						33990		34922				
pGBM	2010						22114		21939				10977
pGBM	2104						20095		12555	2397			
pGBM	2169						49763		37272				
pGBM	2304						16788		13189				
pGBM	2481						14181		14563				
pGBM	2486					1526	25177		22191			1216	
pGBM	2494						13383		10394	2237			
pGBM	2735						22615		30332			2482	
pGBM	2757						13014		16528				
pGBM	2854		1810				27502		17757				
pGBM	2884						9538		11158				
pGBM	2896						21392		15304	2357			
pGBM	3007						40036		32132				
pGBM	3031						35312		23592				
pGBM	3032						37298		26434				
pGBM	3066						8825		7801				
pGBM	3070						9167		6748				
pGBM	3513						21270	2580	19710	3011			
pGBM	3747						21631		25574				
GBM oligo	2655						11793		9233	2176			
GBM RZ	3527						22106		22278				
GBM sark	2643						18032		12070				
GBM sark	3555					4261	11334		9271	5636			
Normal Brain	NBfrontal						9860	6940	6026	6231			
Normal Brain	NBoccipital						8343	8381	5602	7068			
Normal Brain	NBparietal						20994	14305	11481	10482			
Normal Brain	NBtemporal						9343	7008	5371	5927			
All	1418						19617		20652				
pGBM LÜ	820						20257		13442			1764	
pGBMsark	176						9898		5532				
sGBM	677						17046		17065			1621	
sGBM	1214						16456	2722	14162	2717			
sGBM	1329						6742		4778				
sGBM	1430						15947	2555	9824	2453			
sGBM	1944						8971		3747				
sGBM	2007						18669		15918				
sGBM	2727						17089		10782				
sGBM	3475						11656		16539				
GBM cells	A172						20800		12084				
GBM cells	LN229						14344		10688				
GBM cells	LN428						15692		12416				
GBM cells	T98G						27548		7879				
GBM cells	U178						38061		17132				

more abundant in normal brain tissue and reduced or lacking in tumors

more abundant in glioma tissue and reduced or lacking in normal brain tissues

5.2 Alterations of growth properties and cancer-associated parameters in glioblastoma-derived cells mediated by CPEBs

5.2.1 Expression profile of CPEB 1-4 in A172 cultured glioblastoma cells

Altered expression of CPEBs in high- and low-grade gliomas indicated their role in the translational regulation in cancer. CPEB protein activity was studied in human glioma specimens and described in the previous section (see chapter 5.1.3.1). The current investigation addressed a potential influence of CPEBs on glioblastoma cells *in vitro.* With this intention, endogenous CPEB expression was monitored in human A172 glioblastoma culture (Fig. 5.2.1-1). Among CPEB paralogs, the most prominent expression was observed in CPEB 2-4. Proteins were detected as a punctate staining in the cytoplasm of investigated cells. Expression of CPEB1 and phospho-CPEB3 appeared to be reduced. Although all CPEBs are able shuttle to the nucleus (Kan et al., 2010), here, only phospho-CPEB3 and CPEB3 were observed in cell nuclei.

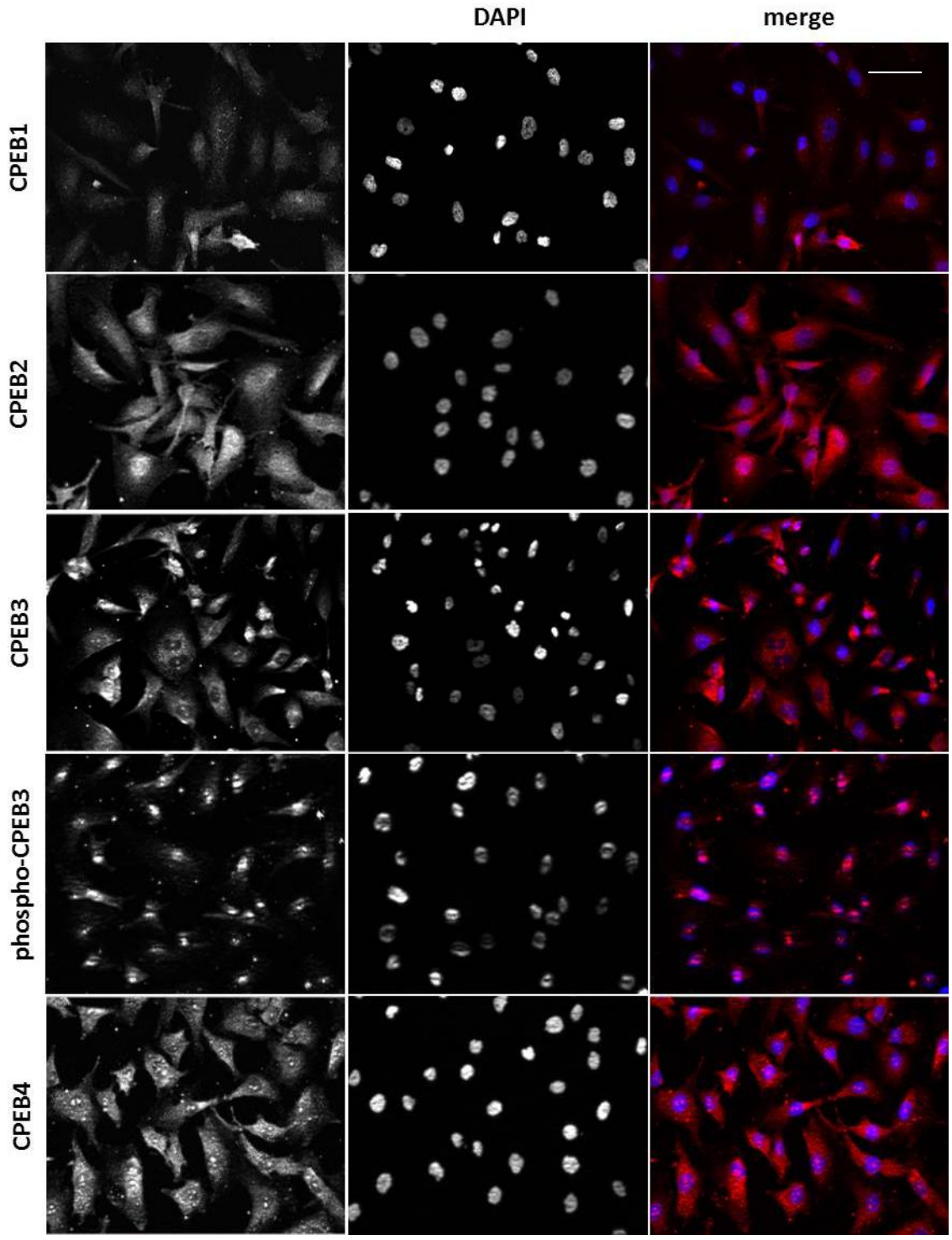

Figure 5.2.1-1. Endogenous expression of CPEB1-4 and phospho-CPEB3 proteins in human A172 glioblastoma culture cells. Starting from the left, the panels show staining of individual CPEBs, DAPI and their merged staining. Scale bars represent 25 μm.

5.2.2 Functional characterization of CPEB1 and CPEB2 protein overexpression in cultured A172 glioblastoma cells

5.2.2.1 Overexpression of CPEB1 and CPEB2 proteins

The contribution of CPEBs to the molecular pathogenesis of glioblastoma was investigated by overexpression of CPEB1 (n=4) and CPEB2 (n=7) proteins in glioblastoma-derived cells (Fig. 5.2.2.1-1). Next, A172 cultures transiently overexpressing CPEB1 or CPEB2 protein were investigated with regard to proliferation, apoptotic activity and migration.

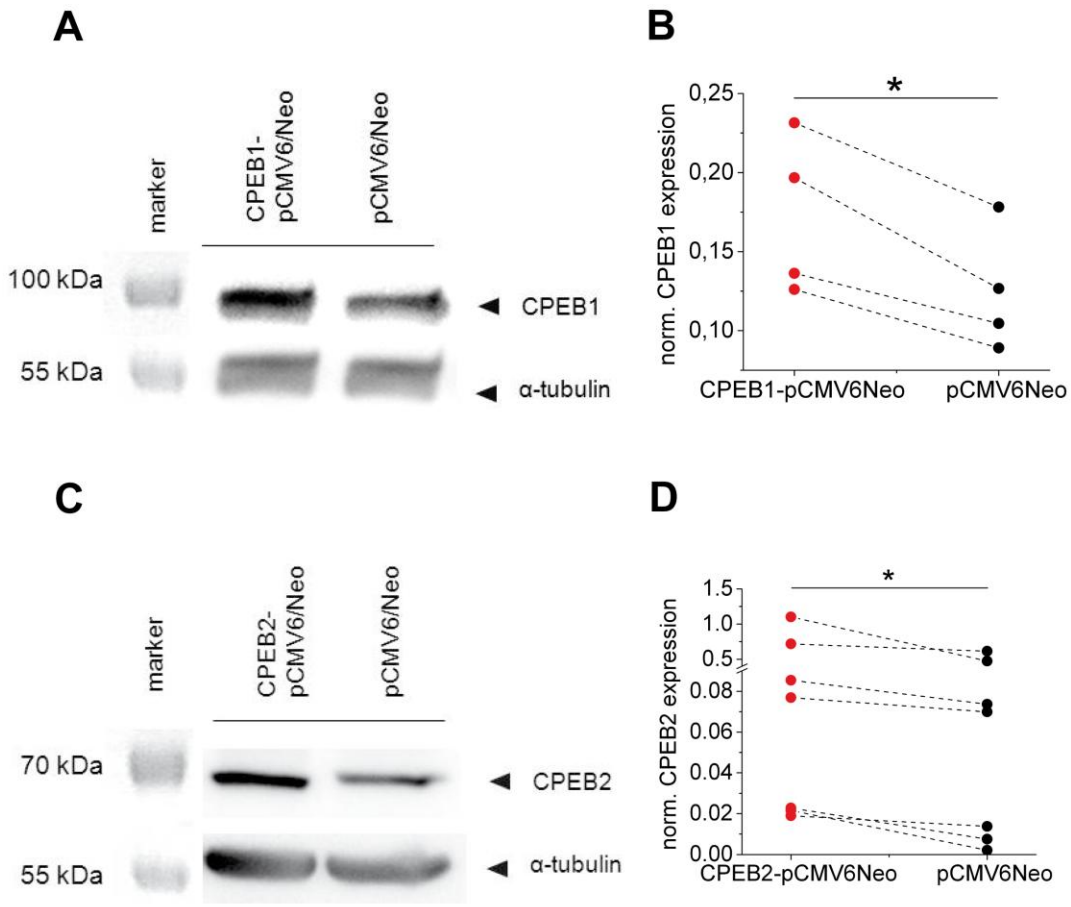

Figure 5.2.2.1-1. Overexpression of CPEB1 and CPEB2 proteins in A172 glioblastoma culture. A, C: Representative immunoblot showing overexpression of CPEB1, CPEB2 proteins and tubulin as an internal control. B, D: Analysis of the immunoblots of CPEB1-pCMV/Neo (n=4) and CPEB2-pCMV/Neo (n=7) transfected cells in comparison to reference pCMV6/Neo vector.

5.2.2.2 Alteration of proliferation and apoptotic activity of glioblastoma cells mediated by CPEB1 and CPEB2 proteins

The influence of CPEB overexpression on proliferation and apoptosis of cultured A172 cells was identified by flow cytometric analysis. In each experiment 100000 GFP-CPEB1-pCMV6/Neo, GFP-CPEB2-pCMV6/Neo or control GFP-pCMV6/Neo transfected cells were analyzed. Apoptotic, cPARP+ cells were labeled by antibodies against poly(ADP-ribose) polymerase (Asp214), while proliferating, pHH3+ cells were detected by antibodies against Ser10-phosphorylated histone H3. Overexpression of CPEB1 resulted in 1.75-fold growth of the apoptotic cellular population. In contrast, overexpression of CPEB2 resulted in a decrease in apoptosis (to 70%). Proliferation appeared to be not affected by CPEB overexpression (Fig. 5.2.2.2-1).

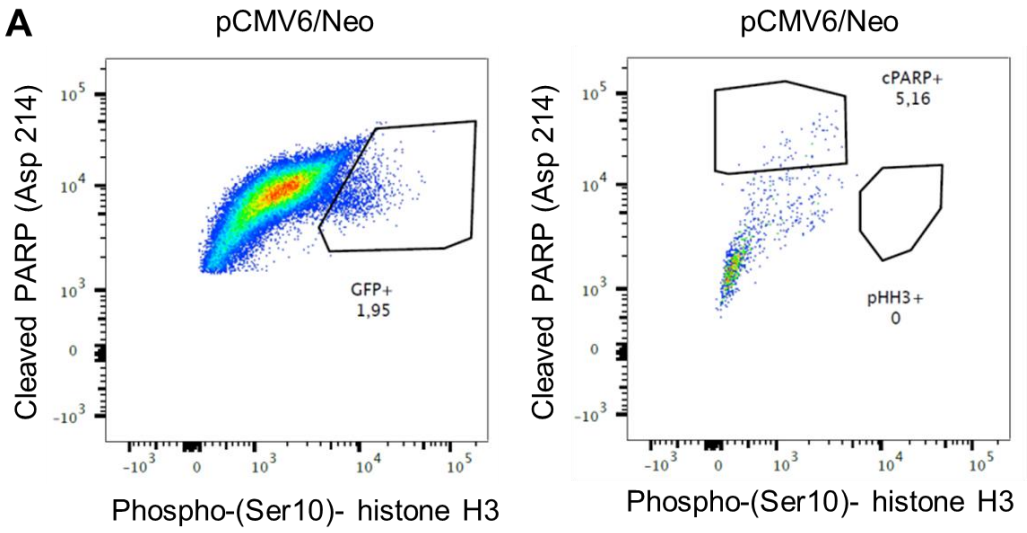

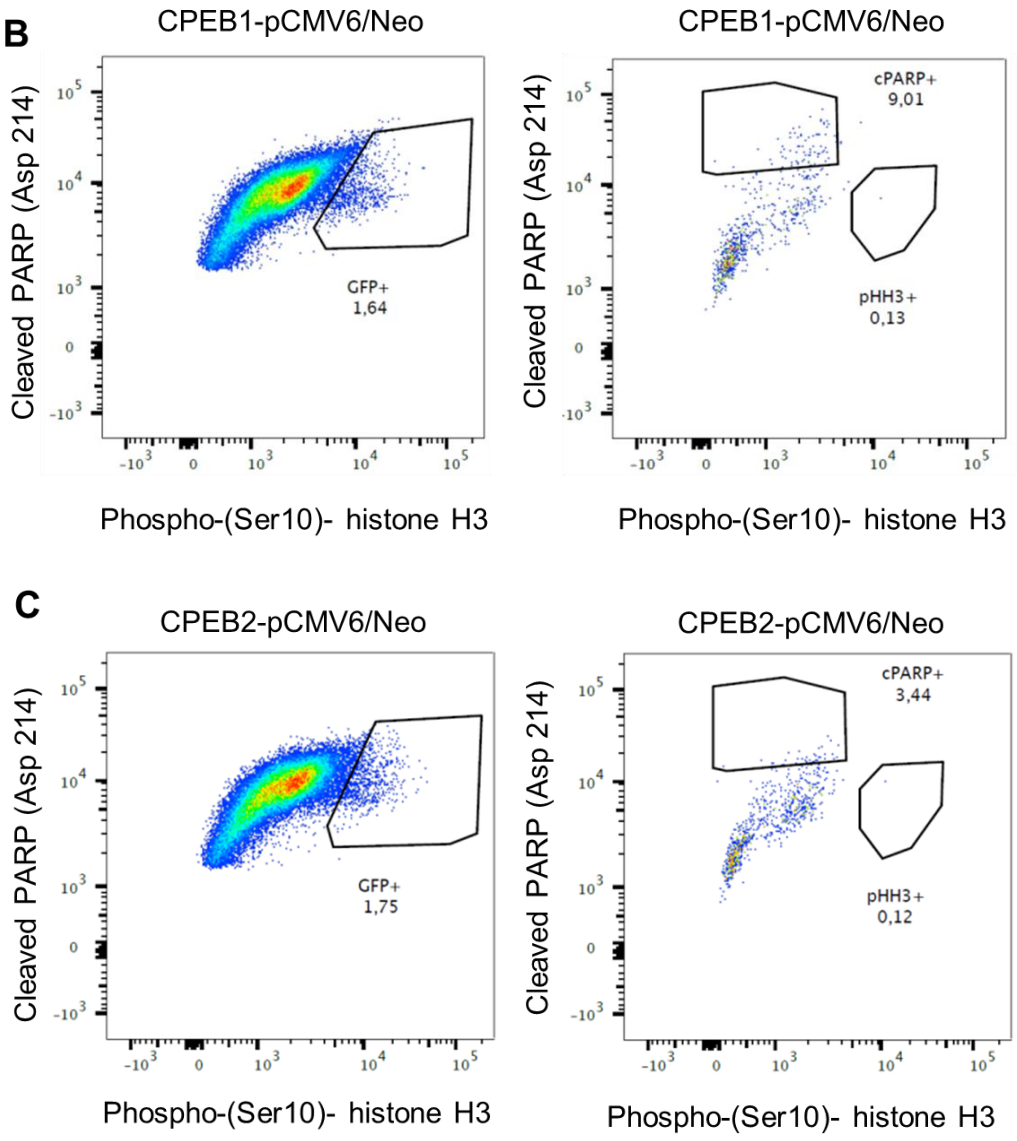

Figure 5.2.2.2-1. Flow cytometric analyses performed in A172 glioblastoma cells overexpressing CPEB1 or CPEB2 protein. Proliferating cells (pHH3+) were detected by antibodies against Ser10-phosphorylated histone H3, whereas apoptotic cells (cPARP+) by antibodies against poly(ADP-ribose) polymerase (Asp214). In each experiment at least 100000 GFP- CPEB1-pCMV6/Neo, GFP- CPEB2-pCMV6/Neo, GFP- pCMV6/Neo or GFP positive cells were analyzed. Cells transfected with GFP- pCMV6/Neo or GFP vector were considered as reference. Non-transfected cells labeled with pHH3 or stimulated with 1 μM staurosporine and stained with PARP antibody were considered as a proliferation and apoptosis control.

5.2.2.3 **Influence of CPEB1 and CPEB2 overexpression on glioblastoma cells migration**

The impact of CPEBs on cell migration was determined by overexpression of CPEB1 or CPEB2 protein in cultured glioblastoma cells followed by an *in vitro* scratch assay (Fig. 5.2.2.3-1A). Since FACS analysis (see Fig. 5.2.2.2-1) did not reveal any effect of increased CPEB expression on proliferation, the presence of cells in the wounded area was associated with their enhanced migratory capability. The change in the area covered by migrating cells over the time was raised up to 30% and 20% by elevated CPEB1 and CPEB2 protein levels, respectively (Fig. 5.2.2.3-1B).

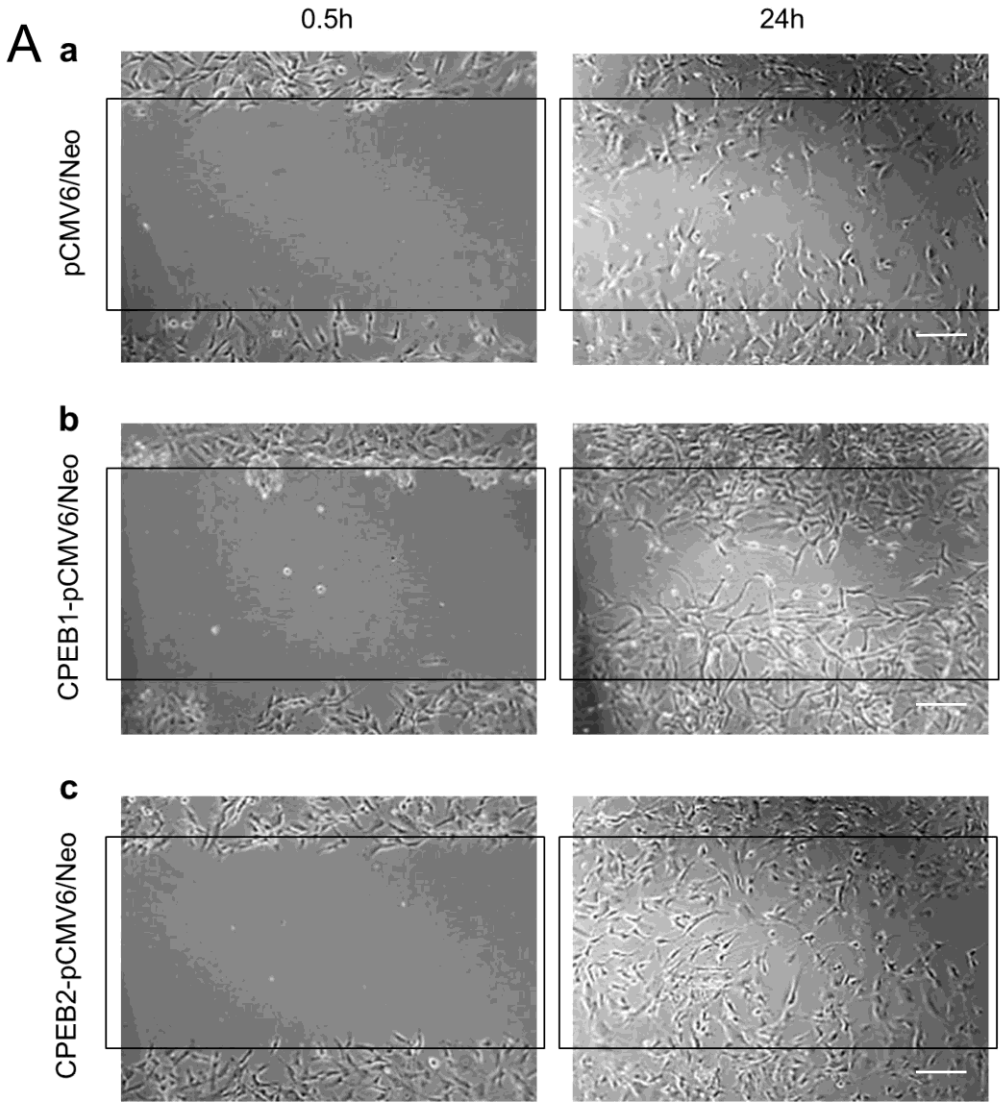

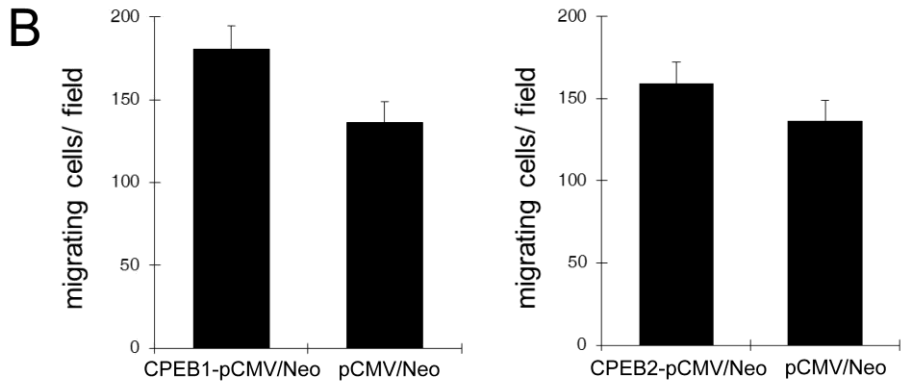

Figure 5.2.2.3-1. Influence of CPEB1 and CPEB2 overexpression on migration of cultured A172 glioblastoma cells A: Motility of CPEB1 and CPEB2 overexpressing cells examined by an *in vitro* wound healing assay. Scale bars represent 100 µm. B: Quantification of the change in the cell-covered area over time (24h) upon elevated expression of CPEB1 (n=4) and CPEB2 (n=4) proteins. Error bars indicate standard error of the mean.

5.2.3 Identification of cancer-associated signaling pathways altered by CPEB1 and CPEB2 proteins

Changes in cancer-associated signaling pathways induced by CPEBs were investigated by a cell-based pathway reporter array. Quantitative evaluation was possible upon overexpression of CPEB1 and CPEB2 in cultured cells and its reverse transfection with reporters of transcription factors present at the array plate. Increased expression of CPEB1 revealed a significant upregulation of estrogen, hedgehog, HNF4 and TGFβ pathways (Fig. 5.2.3-1A). In contrast, elevated expression of CPEB2 protein resulted in upregulation of c-myc, oct4, PI3K/Akt and TGFβ cascades (Fig. 5.2.3-1B). Since overexpression of CPEB1 proteins led to enhancement of TGFβ activity, it might indicate that the detected cascade is a novel target for translational regulation by CPEBs

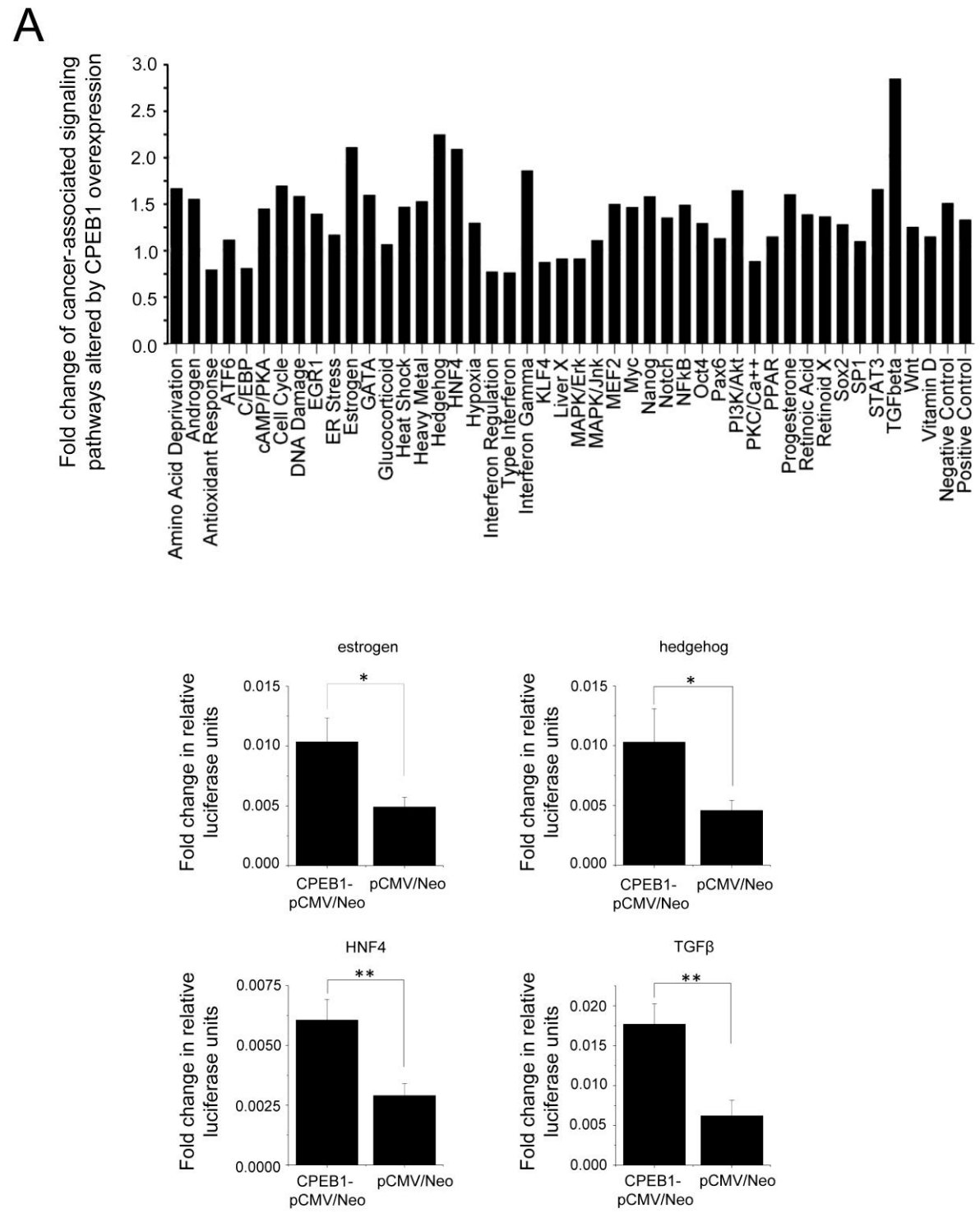
A
Fold change of cancer-associated signaling pathways altered by CPEB1 overexpression
3.0
2.5
2.0
1.5
1.0
0.5
0.0
Amino Acid Deprivation
Androgen
Antioxidant Response
ATF6
C/EBP
cAMP/PKA
Cell Cycle
DNA Damage
EGR1
ER Stress
Estrogen
GATA
Glucocorticoid
Heat Shock
Heavy Metal
Hedgehog
HNF4
Hypoxia
Interferon Regulation
Type Interferon
Interferon Gamma
KLF4
Liver X
MAPK/Erk
MAPK/Jnk
MEF2
Myc
Nanog
Notch
NFkB
Oct4
Pax6
PI3K/Akt
PKC/Ca++
PPAR
Progesterone
Retinoic Acid
Retinoid X
Sox2
SP1
STAT3
TGFbeta
Wnt
Vitamin D
Negative Control
Positive Control
estrogen
hedgehog
HNF4
TGFβ
Fold change in relative luciferase units
CPEB1-pCMV/Neo
pCMV/Neo
*
**

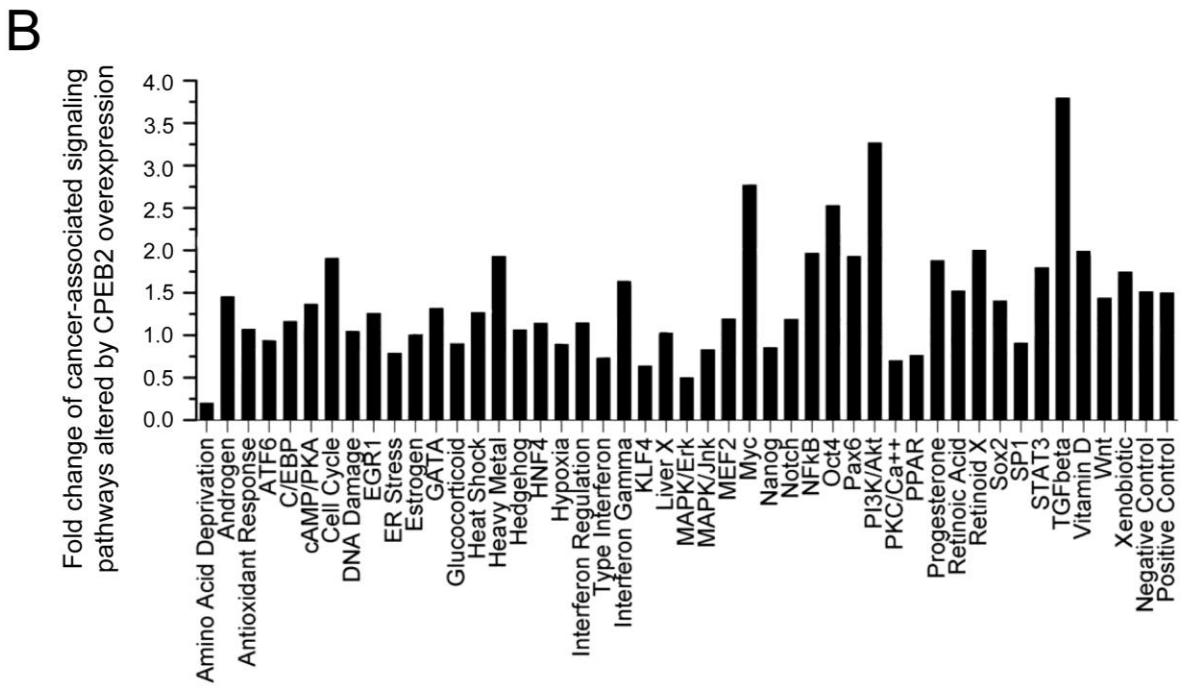

Figure 5.2.3-1. Cancer-associated signaling pathways altered by CPEB1 and CPEB2 proteins. A: Changes in cancer-associated signaling pathways monitored by cell-based reporter assays (n=3) revealed a significant upregulation of estrogen, hedgehog, HNF4 and TGFβ upon CPEB1 overexpression. Error bars indicate SEM. B: Upregulation of myc, oct4, PI3K/Akt and TGFβ signaling pathways upon CPEB2 overexpression (n=2; statistical quantification was not performed).

5.3 Expression profile of CPEB2 protein in mouse brain

5.3.1 Expression of CPEB1 and CPEB2 proteins in primary hippocampal cultures

In neurons, proteins involved in synaptic plasticity are predominantly derived from RNA molecules localized in dendrites. In response to synaptic stimulation, CPE elements present in the 3'UTR of dendritic mRNAs and CPE binding proteins promote translation induced by cytoplasmic polyadenylation. CPEBs also facilitate transport of mRNAs to dendrites. Localization of CPEB1 in cultured neurons has been observed in both, dendrites and cell bodies (Huang et al., 2003). Here, the expression of CPEB1 and CPEB2 was examined in rat primary hippocampal cultures. Neurons were co-stained with antibodies against CPEB1, CPEB2 and neuronal marker MAP2. Subcellular localization of both CPEBs overlapped in cultured neurons. Punctate distribution of expressed CPEB2 was observed in dendrites and the soma, similar to CPEB1 (Fig. 5.3.1-1).

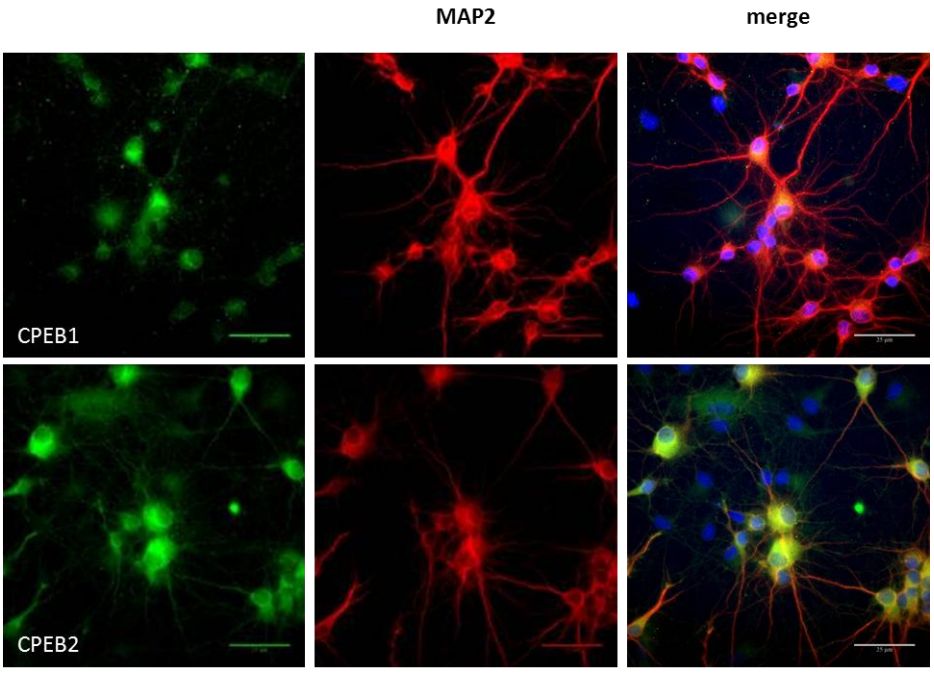

Figure 5.3.1-1. Endogenous expression of CPEB1 and CPEB2 in primary hippocampal neurons. 7 days in vitro hippocampal cultures prepared from Wistar rats were stained with CPEB1 (green), CPEB2 (green), MAP2 (red) antibodies and Hoechst counterstain (blue). Scale bars represent 25 μm.

5.3.2 **Expression of CPEB2 protein in juvenile and adult mouse brain**

Expression pattern of CPEB2 protein in juvenile (p12) and adult (p90) C57Bl6J mouse brain was determined with custom made CPEB2 antibody directed to mouse and human. Antibodies specifically recognized CPEB2a and CPEB2a* splice variants containing the B- and C-region and did not cross-react with other CPEBs (Turimella et al., 2015). Expression of CPEB2 was explored in neurons of different brain areas by immunostaining. Coronal sections from corresponding age groups were stained with antibodies against CPEB2 and the neuronal marker MAP2. The vast majority of MAP2 positive neurons in the CA1 region of the hippocampus, striatum radiatum, thalamus, cortex, and cerebellum displayed immunoreactivity against CPEB2 (Fig. 5.3.2-1). In individual cells of juvenile and adult animals, CPEB2 was located in the cytoplasm and processes. Dendritic localization of CPEB2 seemed to be more prominent in adult animals (Fig. 5.3.2-1B).

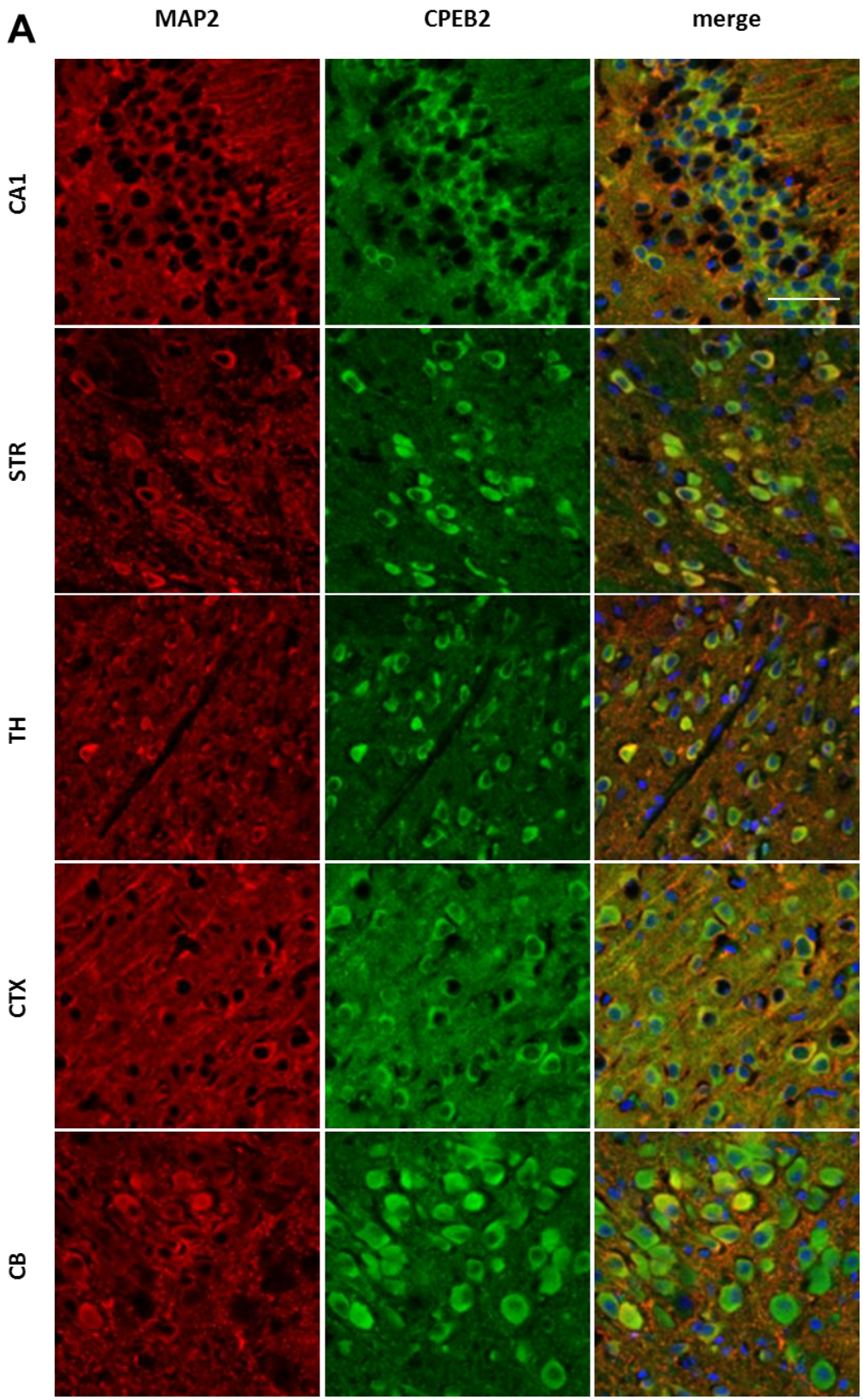
A
MAP2
CPEB2
merge
CA1
STR
TH
CTX
CB

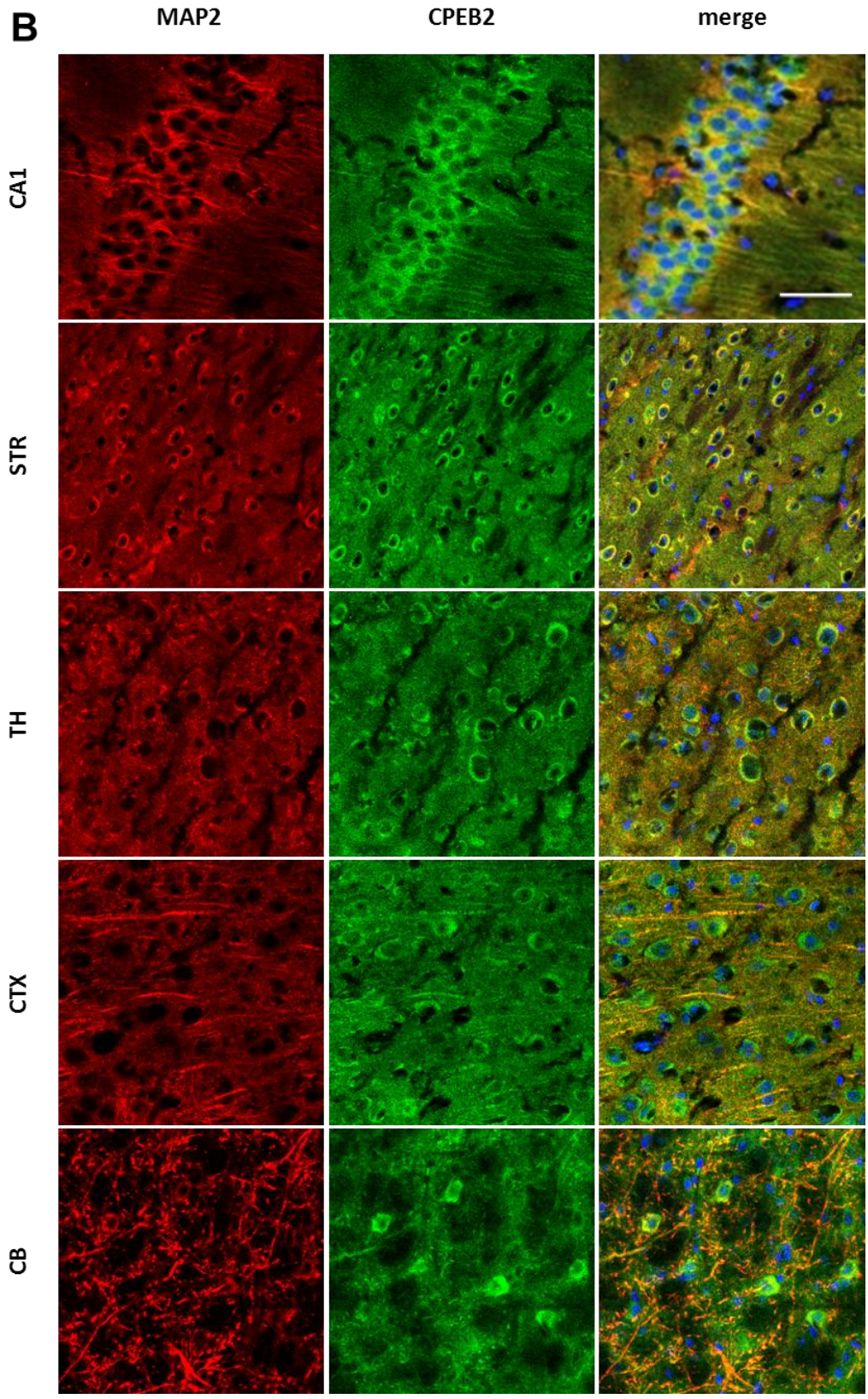

Figure 5.3.2-1.

Figure 5.3.2-1. Examination of CPEB2a and CPEB2a* expression in (A) juvenile (p12) and (B) adult (p90) C57Bl6J mice brains. Representative confocal images of CPEB2 (green), MAP2 (red), and Hoechst (blue) staining in the hippocampal CA1 region, striatum radiatum (STR), thalamus (TH), cortex (CTX), and cerebellum (CB). Scale bars represent 50 μm.

5.3.3 Differential expression of CPEB2 in excitatory, inhibitory and dopaminergic neurons

Differential expression of CPEB2 in excitatory, inhibitory, and dopaminergic neurons was assessed by immunostaining. 42.26±15.9% (n=3) of the GFP positive excitatory neurons in the hippocampus and dentate gyrus demonstrated CPEB2 immunoreactivity in Thy1-GFP mice (Fig. 5.3.3-1.). Further, in wild-type C57Bl6J mice, 93.6±9% (n=3) of the hippocampal inhibitory neurons and 62.36±9% (n=3) of the midbrain dopaminergic neurons demonstrated CPEB2 immunoreactivity (Fig. 5.3.3-1.). CPEB2 protein occurred to be heterogeneously expressed among investigated types of neurons and its strongest expression was observed in parvalbumin positive inhibitory neurons.

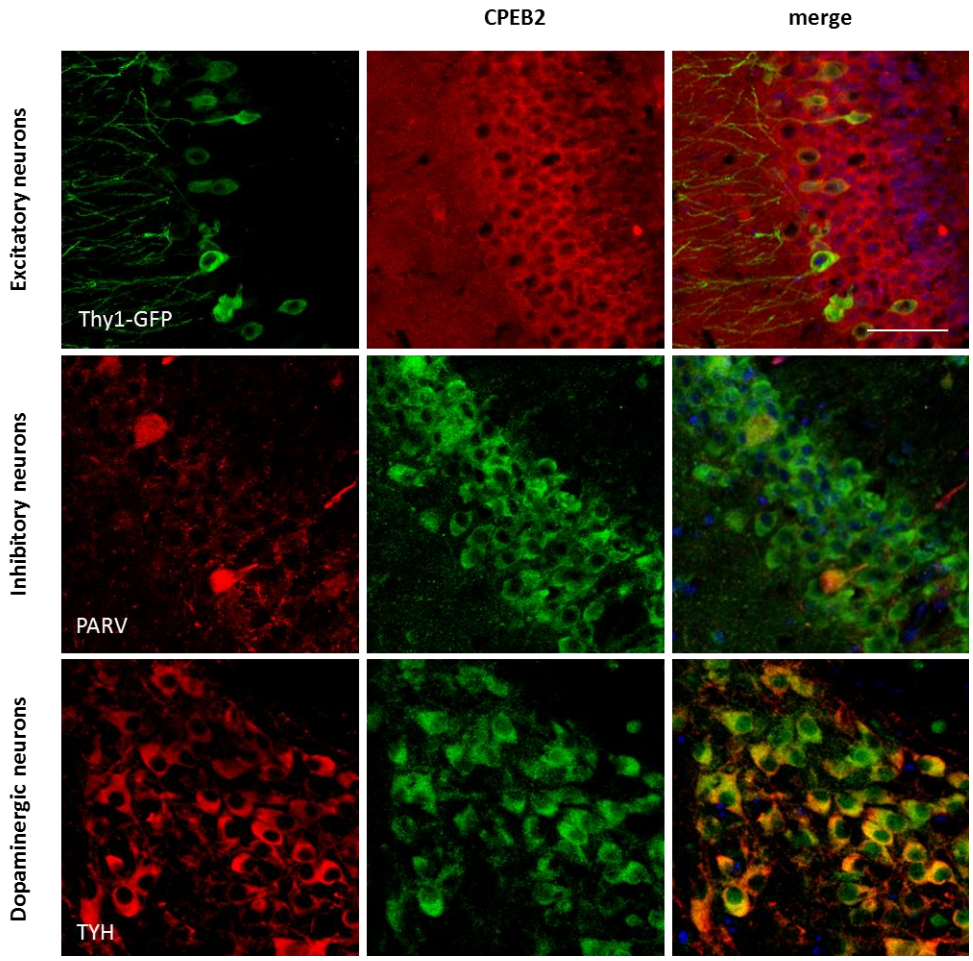

Figure 5.3.3-1. Endogenous expression of CPEB2 in excitatory, inhibitory, and dopaminergic neurons. Staining of GFP (green) and CPEB2 (red) or parvalbumin (PARV; red), tyrosine hydroxylase (TYH; red), and CPEB2 (green) was combined with Hoechst counterstain (blue). Scale bars represent 50 µm.

6 DISCUSSION

Understanding the molecular pathophysiology of tumors is fundamental to identify novel therapeutic and diagnostic factors. Thus far, cancer-related genes were abundantly investigated by transcript-based microarrays (van den Boom et al., 2003; Phillips et al., 2006; Rickman et al., 2001). In addition to these analyses, a recent study emphasizes the importance of post-transcriptional modification regulating gene expression changes under physiological conditions, but also giving rise to the pathology of tumors (Ortiz-Zapater et al., 2012). Translational control is particularly relevant in aggressive and therapy resistant malignancies. Despite reports endorsing the role of CPEBs in polyadenylation-induced translation in gliomas (Hu et al., 2015; Kochanek and Wells, 2013; Ortiz-Zapater et al., 2012), our knowledge of CPEB properties and their physiological relevance is incomplete. Thus far, the main research effort was focused on characterization of CPEB1. However, other members of the CPEB family mediate equally important processes, including synaptic plasticity and cancer formation (Ivshina et al., 2014). Furthermore, regardless of structural similarities, CPEBs are functionally non redundant (Ivshina et al., 2014). Therefore we chose to carefully examine the functional aspects of the CPEB isoforms in the developing and diseased brain.

6.1 The role of CPEBs in development and progression of glioma

6.1.1 Expression of CPEBs is heterogeneous in human glioma tissues

To examine functions of each of the CPEB subtypes in human glioma tissue, the present study focused on the expression patterns by comparing glioma tissues of different WHO grades. For this purpose, the abundance and localization of CPEBs was determined by immunohistochemistry. The vast majority of CPEB1 expression was detected in the infiltration areas of tumor cells into normal brain tissue. Cells in the tumor center, in the

areas of necrosis and angiogenesis, lacked CPEB1 (Fig. 5.1.3.1-1). It is generally known that tumor cells may adapt to the local environment or change the surrounding towards their own benefit (Godlewski et al., 2014). The fact that CPEB1 expression was reduced in GBMs may suggest a proto-oncogenic adaptation. Interestingly, expression of CPEB1 was downregulated with WHO grade, reaching the lowest level in GBMs (Fig. 5.1.3.1-2A; Tab. 5.1.3.1-1). A similar expression course was shown in the recent study of Galardi et al. (2016), where CPEB1 mRNA level was maximum in normal brain and significantly reduced in cancer tissues. In line with these findings, CPEB1 was indicated to be a putative tumor suppressor (D'Ambrogio et al., 2013). Abundant evidence form ovarian, melanoma, and gastric cancers and cell lines derived from breast, myeloma and colorectal cancer (Caldeira et al., 2012; Hansen et al., 2009; Heller et al., 2008; Nairismägi et al., 2012; Shoshan et al., 1999) report reduction in CPEB1 transcript and suggest a potential tumor repressing role. Furthermore, downregulation of CPEB1 in tumor cells disturbs the mitotic regulation of poly(A) tails, pre-mRNA alternative polyadenylation site selection, and inhibits cell proliferation (Bava et al., 2013; Giangarrà et al., 2015b; Novoa et al., 2010). In contrast, reduction of CPEB1 in primary fibroblasts is associated with bypass of senescence (Burns and Richter, 2008; Fernández-Miranda and Méndez, 2012) and the ability of tumor cells to enhance invasion, angiogenesis and to increase resistance to nutritional stress (Grudzien-Nogalska et al., 2014). Also knockout of CPEB1 induces epithelial-to-mesenchymal transition (Grudzien-Nogalska et al., 2014), a process that is associated with increased cancer progression and metastatic potential (Kalluri and Weinberg, 2009). From these results it can be concluded that expression of CPEB1 is reduced in various cancers in order to support tumor development and progression.

To a certain extent, the expression pattern of CPEB2 was similar to CPEB1. Prevalent CPEB2 immunoreactivity was observed in less aggressive AII and AAIII, while pGBM specimens were negative or showed very weak CPEB2 staining (Fig. 5.1.3.1-2B; Tab. 5.1.3.1-1). CPEB2 was found in reactive astrocytes and in endothelial tumors cells, suggesting that protein synthesis takes place in the close proximity of blood vessels during tumor formation (Fig. 5.1.3.1-1). One of the possible explanations for CPEB2 expression in endothelial cells may be association of CPEB2 with stress conditions. It was shown that increased oxidative stress provokes CPEB2 binding to HIF-1α mRNA and regulates its

expression (Hägele et al., 2009). In turn, HIF-1α controls homeostatic responses to oxidative stress by stimulating transcription of genes involved in angiogenesis, metabolism and cell survival (Chen et al., 2015). However, further research is needed to explain the role of CPEB2 in hypoxia and vascularization.

In the investigated cohort of gliomas, CPEB3 was the most abundantly expressed family member (Fig. 5.1.3.1-1). The present study provides the first analysis of CPEB3 in human glioma specimens. In contrast to CPEB1 and CPEB2, its immunoreactivity increased with progressing tumor grade, and achieved the strongest intensity in GBMs (Fig. 5.1.3.1-2C; Tab. 5.1.3.1-1). At the same time, the activity of the protein, determined by its phosphorylation, decreased with WHO grade (Fig. 5.1.3.1-2D; Tab. 5.1.3.1-1). Therefore, despite the strong CPEB3 expression, phospho-CPEB3 in GBMs was distinctly reduced. This suggests that a substantial part of CPEB3 protein in GBM specimens does not undergo phosphorylation and indicates phosphorylation to be the biologically significant mechanism regulating CPEB3 activity in gliomas.

In contrast to the other CPEBs, strong expression of CPEB4 was solely observed in a few of the investigated glioma specimens (Fig. 5.1.3.1-2E; Tab. 5.1.3.1-1), with a prominent immunoreactivity in cell processes (Fig. 5.1.3.1-1). This localization of CPEB4 indicates its involvement in local protein synthesis, which was shown to be particularly important for synaptic plasticity (Kandel, 2001; Zukin et al., 2009), but may also contribute to cancerogenesis. CPEB4 may be implicated in the syntheses of proteins involved in cell-cell communication and tumor-stromal interactions (Ortiz-Zapater et al., 2012), thus indirectly in cancer progression. Indeed, downregulation of CPEB4 was associated with tumor development (Giangarrà et al., 2015). Cells overexpressing CPEB4 showed an advantage for tissue colonization and invasion (Fernández-Miranda and Méndez, 2012), while its downregulation resulted in reduction of cellular proliferation in the GBMs and PDAs (Ortiz-Zapater et al., 2012). Knockdown of CPEB4 contributed to a decrease of tumor size and vascularization, indicating its impact on changes in cell proliferation (Ortiz-Zapater et al., 2012). In the present study the expression pattern of CPEB4 could not be associated with the WHO grade. However Hu et al. (2015) reported CPEB4 to enhance tumor progression in human high-grade gliomas. Considering that high CPEB4 expression

supports tumorigenic properties, this isoform might be involved in local protein synthesis and mediate cancer progression.

Altogether, these observations are in agreement with the fact that CPEB expression is heterogeneous in human gliomas. Destabilization of the normal function of a wide range of transcripts regulated by CPEB favors tumor growth. Therefore, CPEB-dependent translational control may be considered as a mechanism having a significant role during glioma formation and progression.

6.1.2 **CPEB expression patterns associate with clinical prognosis of glioma patients**

Since in the present study a decrease in CPEB1 and phoshop-CPEB3 was observed with increasing tumor grade, the potential prognostic value of CPEB expression in human glioma specimens was assessed by Kaplan-Meier survival analysis. CPEB expression profiles compared with the clinical data revealed an interesting dependency between CPEB1, phospho-CPEB3 and life expectancy. A pronounced association of CPEB1 expression with prolonged survival was observed in AII and AAIII, but not in GBM specimens (Fig. 5.1.3.2-1A, B). Though it is necessary to keep in mind that low-grade astrocytoma patients usually progress better, recent reports support a link between reduced CPEB1 expression and longer survival (Galardi et al., 2016; Yin et al., 2014). Despite the robust expression of CPEB 2-4, none of the proteins showed correlation with patient survival (Fig. 5.1.3.2-1C, D, G). However, Hu et al. (2015) reported that a high CPEB4 expression profile was associated with shorter survival of GBM patients. Interestingly, there was a difference in the survival of patients with and without phospho-CPEB3. A significant correlation between CPEB3 activity and survival was observed in less aggressive low-grade astrocytomas considered to be sGBM precursors (Fig. 5.1.3.2-1E), but not in pGBMs (Fig. 5.1.3.2-1F). In order to ascertain an association between survival and phospho-CPEB3 expression in GBMs, an increased number of specimens should be retested. In general, the data presented here support the hypothesis that CPEBs may serve as a sensitive prognostic factor for glioma patients.

6.1.3 **Methylation of *CPEB1* gene does not correlate with silenced expression**

Hypermethylation of DNA is a frequent condition in cancers (Chen et al., 2014), resulting in stable transcriptional silencing of the associated genes (Jones and Baylin, 2007). This is due to the methyl groups that attach to the CpG islands localized in the promoter region, which impede the binding of transcription factors (Chen et al., 2014). The finding that CPEB1 expression was gradually decreasing with tumor progression, suggested increased DNA methylation (Curradi et al., 2002). To test this hypothesis genome wide DNA methylation analysis was performed. Methylation of *CPEB* genes was formerly studied in tumors (Caldeira et al., 2012; Heller et al., 2008), but hypermethylation in gliomas was never reported. Among the investigated genes, *CPEB1* and *CPEB3* were methylated (Fig. 5.1.1-1), however only *CPEB1* reached prominent hypermethylation level. *CPEB1* methylation was additionally associated with mutation in the *IDH* gene (Fig. 5.1.2-1). Recent studies proved that *IDH* mutations, not only drive an increased promoter methylation, but actually entail hypermethylation (Christensen et al., 2011; Labussiere et al., 2010), and associate with improved prognosis of glioma patients (Cohen et al., 2013).

In the present study a significant reduction in CPEB1 expression on a transcript level was detected in AAIII and sGBM specimens containing increased methylation and *IDH1* mutation (Fig. 5.1.1-1). Although this observed trend was indicating a link between the high CPEB1 methylation and silenced expression it turned out not to be correlated. Therefore, the observed DNA methylation only partially may be involved in transcriptional repression of CPEB1. Interestingly, pGBM specimens, with wild type *IDH1,* where CPEB1 methylation was not detected also revealed reduced expression of CPEB1 transcript (Fig. 5.1.1-1). This allows concluding that CPEB1 expression in pGBM samples was reduced independently of the methylation status. Consequently, other epigenetic and non-epigenetic mechanisms play a role in transcription silencing. For instance microRNAs may contribute to blocking translation or promoting degradation of the transcripts (Burns et al., 2011; Morgan et al., 2010), and explain the reduction of CPEB1 expression. Although in the present study DNA methylation turned out not to be responsible for CPEB1 downregulation, promising results from clinical trials with DNA methylation inhibitors as

well as histone deacetylase inhibitors were recently reported, meaning that epigenetic approaches have a potential in cancer therapy (Chen et al., 2014).

6.1.4 **Expression of CPEB3 and active CPEB3 protein is tissue specific**

The difference between expression levels of CPEB3 and phosphorylated CPEB3 gives a solid foundation to further examine kinases regulating CPEB function (Fig. 5.1.5-2). PKA and CaMKII investigated here are known to activate CPEBs phosphorylation that further triggers polyadenylation-induced translation (Kaczmarczyk et al., 2016; Theis et al., 2003). A recent study demonstrated that phosphorylation of CPEB3 depends on the presence of the alternatively spliced B-region, and can be detected by phospho-specific CPEB3 antibody (Kaczmarczyk et al., 2016). The used antibody allowed for recognition of only one splice form of the protein containing a phosphorylation consensus sequence, namely the B-region adjacent to two serine (S419, S420) residues. The specificity of the phospho-CPEB3 antibody was confirmed in cultured cells transfected with full-length CPEB3a (containing the B-region), CPEB3aKD (S419, S420 mutated to A419, A420), and CPEB3b (lacking the B-region) (Fig. 5.1.5-1), where only full-length CPEB3a was subject for phosphorylation.

Since the alternatively spliced B-region and the overlapping phosphorylation site are conserved between CPEB 2-4, this site is strongly engaged in regulatory functions of CPEBs (Kaczmarczyk et al., 2016). The AII specimens analyzed here were characterized by robust expression of CPEB3 and phospho-CPEB3 (Fig. 5.1.5-2, *right column*), while pGBM specimens showed strong immunoreactivity against CPEB3 (Fig. 5.1.5-2, *left column*). Altogether, CPEB3, PKA and CaMKII kinases were abundantly expressed in both of the investigated groups, while phospho-CPEB3 protein was only present in AII (Fig. 5.1.5-2). Despite the abundant CPEB3 expression and strong activity of kinases initiating polyadenylation, no significant phosphorylation of CPEB3 was observed in GBMs. This strongly suggests the lack of functional regions in the expressed CPEB3 and blockade of presumed targets expression.

6.1.5 Alternative splicing determines the expression pattern and activity of CPEBs

As expression analysis of PKA and CaMKII kinases revealed no change in their immunoreactivity between low- and high-grade gliomas the next step was directed towards the investigation of alternative splicing of CPEBs. In eukaryotes, alternative splicing determines tissue differentiation, controls transcriptional and post- transcriptional mechanisms, and their role in cancer (Kornblihtt et al., 2013). Alternative splicing of CPEBs is particularly relevant in the context of cytoplasmic polyadenylation, because the splice variants of CPEB 2-4 differ in their regulation by phosphorylation due to presence or lack of respective consensus sites (Fig. 1.4.3-1; Fig. 5.1.6-1) (Kaczmarczyk et al., 2016; Theis et al., 2003).

CPEBs are involved in the regulation of synaptic plasticity, and multiple splice variants of CPEB paralogs were observed in a mouse brain (Kaczmarczyk et al., 2016; Theis et al., 2003; Turimella et al., 2015). In hippocampal pyramidal neurons, only CPEB2 splice variants containing the B-region, such as CPEB2 a/c were expressed. Two of the detected isoforms, CPEB2 a*/c*, contained an additional 9-nt E-region (Turimella et al., 2015). Furthermore, changes in the abundance of CPEB3 splice variants were induced by neuronal stimulation. As in the case of CPEB2, increased neuronal activity led to expression of CPEB3 isoforms containing the B-region (Kaczmarczyk et al., 2016). In cancers, alternative splicing of CPEB2 turned out to be a key driving mechanism in human TNBC metastasis (Johnson et al., 2015). The high metastatic potential of TNBC cells was associated with acquiring of anoikis resistance (AnR) and increase in expression of the B-region-lacking isoform. Downregulation of the CPEB2b re-sensitized AnR cells to detachment and induced cell death, whereas overexpression of CPEB2b in TNBC cells generated the AnR and increased their metastatic potential (Johnson et al., 2015). In human glioma specimens, profiling of alternative splice variants revealed that in comparison to normal brain and low-grade astrocytomas, most of the GBMs lacked the full-length CPEBs (CPEB2a, CPEB3a, CPEB4a) (Fig. 5.1.6-2; Tab. 5.1.6-1B, C, D). Furthermore, the majority of GBM samples did not express the CPEB4c variant also containing the B-region (Tab. 5.1.6-1D). Instead, isoforms lacking the B-region (CPEB3b, CPEB3d, CPEB4b,

CPEB4d) were predominantly expressed (Fig. 5.1.6-2; Tab. 5.1.6-1C, D). Interestingly, the recently identified E-region was detected in CPEB2 c*/d* splice variants, but so far its function has not been addressed. Generally this observation indicated the loss of CPEB 2-4 activity in high-grade gliomas. Alternative splicing appeared to be cell type-specific and depended on the grade of tumor malignancy.

Summarizing, in physiological conditions, the B-region-containing splice variants are abundantly expressed (Kaczmarczyk et al., 2016; Turimella et al., 2015). In contrast, TNBC (Johnson et al., 2015) and GBM tumors show enforced expression of isoforms lacking the B-region. However, it is unknown whether similarly to breast cancers, splicing in GMBs is related to their metastasis potential. Certainly, binding of CPEB 2-4 to the target transcripts without the possibility to further activate their translation, might cause their translational-arrest and in consequence silence mRNAs expression. Importantly, a similar pattern was observed for CPEB1. Mutant CPEB1 protein lacking regions of phosphorylation could not be activated, therefore kept the bound mRNAs in translational arrest (Kochanek and Wells, 2013). Thus far, the question how alternative splicing of CPEBs in gliomas is regulated remains open. The finding that CPEB3 in GBMs is expressed as a form that cannot undergo activation suggests its contribution to changes in protein expression of high-grade gliomas. Therefore, CPEB3 may be considered as an attractive therapeutic target.

6.2 The impact of CPEBs on growth properties and cancer-relevant parameters in cultured glioblastoma cells

6.2.1 CPEB3 protein shuttle between nucleus and cytoplasm

The reduction of CPEB1 expression observed in human GBM specimens prompted us to determine whether reversing this process results in acquisition of tumor suppressor properties by GBM cells. Likewise, overexpression of CPEB2 aimed to prove whether enhanced protein levels impact growth properties and cancer-relevant parameters. Therefore, the A172 GBM line was selected as it expressed CPEB1 and CPEB2 (Fig. 5.2.1-1) similar to human glioma specimens (Fig. 5.1.3.1-1).

Similarly to the investigated glioma tissues, endogenous CPEB levels in the cell line were heterogeneous. Weak cytoplasmic expression of CPEB1 was contrasted with abundantly expressed CPEB 2-4 (Fig. 5.2.1-1). Intriguingly, phospho-CPEB3 and partially CPEB3 were observed in the cell nuclei (Fig. 5.2.1-1). However, as this was not the case in the investigated human gliomas the observed pattern was assumed as a culture artefact.

6.2.2 **Forced overexpression of CPEB1 and CPEB2 alters growth properties and cancer-associated parameters of glioblastoma cells**

CPEBs regulate important cellular processes such as astrocyte migration (Jones et al., 2008), or MEF growth and senescence (Fernández-Miranda and Méndez, 2012). Recently CPEBs were found to be expressed in gliomas (Galardi et al., 2016; Ortiz-Zapater et al., 2012). Therefore it is important to identify whether their altered expression evoke changes in growth properties or cancer-associated parameters of GBM cells. The high levels of CPEB1 turned out to be cytotoxic for cultured GBMs. Overexpression of CPEB1 resulted in meagre growth of apoptotic cell population. In contrast, overexpression of CPEB2 slightly decreased apoptotic activity of GBM cells, suggesting that higher CPEB2 level may possibly result in loss of its tumorigenic properties. Alterations in cellular proliferation of CPEB1 and CPEB2 were not observed (Fig. 5.2.2.2-1). Overexpression of CPEB1 was recently reported to reduce proliferation and infiltration of GBM cells (Galardi et al., 2016; Yin et al., 2014). Accordingly, CPEB1 was directly engaged in regulation of $p27^{Kip1}$ expression (Galardi et al., 2016). However, despite CPEB1 reduction, Nagaoka et al., (2016) found no effect on cell proliferation in the investigated mouse mammary epithelial cells. Likewise, knockout of CPEB1 in MEFs resulted in no difference in cell cycle progression. Instead, MEFs as well as primary human cells escaped senescence. This process was shown to be mediated by reduced expression of CPEB1-dependent mRNAs, such *p53* and *c-myc* (Burns and Richter, 2008; Groisman et al., 2006).

Enhanced migration of transformed astrocytes leads to spread of tumors and a high recurrence rate (Stupp et al., 2005). This process not only involves changes in the cytoskeleton, but also depends on the synthesis of new proteins (Jones et al., 2008). New

protein synthesis was shown to be especially important in the migration of astrocytes into a site of the injury, and the process was precisely regulated by CPEB1-mediated synthesis of β-catenin in the leading edge of invading cells (Jones et al., 2008). In the present study, forced overexpression of CPEB1 and CPEB2 also enhanced the cell motility (Fig. 5.2.2.3-1). Therefore, it is highly possible that migration of cultured GBM cells is regulated by CPEB-dependent synthesis of β-catenin. Additionally, based on findings from FACS analysis, the wound healing was speeded up rather by elevated cell motility than by increased proliferation.

One of the possible explanations for enhanced apoptotic activity and migration by CPEB1 might be that the faster migration generates rapid changes in cytoskeleton. These morphological alterations on one hand may contribute to increased cell motility, but may also raise a chance of mistakes turning GBM cells towards an apoptotic pathway. In contrast, decreased apoptotic activity and enhanced migration through CPEB2 may indicate that CPEB2 overexpressing cells are losing their cancerous properties.

6.2.3 **Elevated expression of CPEB1 upregulates cancer-associated signaling pathways**

Altered expression of CPEBs in human glioma specimens may entail changes in associated signaling pathways. Therefore, cultured GBM cells overexpressing CPEBs were seeded on multi-pathway assay plates that allowed for identification of CPEB-mediated changes in cancer-relevant cascades. Overexpression of CPEB1 enhanced the activity of estrogen, hedgehog, HNF4 and TGFβ (Fig. 5.2.3-1A). Overexpression of CPEB2 could not be quantitatively asset because the experiments number was too low (Fig. 5.2.3-1B). Among the upregulated pathways, TGFβ appeared to be the most prominent. Depending on the cellular context, TGFβ may result in tumor-suppressing or tumor-promoting activity (Derynck et al., 2001; Siegel and Massagué, 2003). In order to bypass a cell cycle inhibition, a majority of the cancers accumulate mutations in this pathway. TGFβ restrains proliferation of astrocytes, epithelial, and immune cells. However, in gliomas TGFβ may act as an oncogenic factor due to enhancement of cell proliferation, invasion, angiogenesis

and inhibition of immune response (Massagué, 2008; Seoane, 2006; Wesolowska et al., 2008; Zhang et al., 2012).

An association between CPEB1 and TGFβ pathway was independently confirmed by Nagaoka et al. (2016). They found that mouse mammary epithelial cells deprived of CPEB1 and treated with TGFβ show enhanced epithelial-to-mesenchymal transition and metastatic potential. Thus far, the mechanism triggering CPEB1-mediated TGFβ activation is unclear. However, TGFβ downstream targets, including Smad 2-4 were abundantly studied in gliomas (Bruna et al., 2007). High TGFβ-Smad activity was predominantly present in aggressive gliomas and related to the poor patient prognosis (Bruna et al., 2007). Therefore, inhibitors of the TGFβ pathway results in anti-tumor properties, such as reduction of cell viability and invasion (Kaminska et al., 2013). Inhibitor of the TGFβ receptor I kinase (galunisertib, LY2157299) that downregulates the phosphorylation of Smad2 and selectively block TGFβ pathway is currently investigated with a temozolomide-based radio-chemotherapy in newly diagnosed GBM patients. Summing up, CPEBs are involved in regulation of the TGFβ signaling cascade. However, further studies are needed to fully explain the interaction between CPEB1-mediated translational control and the activation of the TGFβ pathway.

6.3 Expression of CPEB2 in different cellular populations, brain regions, and stages of development

Expression of CPEB1 was well described in the hippocampal neurons (Theis et al., 2003), therefore it served as a reference for the present study of CPEB2. Both CPEB paralogs demonstrated analogous subcellular localization and immunoreactivity in primary hippocampal neurons (Fig. 5.3.1-1). Expression of CPEB2 was present in most of the neurons throughout the investigated mouse brain regions (Fig. 5.3.2-1), including majority of excitatory, inhibitory and dopaminergic cells (Fig. 5.3.3-1). This indicated a role of CPEB2 in physiology of the juvenile and adult brain. In addition, localization of CPEB2 in cell bodies and dendrites, pointed at its role in control of local protein synthesis. This raised

the question of which neuronal mRNAs are regulated by CPEB2. Indeed, CPEB2 may regulate CaMKII, the kinase engaged in LTP (Atkins et al., 2005) and β-catenin, which is involved in neuronal morphogenesis (Yu and Malenka, 2003). Additionally, Turimella et al. (2015) identified EphA4 as a novel CPEB2 target. EphA4 not only participates in the neuron–glia crosstalk (Carmona et al., 2009), but also controls LTP at excitatory synapses (Filosa et al., 2009). Overall, this indicates involvement of CPEB2 in synaptic plasticity and local protein synthesis in the hippocampal neurons of developing and adult brain.

7 SUMMARY

Gliomas are the most common primary brain tumors with aggressive progression and devastating prognosis. Therefore identification of new therapeutic and diagnostic factors is necessary to improve the dramatic situation of glioma patients. Thus far, cancer-related genes were thoroughly analyzed by transcript-based microarrays (van den Boom et al., 2003; Phillips et al., 2006; Rickman et al., 2001). However, recent research shed light on the importance of post-transcriptional modifications of mRNAs that alter gene expression under physiological conditions, but also gives rise to the pathology of gliomas.

The main goal of the present study was to investigate CPEB expression in human glioma specimens. CPEBs are auxiliary regulators associating with consensus sequences present in 3'UTRs of mRNAs, which activate or repress their translation. Via this mechanism CPEBs regulate essential cellular processes, such as development (Groisman et al., 2002; Novoa et al., 2010), memories formation (Theis et al., 2003) and progression of cancer (Ortiz-Zapater et al., 2012). In the current work aberrant CPEB expression was found to be a frequent phenomenon in both, low- and high-grade gliomas. Decreased CPEB1 expression was associated with the rising grade of tumor malignancy, suggesting it being a putative tumor suppressor. One of the mechanisms potentially underlying transcriptional silencing of cancer-related genes might be DNA methylation. However, despite hypermethylation of the *CPEB1* gene, DNA methylation proved not to be directly responsible for its downregulation in gliomas. Thus, the underlying mechanism remains elusive. Abundant expression of CPEB 2-4 was detected in numerous human glioma specimens. CPEB2 expression in endothelial tumor cells suggested that CPEB2-mediated protein synthesis takes place in the close proximity of blood vessels within tumor tissue. On the other hand, CPEB4 expression appeared to support tumorigenic properties by its putative entanglement into local protein synthesis in transformed cells. Intriguingly, only CPEB3 expression was correlated positively with tumor progression. Phosphorylation of CPEB3 within the alternatively spliced region was negatively correlated with tumor malignancy. The loss of

CPEB3 activity in high-grade gliomas is likely caused by the expression of alternatively spliced variants. This suggests that a substantial part of the CPEB3 in GBM specimens does not undergo phosphorylation and indicates phosphorylation to be a biologically important mechanism regulating CPEB3 activity. Furthermore, a significant correlation between CPEB3 activity and survival was observed in less aggressive low-grade astrocytomas considered to be sGBM precursors. Consequently, CPEB3 may be considered as an attractive therapeutic target in gliomas.

To further investigate the relationship between CPEB activity, growth properties and cancer-relevant parameters an *in vitro* overexpression study was performed. This revealed a striking link between CPEB1, enhanced apoptotic activity and enhanced migration. One explanation could be that through rapid changes in the cytoskeleton of migrating cell the chance of mistakes rises, turning GBM cells towards an apoptotic pathway. On the other hand, CPEB2 overexpression decreased apoptotic activity, enhanced migration and by this additionally strengthened the cancerous properties of the cells. Importantly, CPEBs were also found to regulate various cancer pathways, including the TGF-β signaling cascade. However, further studies are needed to fully understand the interaction between CPEBs translational control and the pathophysiology of cultured GMB cells and human gliomas.

Finally, the study revealed that CPEB2 is expressed in different cellular populations, brain regions, and stages of development, which indicates that this protein plays an important role in regulation of local protein synthesis, synaptic plasticity, and neuronal morphogenesis.

The present study does not only increase our understanding of the function of CPEBs but also shows the importance of post-transcriptional modifications of mRNAs as a pathophysiological mechanism in gliomas and potentially other cancers. Therefore, these results may serve as a valuable basis for the identification of new therapeutic and diagnostic factors in cancer treatment.

8 PERSPECTIVE

Aberrant expression of CPEBs in human gliomas indicates the importance of post-transcriptional regulation in cancer cells. However, to fully understand the role of CPEBs in this relatively young research filed further investigations are required.

As increasing evidence confirms the implication of CPEBs in multiple pathological processes, most likely CPEB-dependent translation is a more general event in tumorigenesis. Therefore, particular attention should be paid to metastatic brain tumors, namely cancers beginning in lungs, breast, melanoma, colon, and kidney, and subsequently invade the brain. Further investigations of CPEB expression in different kinds of cancer may be performed by tissue microarrays or meta-analysis.

Knowing that CPEBs control the translation of various genes, the identification of target transcripts should be a major future task to understand their role in the complex tumor environment. Experiments with the objective of identifying mRNAs bound by CPEBs in normal versus cancer cells might involve RNA immunoprecipitation followed by DNA chip microarray analysis. As an alternative method, crosslinking and immunoprecipitation of RNA binding proteins followed by cloning and deep sequencing of the attached RNAs might be used.

Having in mind that solely CPEB splice variants containing the B-region may undergo activation, the variants lacking B-region may arrest cytoplasmic polyadenylation and translation of bound mRNAs. Therefore, it ought to be examined which mRNAs are silenced with the help of this mechanism. The answer may be provided by evaluation of the elongation of poly(A) tails of bound mRNAs in normal and cancer cells. Polyadenylation may be investigated by a whole-transcriptome approach, such as deep sequencing of mRNAs with poly(A) tails.

Finally, it ought to be considered whether CPEBs might be involved in therapy. For this purpose, a straightforward approach of animal models might be used. Xenografts or

syngeneic animal models reflecting conditions observed in human GBMs might be valuable for personalized therapy of brain tumor patients. This might be particularly important for patients who suffered a relapse or whose tumor continues to grow after standard treatment. Moreover, this might be the key to test CPEB function *in vivo* and to translate the latest findings on the molecular causes of brain tumors, their risk valuation and new therapeutic methods into innovative treatment concepts.

REFERENCES

Alarcon, J.M., Hodgman, R., Theis, M., Huang, Y.-S., Kandel, E.R., and Richter, J.D. (2004). Selective Modulation of Some Forms of Schaffer Collateral-CA1 Synaptic Plasticity in Mice With a Disruption of the CPEB-1 Gene. Learning & Memory *11*, 318–327.

Atkins, C.M., Nozaki, N., Shigeri, Y., and Soderling, T.R. (2004). Cytoplasmic Polyadenylation Element Binding Protein-Dependent Protein Synthesis Is Regulated by Calcium/Calmodulin-Dependent Protein Kinase II. The Journal of Neuroscience *24*, 5193–5201.

Atkins, C.M., Davare, M.A., Oh, M.C., Derkach, V., and Soderling, T.R. (2005). Bidirectional regulation of cytoplasmic polyadenylation element-binding protein phosphorylation by Ca2+/calmodulin-dependent protein kinase II and protein phosphatase 1 during hippocampal long-term potentiation. The Journal of Neuroscience *25*, 5604–5610.

Barbashina, V., Salazar, P., Holland, E.C., Rosenblum, M.K., and Ladanyi, M. (2005). Allelic losses at 1p36 and 19q13 in gliomas: correlation with histologic classification, definition of a 150-kb minimal deleted region on 1p36, and evaluation of CAMTA1 as a candidate tumor suppressor gene. Clinical Cancer Research *11*, 1119–1128.

Barnard, D.C., Ryan, K., Manley, J.L., and Richter, J.D. (2004). Symplekin and xGLD-2 are required for CPEB-mediated cytoplasmic polyadenylation. Cell *119*, 641–651.

Bava, F.-A., Eliscovich, C., Ferreira, P.G., Miñana, B., Ben-Dov, C., Guigó, R., Valcárcel, J., and Méndez, R. (2013). CPEB1 coordinates alternative 3'-UTR formation with translational regulation. Nature *495*, 121–125.

Baylin, S.B. (2005). DNA methylation and gene silencing in cancer. Nature Clinical Practice Oncology *2*, S4–S11.

Berger-Sweeney, J., Zearfoss, N.R., and Richter, J.D. (2006). Reduced extinction of hippocampal-dependent memories in CPEB knockout mice. Learning & Memory *13*, 4–7.

Berget, S.M., Moore, C., and Sharp, P.A. (1977). Spliced segments at the 5′ terminus of adenovirus 2 late mRNA. Proceedings of the National Academy of Sciences *74*, 3171–3175.

Bleeker, F.E., Lamba, S., Leenstra, S., Troost, D., Hulsebos, T., Vandertop, W.P., Frattini, M., Molinari, F., Knowles, M., and Cerrato, A. (2009). IDH1 mutations at residue p. R132 (IDH1R132) occur frequently in high-grade gliomas but not in other solid tumors. Human Mutation *30*, 7–11.

Bohman, L.-E., Swanson, K.R., Moore, J.L., Rockne, R., Mandigo, C., Hankinson, T., Assanah, M., Canoll, P., and Bruce, J.N. (2010). Magnetic resonance imaging characteristics of glioblastoma multiforme: implications for understanding glioma ontogeny. Neurosurgery *67*, 1319.

van den Boom, J., Wolter, M., Kuick, R., Misek, D.E., Youkilis, A.S., Wechsler, D.S., Sommer, C., Reifenberger, G., and Hanash, S.M. (2003). Characterization of gene expression profiles associated

with glioma progression using oligonucleotide-based microarray analysis and real-time reverse transcription-polymerase chain reaction. The American Journal of Pathology *163*, 1033–1043.

Bruna, A., Darken, R.S., Rojo, F., Ocaña, A., Peñuelas, S., Arias, A., Paris, R., Tortosa, A., Mora, J., and Baselga, J. (2007). High TGFβ-Smad activity confers poor prognosis in glioma patients and promotes cell proliferation depending on the methylation of the PDGF-B gene. Cancer Cell *11*, 147–160.

Burns, D.M., and Richter, J.D. (2008). CPEB regulation of human cellular senescence, energy metabolism, and p53 mRNA translation. Genes & Development *22*, 3449–3460.

Burns, D.M., D'Ambrogio, A., Nottrott, S., and Richter, J.D. (2011). CPEB and two poly (A) polymerases control miR-122 stability and p53 mRNA translation. Nature *473*, 105–108.

Caldeira, J., Simões-Correia, J., Paredes, J., Pinto, M.T., Sousa, S., Corso, G., Marrelli, D., Roviello, F., Pereira, P.S., and Weil, D. (2012). CPEB1, a novel gene silenced in gastric cancer: a Drosophila approach. Gut *61*, 1115–1123.

Cao, Q., and Richter, J.D. (2002). Dissolution of the maskin–eIF4E complex by cytoplasmic polyadenylation and poly (A)-binding protein controls cyclin B1 mRNA translation and oocyte maturation. The EMBO Journal *21*, 3852–3862.

Cao, Q., Kim, J.H., and Richter, J.D. (2006). CDK1 and calcineurin regulate Maskin association with eIF4E and translational control of cell cycle progression. Nature Structural & Molecular Biology *13*, 1128–1134.

Carmona, M.A., Murai, K.K., Wang, L., Roberts, A.J., and Pasquale, E.B. (2009). Glial ephrin-A3 regulates hippocampal dendritic spine morphology and glutamate transport. Proceedings of the National Academy of Sciences *106*, 12524–12529.

Chen, P., and Huang, Y. (2012). CPEB2–eEF2 interaction impedes HIF-1α RNA translation. The EMBO Journal *31*, 959–971.

Chen, P.-J., Weng, J.-Y., Hsu, P.-H., Shew, J.-Y., Huang, Y.-S., and Lee, W.-H. (2015). NPGPx modulates CPEB2-controlled HIF-1α RNA translation in response to oxidative stress. Nucleic Acids Research.

Chen, Q.W., Zhu, X.Y., Li, Y.Y., & Meng, Z.Q. (2014). Epigenetic regulation and cancer (Review). Oncology Reports *31*, 523-532.

Chow, L.T., Gelinas, R.E., Broker, T.R., and Roberts, R.J. (1977). An amazing sequence arrangement at the 5′ ends of adenovirus 2 messenger RNA. Cell *12*, 1–8.

Christensen, B.C., Smith, A.A., Zheng, S., Koestler, D.C., Houseman, E.A., Marsit, C.J., Wiemels, J.L., Nelson, H.H., Karagas, M.R., and Wrensch, M.R. (2011). DNA methylation, isocitrate dehydrogenase mutation, and survival in glioma. Journal of the National Cancer Institute *103*, 143–153.

Cohen, A.L., Holmen, S.L., and Colman, H. (2013). IDH1 and IDH2 mutations in gliomas. Current Neurology and Neuroscience Reports *13*, 1–7.

Curradi, M., Izzo, A., Badaracco, G., and Landsberger, N. (2002). Molecular mechanisms of gene silencing mediated by DNA methylation. Molecular and Cellular Biology *22*, 3157–3173.

D'Ambrogio, A., Nagaoka, K., and Richter, J.D. (2013). Translational control of cell growth and malignancy by the CPEBs. Nat Rev Cancer *13*, 283–290.

Dang, L., White, D.W., Gross, S., Bennett, B.D., Bittinger, M.A., Driggers, E.M., Fantin, V.R., Jang, H.G., Jin, S., Keenan, M.C., et al. (2010). Cancer-associated IDH1 mutations produce 2-hydroxyglutarate. Nature *465*, 966–966.

Darnell, J.C., and Richter, J.D. (2012). Cytoplasmic RNA-binding proteins and the control of complex brain function. Cold Spring Harbor Perspectives in Biology *4*, a012344.

Derynck, R., Akhurst, R.J., and Balmain, A. (2001). TGF-β signaling in tumor suppression and cancer progression. Nature Genetics *29*, 117–129.

Dever, T.E. (2002). Gene-specific regulation by general translation factors. Cell *108*, 545–556.

Du, L., and Richter, J.D. (2005). Activity-dependent polyadenylation in neurons. RNA *11*, 1340–1347.

Ehrlich, M. (2002). DNA methylation in cancer: too much, but also too little. Oncogene *21*, 5400–5413.

Emini, E.A., Hughes, J.V., Perlow, D., and Boger, J. (1985). Induction of hepatitis A virus-neutralizing antibody by a virus-specific synthetic peptide. Journal of Virology *55*, 836–839.

Fernández-Miranda, G., and Méndez, R. (2012). The CPEB-family of proteins, translational control in senescence and cancer. Ageing Research Reviews *11*, 460–472.

Filosa, A., Paixão, S., Honsek, S.D., Carmona, M.A., Becker, L., Feddersen, B., Gaitanos, L., Rudhard, Y., Schoepfer, R., and Klopstock, T. (2009). Neuron-glia communication via EphA4/ephrin-A3 modulates LTP through glial glutamate transport. Nature Neuroscience *12*, 1285–1292.

Galardi, S., Petretich, M., Pinna, G., D'Amico, S., Loreni, F., Michienzi, A., Groisman, I., and Ciafrè, S.A. (2016). CPEB1 restrains proliferation of Glioblastoma cells through the regulation of p27Kip1 mRNA translation. Scientific Reports *6*.

Garber, K. (2010). Oncometabolite? IDH1 discoveries raise possibility of new metabolism targets in brain cancers and leukemia. Journal of the National Cancer Institute.

Gebauer, F., and Richter, J.D. (1996). Mouse cytoplasmic polyadenylylation element binding protein: an evolutionarily conserved protein that interacts with the cytoplasmic polyadenylylation elements of c-mos mRNA. Proceedings of the National Academy of Sciences *93*, 14602–14607.

Giangarrà, V., Igea, A., Castellazzi, C.L., Bava, F.-A., and Mendez, R. (2015a). Global Analysis of CPEBs Reveals Sequential and Non-Redundant Functions in Mitotic Cell Cycle. PloS One *10*, e0138794.

Gibson, P., Tong, Y., Robinson, G., Thompson, M.C., Currle, D.S., Eden, C., Kranenburg, T.A., Hogg, T., Poppleton, H., and Martin, J. (2010). Subtypes of medulloblastoma have distinct developmental origins. Nature *468*, 1095–1099.

Godlewski, J., Krichevsky, A.M., Johnson, M.D., Chiocca, E.A., and Bronisz, A. (2014). Belonging to a network—microRNAs, extracellular vesicles, and the glioblastoma microenvironment. Neuro-Oncology.

Goll, M.G., and Bestor, T.H. (2005). Eukaryotic cytosine methyltransferases. Annu. Rev. Biochem. *74*, 481–514.

Groisman, I., Jung, M.-Y., Sarkissian, M., Cao, Q., and Richter, J.D. (2002). Translational control of the embryonic cell cycle. Cell *109*, 473–483.

Groisman, I., Ivshina, M., Marin, V., Kennedy, N.J., Davis, R.J., and Richter, J.D. (2006). Control of cellular senescence by CPEB. Genes & Development *20*, 2701–2712.

Groppo, R., and Richter, J.D. (2009). Translational control from head to tail. Current Opinion in Cell Biology *21*, 444–451.

Grudzien-Nogalska, E., Reed, B.C., and Rhoads, R.E. (2014). CPEB1 promotes differentiation and suppresses EMT in mammary epithelial cells. J Cell Sci *127*, 2326–2338.

Hägele, S., Kühn, U., Böning, M., and Katschinski, D.M. (2009). Cytoplasmic polyadenylation-element-binding protein (CPEB) 1 and 2 bind to the HIF-1α mRNA 3′-UTR and modulate HIF-1α protein expression. Biochemical Journal *417*, 235–246.

Hake, L.E., and Richter, J.D. (1994). CPEB is a specificity factor that mediates cytoplasmic polyadenylation during Xenopus oocyte maturation. Cell *79*, 617–627.

Hansen, C.N., Ketabi, Z., Rosenstierne, M.W., Palle, C., Boesen, H.C., and Norrild, B. (2009). Expression of CPEB, GAPDH and U6snRNA in cervical and ovarian tissue during cancer development. Apmis *117*, 53–59.

Heller, G., Schmidt, W.M., Ziegler, B., Holzer, S., Müllauer, L., Bilban, M., Zielinski, C.C., Drach, J., and Zöchbauer-Müller, S. (2008). Genome-wide transcriptional response to 5-aza-2′-deoxycytidine and trichostatin a in multiple myeloma cells. Cancer Research *68*, 44–54.

Herman, J.G., and Baylin, S.B. (2003). Gene silencing in cancer in association with promoter hypermethylation. New England Journal of Medicine *349*, 2042–2054.

Hu, W., Yang, Y., Xi, S., Sai, K., Su, D., Zhang, X., Lin, S., and Zeng, J. (2015). Expression of CPEB4 in Human Glioma and Its Correlations With Prognosis. Medicine *94*.

Huang, Y., Kan, M., Lin, C., and Richter, J.D. (2006). CPEB3 and CPEB4 in neurons: analysis of RNA-binding specificity and translational control of AMPA receptor GluR2 mRNA. The EMBO Journal *25*, 4865–4876.

Huang, Y.-S., Jung, M.-Y., Sarkissian, M., and Richter, J.D. (2002). N-methyl-d-aspartate receptor signaling results in Aurora kinase-catalyzed CPEB phosphorylation and αCaMKII mRNA polyadenylation at synapses. The EMBO Journal *21*, 2139–2148.

Huang, Y.-S., Carson, J.H., Barbarese, E., and Richter, J.D. (2003). Facilitation of dendritic mRNA transport by CPEB. Genes & Development *17*, 638–653.

Ichimura, K., Schmidt, E.E., Goike, H.M., and Collins, V.P. (1996). Human glioblastomas with no alterations of the CDKN2A (p16INK4A, MTS1) and CDK4 genes have frequent mutations of the retinoblastoma gene. Oncogene *13*, 1065–1072.

Igea, A., and Méndez, R. (2010). Meiosis requires a translational positive loop where CPEB1 ensues its replacement by CPEB4. The EMBO Journal *29*, 2182–2193.

Ivshina, M., Lasko, P., and Richter, J.D. (2014). Cytoplasmic polyadenylation element binding proteins in development, health, and disease. Annual Review of Cell and Developmental Biology *30*, 393–415.

Jameson, B., and Wolf, H. (1988). The antigenic index: a novel algorithm for predicting antigenic determinants. Computer Applications in the Biosciences: CABIOS *4*, 181–186.

Jin, G., Reitman, Z.J., Spasojevic, I., Batinic-Haberle, I., Yang, J., Schmidt-Kittler, O., Bigner, D.D., and Yan, H. (2011). 2-hydroxyglutarate production, but not dominant negative function, is conferred by glioma-derived NADP+-dependent isocitrate dehydrogenase mutations. PloS One *6*, e16812.

Johnson, R.A., Wright, K.D., Poppleton, H., Mohankumar, K.M., Finkelstein, D., Pounds, S.B., Rand, V., Leary, S.E., White, E., and Eden, C. (2010). Cross-species genomics matches driver mutations and cell compartments to model ependymoma. Nature *466*, 632–636.

Johnson, R.M., Vu, N.T., Griffin, B.P., Gentry, A.E., Archer, K.J., Chalfant, C.E., and Park, M.A. (2015). The alternative splicing of cytoplasmic polyadenylation element binding protein 2 drives anoikis resistance and the metastasis of triple negative breast cancer. Journal of Biological Chemistry *290*, 25717–25727.

Jones, P.A., and Baylin, S.B. (2007). The epigenomics of cancer. Cell *128*, 683–692.

Jones, K.J., Korb, E., Kundel, M.A., Kochanek, A.R., Kabraji, S., McEvoy, M., Shin, C.Y., and Wells, D.G. (2008). CPEB1 regulates β-catenin mRNA translation and cell migration in astrocytes. Glia *56*, 1401–1413.

Jung, M., and Pfeifer, G. P. (2015). Aging and DNA methylation. BMC Biology, 13, 7.

Kaczmarczyk, L., Labrie-Dion, É., Sehgal, K., Sylvester, M., Skubal, M., Josten, M., Steinhäuser, C., De Koninck, P., and Theis, M. (2016). New Phosphospecific Antibody Reveals Isoform-Specific Phosphorylation of CPEB3 Protein. PLoS ONE *11*, e0150000.

Kalluri, R., and Weinberg, R.A. (2009). The basics of epithelial-mesenchymal transition. The Journal of Clinical Investigation *119*, 1420–1428.

Kaminska, B., Kocyk, M., and Kijewska, M. (2013). TGF beta signaling and its role in glioma pathogenesis. In Glioma Signaling, (Springer), pp. 171–187.

Kan, M.-C., Oruganty-Das, A., Cooper-Morgan, A., Jin, G., Swanger, S.A., Bassell, G.J., Florman, H., van Leyen, K., and Richter, J.D. (2010). CPEB4 is a cell survival protein retained in the nucleus

upon ischemia or endoplasmic reticulum calcium depletion. Molecular and Cellular Biology *30*, 5658–5671.

Kandel, E.R. (2001). The molecular biology of memory storage: a dialogue between genes and synapses. Science *294*, 1030–1038.

Kang, H., and Schuman, E.M. (1996). A requirement for local protein synthesis in neurotrophin-induced hippocampal synaptic plasticity. Science *273*, 1402.

Kim, J.H., and Richter, J.D. (2006). Opposing polymerase-deadenylase activities regulate cytoplasmic polyadenylation. Molecular Cell *24*, 173–183.

Kim, J.H., and Richter, J.D. (2007). RINGO/cdk1 and CPEB mediate poly (A) tail stabilization and translational regulation by ePAB. Genes & Development *21*, 2571–2579.

Kim, Y.-W., Koul, D., Kim, S.H., Lucio-Eterovic, A.K., Freire, P.R., Yao, J., Wang, J., Almeida, J.S., Aldape, K., and Yung, W.A. (2013). Identification of prognostic gene signatures of glioblastoma: a study based on TCGA data analysis. Neuro-Oncology *15*, 829–839.

Kochanek, D.M., and Wells, D.G. (2013). CPEB1 regulates the expression of MTDH/AEG-1 and glioblastoma cell migration. Molecular Cancer Research *11*, 149–160.

Kornblihtt, A.R., Schor, I.E., Alló, M., Dujardin, G., Petrillo, E., and Muñoz, M.J. (2013). Alternative splicing: a pivotal step between eukaryotic transcription and translation. Nature Reviews Molecular Cell Biology *14*, 153–165.

Kyte, J., and Doolittle, R.F. (1982). A simple method for displaying the hydropathic character of a protein. Journal of Molecular Biology *157*, 105–132.

Labussiere, M., Idbaih, A., Wang, X.-W., Marie, Y., Boisselier, B., Falet, C., Paris, S., Laffaire, J., Carpentier, C., and Criniere, E. (2010). All the 1p19q codeleted gliomas are mutated on IDH1 or IDH2. Neurology *74*, 1886–1890.

Lazaris-Karatzas, A., Smith, M.R., Frederickson, R.M., Jaramillo, M.L., Liu, Y., Kung, H., and Sonenberg, N. (1992). Ras mediates translation initiation factor 4E-induced malignant transformation. Genes & Development *6*, 1631–1642.

Lim, D.A., Cha, S., Mayo, M.C., Chen, M.-H., Keles, E., VandenBerg, S., and Berger, M.S. (2007). Relationship of glioblastoma multiforme to neural stem cell regions predicts invasive and multifocal tumor phenotype. Neuro-Oncology *9*, 424–429.

Lin, C.-L., Evans, V., Shen, S., Xing, Y., and Richter, J.D. (2010). The nuclear experience of CPEB: implications for RNA processing and translational control. RNA *16*, 338–348.

Lin, C.-L., Huang, Y.-T., and Richter, J.D. (2012). Transient CPEB dimerization and translational control. RNA *18*, 1050–1061.

Liu, J., and Maller, J.L. (2005). Xenopus Polo-like kinase Plx1: a multifunctional mitotic kinase. Oncogene *24*, 238–247.

Louis, D.N. (2006). Molecular pathology of malignant gliomas. Annu. Rev. Pathol. Mech. Dis. *1*, 97–117.

Louis, D.N., Ohgaki, H., Wiestler, O.D., Cavenee, W.K., Burger, P.C., Jouvet, A., Scheithauer, B.W., and Kleihues, P. (2007). The 2007 WHO classification of tumours of the central nervous system. Acta Neuropathologica *114*, 97–109.

Louis, D.N., Perry, A., Reifenberger, G., von Deimling, A., Figarella-Branger, D., Cavenee, W.K., Ohgaki, H., Wiestler, O.D., Kleihues, P., and Ellison, D.W. (2016). The 2016 World Health Organization classification of tumors of the central nervous system: A summary. Acta Neuropathologica *131*, 803–820.

Massagué, J. (2008). TGFβ in cancer. Cell *134*, 215–230.

Mayford, M., Siegelbaum, S.A., and Kandel, E.R. (2012). Synapses and memory storage. Cold Spring Harbor Perspectives in Biology *4*, a005751.

Mendez, R., and Richter, J.D. (2001). Translational control by CPEB: a means to the end. Nature Reviews Molecular Cell Biology *2*, 521–529.

Mendez, R., Murthy, K.G., Ryan, K., Manley, J.L., and Richter, J.D. (2000a). Phosphorylation of CPEB by Eg2 mediates the recruitment of CPSF into an active cytoplasmic polyadenylation complex. Molecular Cell *6*, 1253–1259.

Mendez, R., Hake, L.E., Andresson, T., Littlepage, L.E., Ruderman, J.V., and Richter, J.D. (2000b). Phosphorylation of CPE binding factor by Eg2 regulates translation of c-mos mRNA. Nature *404*, 302–307.

Modrek, A.S., Bayin, N.S., and Placantonakis, D.G. (2014). Brain stem cells as the cell of origin in glioma. World J Stem Cells *6*, 43–52.

Morgan, M., Iaconcig, A., and Muro, A.F. (2010). CPEB2, CPEB3 and CPEB4 are coordinately regulated by miRNAs recognizing conserved binding sites in paralog positions of their 3′-UTRs. Nucleic Acids Research *38*, 7698–7710.

Nagaoka, K., Udagawa, T., and Richter, J.D. (2012). CPEB-mediated ZO-1 mRNA localization is required for epithelial tight-junction assembly and cell polarity. Nature Communications *3*, 675.

Nagaoka, K., Fujii, K., Zhang, H., Usuda, K., Watanabe, G., Ivshina, M., and Richter, J. (2016). CPEB1 mediates epithelial-to-mesenchyme transition and breast cancer metastasis. Oncogene *35*, 2893–2901.

Nairismägi, M.-L., Vislovukh, A., Meng, Q., Kratassiouk, G., Beldiman, C., Petretich, M., Groisman, R., Füchtbauer, E., Harel-Bellan, A., and Groisman, I. (2012). Translational control of TWIST1 expression in MCF-10A cell lines recapitulating breast cancer progression. Oncogene *31*, 4960–4966.

Nan, X., Ng, H.-H., Johnson, C.A., Laherty, C.D., Turner, B.M., Eisenman, R.N., and Bird, A. (1998). Transcriptional repression by the methyl-CpG-binding protein MeCP2 involves a histone deacetylase complex. Nature *393*, 386–389.

Noushmehr, H., Weisenberger, D.J., Diefes, K., Phillips, H.S., Pujara, K., Berman, B.P., Pan, F., Pelloski, C.E., Sulman, E.P., and Bhat, K.P. (2010). Identification of a CpG island methylator phenotype that defines a distinct subgroup of glioma. Cancer Cell *17*, 510–522.

Novoa, I., Gallego, J., Ferreira, P.G., and Mendez, R. (2010). Mitotic cell-cycle progression is regulated by CPEB1 and CPEB4-dependent translational control. Nature Cell Biology *12*, 447–456.

Ohgaki, H., Dessen, P., Jourde, B., Horstmann, S., Nishikawa, T., Di Patre, P.-L., Burkhard, C., Schüler, D., Probst-Hensch, N.M., and Maiorka, P.C. (2004). Genetic pathways to glioblastoma A population-based study. Cancer Research *64*, 6892–6899.

Olar, A., and Aldape, K.D. (2012). Biomarkers classification and therapeutic decision-making for malignant gliomas. Current Treatment Options in Oncology *13*, 417–436.

Ortiz-Zapater, E., Pineda, D., Martínez-Bosch, N., Fernández-Miranda, G., Iglesias, M., Alameda, F., Moreno, M., Eliscovich, C., Eyras, E., and Real, F.X. (2012). Key contribution of CPEB4-mediated translational control to cancer progression. Nature Medicine *18*, 83–90.

Parsons, D.W., Jones, S., Zhang, X., Lin, J.C.-H., Leary, R.J., Angenendt, P., Mankoo, P., Carter, H., Siu, I.-M., and Gallia, G.L. (2008). An integrated genomic analysis of human glioblastoma multiforme. Science *321*, 1807–1812.

Peng, A., and Maller, J. (2010). Serine/threonine phosphatases in the DNA damage response and cancer. Oncogene *29*, 5977–5988.

Phillips, H.S., Kharbanda, S., Chen, R., Forrest, W.F., Soriano, R.H., Wu, T.D., Misra, A., Nigro, J.M., Colman, H., and Soroceanu, L. (2006). Molecular subclasses of high-grade glioma predict prognosis, delineate a pattern of disease progression, and resemble stages in neurogenesis. Cancer Cell *9*, 157–173.

Reya, T., Morrison, S.J., Clarke, M.F., and Weissman, I.L. (2001). Stem cells, cancer, and cancer stem cells. Nature *414*, 105–111.

Richter, J.D. (2001). Think globally, translate locally: what mitotic spindles and neuronal synapses have in common. Proceedings of the National Academy of Sciences *98*, 7069–7071.

Richter, J.D. (2007). CPEB: a life in translation. Trends in Biochemical Sciences *32*, 279–285.

Richter, J.D., and Klann, E. (2009). Making synaptic plasticity and memory last: mechanisms of translational regulation. Genes & Development *23*, 1–11.

Richter, J.D., and Sonenberg, N. (2005). Regulation of cap-dependent translation by eIF4E inhibitory proteins. Nature *433*, 477–480.

Rickman, D.S., Bobek, M.P., Misek, D.E., Kuick, R., Blaivas, M., Kurnit, D.M., Taylor, J., and Hanash, S.M. (2001). Distinctive molecular profiles of high-grade and low-grade gliomas based on oligonucleotide microarray analysis. Cancer Research *61*, 6885–6891.

Riemenschneider, M.J., Koy, T.H., and Reifenberger, G. (2004). Expression of oligodendrocyte lineage genes in oligodendroglial and astrocytic gliomas. Acta Neuropathologica *107*, 277–282.

Rousseau, A., Nutt, C.L., Betensky, R.A., Iafrate, A.J., Han, M., Ligon, K.L., Rowitch, D.H., and Louis, D.N. (2006). Expression of oligodendroglial and astrocytic lineage markers in diffuse gliomas: use of YKL-40, ApoE, ASCL1, and NKX2-2. Journal of Neuropathology & Experimental Neurology *65*, 1149–1156.

Ruggero, D., Montanaro, L., Ma, L., Xu, W., Londei, P., Cordon-Cardo, C., and Pandolfi, P.P. (2004). The translation factor eIF-4E promotes tumor formation and cooperates with c-Myc in lymphomagenesis. Nature Medicine *10*, 484–486.

Sarkissian, M., Mendez, R., and Richter, J.D. (2004). Progesterone and insulin stimulation of CPEB-dependent polyadenylation is regulated by Aurora A and glycogen synthase kinase-3. Genes & Development *18*, 48–61.

Schonberg, D.L., Lubelski, D., Miller, T.E., and Rich, J.N. (2014). Brain tumor stem cells: molecular characteristics and their impact on therapy. Molecular Aspects of Medicine *39*, 82–101.

Seifert, G., and Steinhäuser, C. (2007). Structure-Function Analyses of Single Cells by Combining Patch-Clamp Techniques with Reverse Transcription-Polymerase Chain Reaction. In Patch-Clamp Analysis, (Springer), pp. 373–409.

Seoane, J. (2006). Escaping from the TGFβ anti-proliferative control. Carcinogenesis *27*, 2148–2156.

Sharma, S., Kelly, T.K., and Jones, P.A. (2010). Epigenetics in cancer. Carcinogenesis *31*, 27–36.

Shin, J., Shen, F., and Huguenard, J.R. (2005). Polyamines modulate AMPA receptor–dependent synaptic responses in immature layer V pyramidal neurons. Journal of Neurophysiology *93*, 2634–2643.

Shoshan, Y., Nishiyama, A., Chang, A., Mörk, S., Barnett, G.H., Cowell, J.K., Trapp, B.D., and Staugaitis, S.M. (1999). Expression of oligodendrocyte progenitor cell antigens by gliomas: implications for the histogenesis of brain tumors. Proceedings of the National Academy of Sciences *96*, 10361–10366.

Siegel, P.M., and Massagué, J. (2003). Cytostatic and apoptotic actions of TGF-β in homeostasis and cancer. Nature Reviews Cancer *3*, 807–820.

Skubal, M., Gielen, G.H., Waha, A., Gessi, M., Kaczmarczyk, L., Seifert, G., Freihoff, D., Freihoff, J., Pietsch, T., and Simon, M. (2016). Altered splicing leads to reduced activation of CPEB3 in high-grade gliomas. Oncotarget.

Sonenberg, N. (1993). Translation factors as effectors of cell growth and tumorigenesis. Current Opinion in Cell Biology *5*, 955–960.

Sonenberg, N., and Hinnebusch, A.G. (2009). Regulation of translation initiation in eukaryotes: mechanisms and biological targets. Cell *136*, 731–745.

Stebbins-Boaz, B., Hake, L., and Richter, J. (1996). CPEB controls the cytoplasmic polyadenylation of cyclin, Cdk2 and c-mos mRNAs and is necessary for oocyte maturation in Xenopus. The EMBO Journal *15*, 2582.

Stupp, R., Mason, W.P., Van Den Bent, M.J., Weller, M., Fisher, B., Taphoorn, M.J., Belanger, K., Brandes, A.A., Marosi, C., and Bogdahn, U. (2005). Radiotherapy plus concomitant and adjuvant temozolomide for glioblastoma. New England Journal of Medicine *352*, 987–996.

Sutton, M.A., and Schuman, E.M. (2006). Dendritic protein synthesis, synaptic plasticity, and memory. Cell *127*, 49–58.

Swanger, S.A., He, Y.A., Richter, J.D., and Bassell, G.J. (2013). Dendritic GluN2A synthesis mediates activity-induced NMDA receptor insertion. The Journal of Neuroscience *33*, 8898–8908.

Tam, W.L., and Weinberg, R.A. (2013). The epigenetics of epithelial-mesenchymal plasticity in cancer. Nature Medicine *19*, 1438–1449.

Teleman, A.A., Chen, Y.-W., and Cohen, S.M. (2005). 4E-BP functions as a metabolic brake used under stress conditions but not during normal growth. Genes & Development *19*, 1844–1848.

Thakkar, J.P., Dolecek, T.A., Horbinski, C., Ostrom, Q.T., Lightner, D.D., Barnholtz-Sloan, J.S., and Villano, J.L. (2014). Epidemiologic and molecular prognostic review of glioblastoma. Cancer Epidemiology Biomarkers & Prevention *23*, 1985–1996.

Theis, M., Si, K., and Kandel, E.R. (2003). Two previously undescribed members of the mouse CPEB family of genes and their inducible expression in the principal cell layers of the hippocampus. Proceedings of the National Academy of Sciences *100*, 9602–9607.

Tsai, L.-Y., Chang, Y.-W., Lin, P.-Y., Chou, H.-J., Liu, T.-J., Lee, P.-T., Huang, W.-H., Tsou, Y.-L., and Huang, Y.-S. (2013). CPEB4 knockout mice exhibit normal hippocampus-related synaptic plasticity and memory. PLoS One *8*, e84978.

Turimella, S.L., Bedner, P., Skubal, M., Vangoor, V.R., Kaczmarczyk, L., Karl, K., Zoidl, G., Gieselmann, V., Seifert, G., and Steinhäuser, C. (2015). Characterization of cytoplasmic polyadenylation element binding 2 protein expression and its RNA binding activity. Hippocampus *25*, 630–642.

Udagawa, T., Swanger, S.A., Takeuchi, K., Kim, J.H., Nalavadi, V., Shin, J., Lorenz, L.J., Zukin, R.S., Bassell, G.J., and Richter, J.D. (2012). Bidirectional control of mRNA translation and synaptic plasticity by the cytoplasmic polyadenylation complex. Molecular Cell *47*, 253–266.

Vander Heiden, M.G., Cantley, L.C., and Thompson, C.B. (2009). Understanding the Warburg effect: the metabolic requirements of cell proliferation. Science *324*, 1029–1033.

Verhaak, R.G., Hoadley, K.A., Purdom, E., Wang, V., Qi, Y., Wilkerson, M.D., Miller, C.R., Ding, L., Golub, T., and Mesirov, J.P. (2010). Integrated genomic analysis identifies clinically relevant subtypes of glioblastoma characterized by abnormalities in PDGFRA, IDH1, EGFR, and NF1. Cancer Cell *17*, 98–110.

Vigneswaran, K., Neill, S., and Hadjipanayis, C.G. (2015). Beyond the World Health Organization grading of infiltrating gliomas: advances in the molecular genetics of glioma classification. Annals of Translational Medicine *3*.

Wang, X.-P., and Cooper, N.G. (2009). Characterization of the transcripts and protein isoforms for cytoplasmic polyadenylation element binding protein-3 (CPEB3) in the mouse retina. BMC Molecular Biology *10*, 109.

Wang, X.-P., and Cooper, N.G. (2010). Comparative in silico analyses of cpeb1–4 with functional predictions. Bioinformatics and Biology Insights *4*, 61.

Watt, F., and Molloy, P.L. (1988). Cytosine methylation prevents binding to DNA of a HeLa cell transcription factor required for optimal expression of the adenovirus major late promoter. Genes & Development *2*, 1136–1143.

Weber, M., Hellmann, I., Stadler, M.B., Ramos, L., Pääbo, S., Rebhan, M., and Schübeler, D. (2007). Distribution, silencing potential and evolutionary impact of promoter DNA methylation in the human genome. Nature Genetics *39*, 457–466.

Wesolowska, A., Kwiatkowska, A., Slomnicki, L., Dembinski, M., Master, A., Sliwa, M., Franciszkiewicz, K., Chouaib, S., and Kaminska, B. (2008). Microglia-derived TGF-β as an important regulator of glioblastoma invasion—an inhibition of TGF-β-dependent effects by shRNA against human TGF-β type II receptor. Oncogene *27*, 918–930.

Wessagowit, V., Nalla, V.K., Rogan, P.K., and McGrath, J.A. (2005). Normal and abnormal mechanisms of gene splicing and relevance to inherited skin diseases. Journal of Dermatological Science *40*, 73–84.

Wilczynska, A., Aigueperse, C., Kress, M., Dautry, F., and Weil, D. (2005). The translational regulator CPEB1 provides a link between dcp1 bodies and stress granules. J Cell Sci *118*, 981–992.

Wilkins, J.F. (2005). Genomic imprinting and methylation: epigenetic canalization and conflict. TRENDS in Genetics *21*, 356–365.

Wilson, T., Karajannis, M., and Harter, D. (2014). Glioblastoma multiforme: State of the art and future therapeutics. Surgical Neurology International *5*, 64.

Wu, L., Wells, D., Tay, J., Mendis, D., Abbott, M.-A., Barnitt, A., Quinlan, E., Heynen, A., Fallon, J.R., and Richter, J.D. (1998). CPEB-mediated cytoplasmic polyadenylation and the regulation of experience-dependent translation of α-CaMKII mRNA at synapses. Neuron *21*, 1129–1139.

Yamada, Y., Watanabe, H., Miura, F., Soejima, H., Uchiyama, M., Iwasaka, T., Mukai, T., Sakaki, Y., and Ito, T. (2004). A comprehensive analysis of allelic methylation status of CpG islands on human chromosome 21q. Genome Research *14*, 247–266.

Yan, H., Parsons, D.W., Jin, G., McLendon, R., Rasheed, B.A., Yuan, W., Kos, I., Batinic-Haberle, I., Jones, S., and Riggins, G.J. (2009). IDH1 and IDH2 mutations in gliomas. New England Journal of Medicine *360*, 765–773.

Yin, J., Park, G., Lee, J.E., Park, J.Y., Kim, T.-H., Kim, Y.-J., Lee, S.-H., Yoo, H., Kim, J.H., and Park, J.B. (2014). CPEB1 modulates differentiation of glioma stem cells via downregulation of HES1 and SIRT1 expression. Oncotarget *5*, 6756–6769.

Yu, X., and Malenka, R.C. (2003). β-catenin is critical for dendritic morphogenesis. Nature Neuroscience *6*, 1169–1177.

Zhang, M., Lahn, M., and Huber, P.E. (2012). Translating the combination of TGFβ blockade and radiotherapy into clinical development in glioblastoma. Oncoimmunology *1*, 943–945.

Zilberman, D., and Henikoff, S. (2007). Genome-wide analysis of DNA methylation patterns. Development *134*, 3959–3965.

Zong, H., Verhaak, R.G., and Canoll, P. (2012). The cellular origin for malignant glioma and prospects for clinical advancements. Expert Review of Molecular Diagnostics *12*, 383–394.

Zukin, R.S., Richter, J., and Bagni, C. (2009). Signals, synapses, and synthesis: how new proteins control plasticity. Frontiers in Neural Circuits *3*, 14.

APPENDIX I

pCMV6-Neo vector map

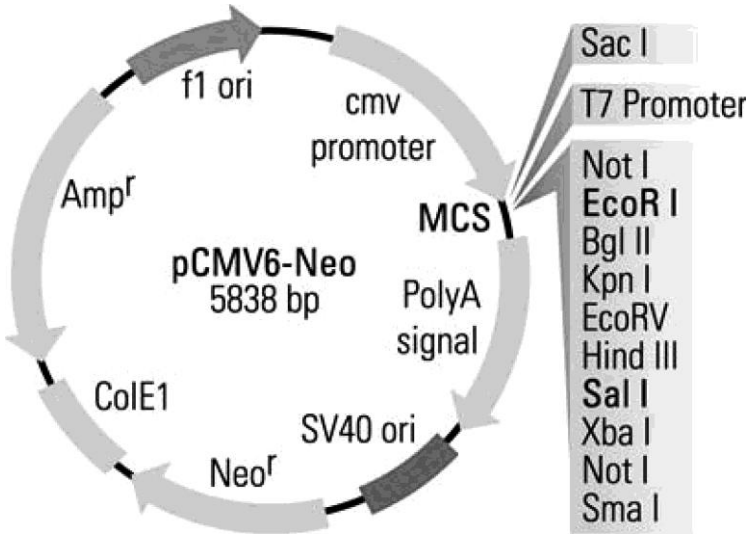

pmaxGFP vector map

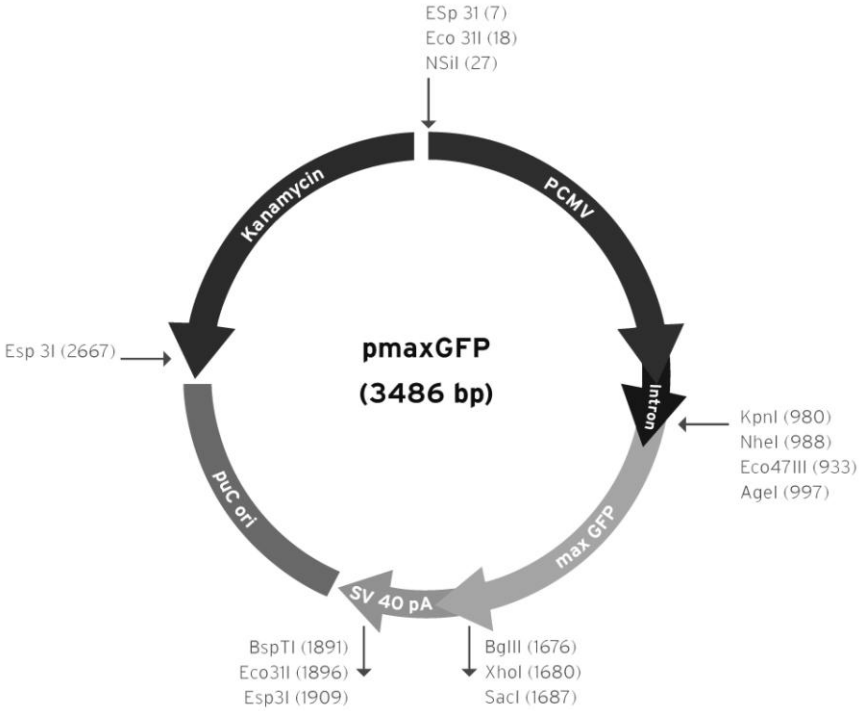

pEGFP-N1 vector map

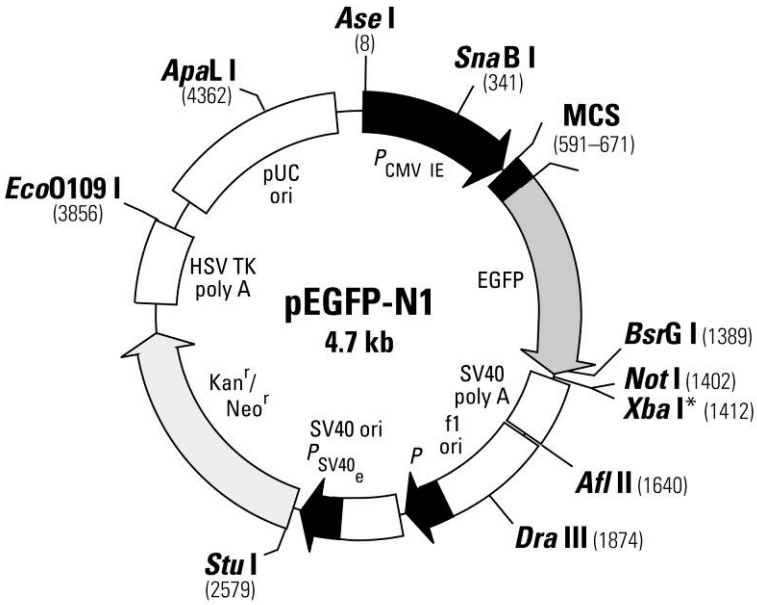
Ase I
(8)
Sna B I
(341)
MCS
(591–671)
ApaL I
(4362)
Eco0109 I
(3856)
pUC
ori
P CMV IE
EGFP
HSV TK
poly A
pEGFP-N1
4.7 kb
BsrG I (1389)
Not I (1402)
Xba I* (1412)
SV40
poly A
Kanr/
Neor
SV40 ori
P SV40e
f1
ori
P
Afl II (1640)
Dra III (1874)
Stu I
(2579)